Interaction Notes

Note 525

21 April 1997

Use of Modified Pole Series in the Singularity Expansion Method

Carl E. Baum
Phillips Laboratory WSQW

Jon E. Mooney and Lloyd S. Riggs
Electrical Engineering Dept.
Auburn University

Abstract

The singularity expansion method (SEM) is an efficient representation of electromagnetic scattering in terms of poles in the resonance region. However, in the low-frequency region, the scattering is proportional to the square of the frequency and is dominated by the induced electric and magnetic dipole moments. This paper develops a hybrid representation involving both the dipole and pole terms for a more efficient low-frequency representation.

Interaction Notes
Note 525
21 April 1997

Use of Modified Pole Series in the Singularity Expansion Method

Carl E. Baum
Phillips Laboratory WSQW

Jon E. Mooney and Lloyd S. Riggs
Electrical Engineering Dept.
Auburn University

Abstract

The singularity expansion method (SEM) is an efficient representation of electromagnetic scattering in terms of poles in the resonance region. However, in the low-frequency region, the scattering is proportional to the square of the frequency and is dominated by the induced electric and magnetic dipole moments. This paper develops a hybrid representation involving both the dipole and pole terms for a more efficient low-frequency representation.

Contents

1. Introduction

The singularity expansion method (SEM) is by now well established as a way to represent and efficiently calculate the interaction and scattering of electromagnetic fields in the time and frequency domains (with emphasis on the resonance region) [5,7,21,22,27,28]. Considered in the general context of complex-variable theory (vis a vis the complex frequency s), there are various ways to represent a function of a complex variable. There are power (Taylor) series around some point, say s_0, in the complex plane, converging within some radius given by the nearest singularity. In the electromagnetic context, this can be applied with $s_0 = 0$ to obtain a series expansion of the scattering (Rayleigh scattering or low-frequency method (LFM)). One can use the singularities (poles, branch cuts, singularity at ∞ (entire function)) to represent the response (hence SEM). As $s \to \infty$ (in appropriate directions) one can obtain various high-frequency asymptotic expansions (e.g. GTD, UTD, etc.) to give a high frequency method (HFM).

In this paper, we explore the connection of LFM and SEM for electromagnetic scattering. At low frequencies, it is well known that the induced dipole moments (electric and magnetic) of the target dominate the scattering and give a scattering dyadic proportional to s^2. This suggests a hybrid expansion in which the dipole terms are first pulled out, and then the SEM is applied in an appropriate fashion to give a representation which is accurate for low frequencies up through the first few resonances and requires a minimum number of terms for reasonable accuracy. This paper approaches this problem by removing successive powers of s (in a multiplicative sense) and then applying the SEM to the resulting functions.

The appendices apply the theory to two classical scatterers, the thin wire and the thin circular loop. Various comparisons are made to indicate the range of applicability of this approach. Some preliminary results of this study were reported in [23].

2. Modified Pole Series

Consider some $F(t)$ and its two-sided Laplace transform $\tilde{F}(s)$ which is written in its SEM representation

$$\begin{aligned} \tilde{F}(s) &= \sum_\alpha F_\alpha e^{-(s-s_\alpha)t_i} [s-s_\alpha]^{-1} + \text{other singularities} \\ F(t) &= \sum_\alpha F_\alpha e^{s_\alpha t} u(t-t_i) + \text{other singularities} \end{aligned} \tag{2.1}$$

where the starting or initial time for the pole terms is t_i, noting that for our problems of interest, time-translation symmetry makes the definition of $t = 0$ arbitrary. Typically $F(t)$ is assumed real, making $\tilde{F}(s)$ conjugate symmetric. While the above notation is for scalars, the results will apply for vectors and dyadics as well. Note that the poles here are assumed to be first order, but that the analysis can be extended to higher order poles using the techniques in [28].

As discussed in [4], modified poles are introduced to shift the pole terms by subtraction of the value at $s = 0$. In our more general form in (2.1) with an initial time t_i, let us first change the series to

$$\begin{aligned} \tilde{F}'(s) &= e^{st_i} \tilde{F}(s) = \sum_\alpha F'_\alpha [s-s_\alpha]^{-1} + \text{other singularities} \\ F'_\alpha &\equiv e^{s_\alpha t_i} F_\alpha \\ F'(t) &= F(t+t_i) = \sum_\alpha F'_\alpha e^{s_\alpha t} u(t) + \text{other singularities} \end{aligned} \tag{2.2}$$

where for some applications we can assume the $F'(t)$ is zero for negative t. In the complex frequency domain, this has the form for modified poles as

$$\begin{aligned} \tilde{F}'(s) &= \sum_\alpha F'_\alpha \left[[s-s_\alpha]^{-1} + s_\alpha^{-1} \right] + \tilde{F}'(0) + \text{other singularities} \\ &= \sum_\alpha F'_\alpha \frac{s}{s_\alpha} [s-s_\alpha]^{-1} + \tilde{F}'(0) + \text{other singularities} \\ \tilde{F}(s) &= \sum_\alpha F_\alpha e^{-(s-s_\alpha)t_i} \frac{s}{s_\alpha} [s-s_\alpha]^{-1} + e^{-st_i} \tilde{F}(0) + \text{other singularities} \end{aligned} \tag{2.3}$$

In this form, the term corresponding to $s = 0$ clearly represents $\tilde{F}(s)$ well near $s = 0$, in effect making the series more rapidly convergent near there. Note that this term also includes any contribution for $s = 0$ from any other singularity terms, such as an entire function. Of course, this assumes that $\tilde{F}(s)$ exists at $s = 0$ and is continuous near there. Suppose then that we know that $\tilde{F}(0) = 0$ (e.g. in far-field scattering). Then the pole series has the convenient property that each term is zero at $s = 0$, and one does not have the numerical problem of summing comparatively large magnitude numbers to get a small number for s near zero.

In the time domain, this modified pole series introduces a set of delta functions at $t = t_i$, one for each pole term and one for $\tilde{F}(0)$. However, after $t = t_i$, the series gives the same result as for unmodified poles.

Now let us generalize the foregoing by subtracting successive powers of s from each term in the pole series. Note first that

$$\left[\frac{s}{s_\alpha}\right]^n [s - s_\alpha]^{-1} + \left[\frac{s}{s_\alpha}\right]^n s_\alpha^{-1} = \left[\frac{s}{s_\alpha}\right]^{n+1} [s - s_\alpha]^{-1} \tag{2.4}$$

so subtracting the term proportional to s^n just changes the exponent to $n+1$. Then applying this to $\tilde{F}'(s)$ including terms up to s^{p-1} gives

$$\begin{aligned} \tilde{F}'(s) &= \sum_\alpha F'_\alpha \left[\frac{s}{s_\alpha}\right]^p [s - s_\alpha]^{-1} + \sum_{n=0}^{p-1} \frac{1}{n!} \left.\frac{d^n \tilde{F}'(s)}{ds^n}\right|_{s=0} s^n + \text{other singularities} \\ p &\equiv \text{order of representation} \\ &= \text{integer} \geq 0 \end{aligned} \tag{2.5}$$

with the power series up to s^{p-1} taking care of the behavior near $s = 0$. Again sufficient analytic properties of $\tilde{F}'(s)$ near $s = 0$ are required. In terms of $\tilde{F}(s)$, we have

$$\begin{aligned} \tilde{F}(s) = &\sum_\alpha F_\alpha e^{-(s-s_\alpha)t_i} \left[\frac{s}{s_\alpha}\right]^p [s - s_\alpha]^{-1} + \sum_{n=0}^{p-1} \frac{1}{n!} \frac{d^n}{ds^n} \left[e^{st_i} \tilde{F}(s)\right]\Big|_{s=0} e^{-st_i} s^n \\ &+ \text{other singularities} \end{aligned} \tag{2.6}$$

Now if successive derivatives with respect to s up through $p-1$ are known to be zero, this gives an efficient representation for low frequencies. At high frequencies, however, if say $\tilde{F}'(s)$ is to be bounded for $s = j\omega$ (or more generally in the right half plane), then the pole terms behave as s^{p-1} and the series may not converge as well. This corresponds to the higher order distributions (doublets, etc.) introduced in the time domain.

3. Alternate Approach: Pole Expansion of $s^{-p}\tilde{F}(s)$

Now consider the SEM representation of $s^{-p}\,\tilde{F}(s)$. Using $s^{-p}\tilde{F}'(s)$, the pole series in (2.5) is directly produced with s^{-p} contributing to the residues as s_α^{-p}. Multiplying through by s^p gives the form in (2.5) and subsequently (2.6). So instead of thinking of successive corrections at $s = 0$, one can recast the problem as *the SEM expansion of s^{-p} times the original function.*

In this new approach, we have the problem of what happens near $s = 0$ since s^{-p} is a pth order pole there. Multiplying (2.5) and (2.6) by s^{-p} shows the form the expansion takes near $s = 0$ with terms from s^{-p} up to s^{-1}, and these formulas can be considered one way to find this expansion.

Next, restrict $\tilde{F}(s)$ to have only poles and an entire function. This leaves the parameter t_i which one can choose so as to minimize the entire function in some sense, or in some cases even remove it. Suppose that there is some time window between say $t = t'$ and $t = t''$ with

$$t_\mathrm{w} = t'' - t' > 0 \tag{3.1}$$

for which the Bromwich contour for the inverse transform of $\tilde{F}(s)$ can be closed in both half planes. Assuming no singularities in the RHP, then

$$F(t) = \begin{cases} 0 \text{ for } t < t'' \\ \displaystyle\sum_\alpha F_\alpha\, \mathrm{e}^{s_\alpha t}\, u(t - t_\mathrm{i}) \text{ with } t' < t_\mathrm{i} < t'' \end{cases} \tag{3.2}$$

with both representations applicable for t in the the time window. The initial time t_i is the time in the time window one chooses to close in the LHP. As discussed in [11], this is associated with the high frequency behavior as

$$\begin{aligned} \tilde{F}(s) &= \begin{cases} O_\mathrm{e}(-st') \text{ in RHP } (\mathrm{Re}[s] \to +\infty) \\ O_\mathrm{e}(st'') \text{ in LHP } (\mathrm{Re}[s] \to -\infty) \end{cases} \\ \mathrm{RHP} &\equiv \text{right half plane} \\ \mathrm{LHP} &\equiv \text{left half plane} \end{aligned} \tag{3.3}$$

where the O_e(exponential order) symbol bounds the function by the exponential of the argument times some function which grows slower than any exponential. Note that for this restricted class of functions, there is no additional entire function required in (3.2) or in the corresponding frequency form

$$\tilde{F}(s) = \sum_\alpha F_\alpha \mathrm{e}^{-(s - s_\alpha)t_\mathrm{i}}\, [s - s_\alpha]^{-1} \tag{3.4}$$

Note that the term "entire function" (as the term "pole") applies strictly in the s-domain, but is applied by extension to its corresponding time-domain form.

Applying these results to $s^{-p}\tilde{F}(s)$, note that for high frequencies we still have

$$s^{-p}\tilde{F}(s) = \begin{cases} O_e(-st') \text{ in RHP} \\ O_e(st'') \text{ in LHP} \end{cases} \tag{3.5}$$

the power $-p$ not contributing to the exponential order. Then we can apply the result for the case of the closure-time window t_w (still positive) and obtain the result in (2.6) (or (2.5)) with no "other singularities," noting, of course, the presence of the s^{-p} term at zero with which to be dealt. Multiplying across by s^p we have

$$\begin{aligned} \tilde{F}(s) &= \sum_\alpha F_\alpha \, e^{-(s-s_\alpha)t_i} \left[\frac{s}{s_\alpha}\right]^p [s-s_\alpha]^{-1} + \sum_{n=0}^{p-1} \frac{1}{n!} \frac{d^n}{ds^n} \left[e^{st_i}\,\tilde{F}(s)\right]\Big|_{s=0} e^{-st_i} s^n \\ &\quad \text{with } t' < t_i < t'' \end{aligned} \tag{3.6}$$

As previously noted, this can also be expressed in the time domain by including distributions at $t = t_i$. For $t > t_i$, the usual series of complex exponentials is obtained.

This form is valid for general integer $p \geq 0$ and can be extended to negative integer p if desired. One motivation for constructing such a form is to improve the convergence rate for low frequencies, particularly if $\tilde{F}(s)$ and some number of successive derivatives with respect to s are zero there. Suppose we know that

$$\tilde{F}(s) = O(s^p) \quad \text{as} \quad s \to 0 \tag{3.7}$$

Then we can use

$$\tilde{F}(s) = \sum_\alpha F_\alpha \, e^{-(s-s_\alpha)t_i} \left[\frac{s}{s_\alpha}\right]^p [s-s_\alpha]^{-1} \quad \text{with } t' < t_i < t'' \tag{3.8}$$

Alternately, we can explicitly call out the first non-zero term as

$$\begin{aligned} \tilde{F}(s) &= O(s^{p'}) \quad \text{as} \quad s \to 0 \\ \tilde{F}(s) &= \sum_\alpha F_\alpha \, e^{-(s-s_\alpha)t_i} \left[\frac{s}{s_\alpha}\right]^{p'+1} [s-s_\alpha]^{-1} + \frac{d^{p'}}{ds^{p'}} \tilde{F}(s)\Big|_{s=0} e^{-st_i} s^{p'} \\ p' &= \text{integer} \geq 0 \end{aligned} \tag{3.9}$$

4. Surface Current Density on Perfectly Conducting Scatterers

Consider a perfectly conducting scatterer as in fig. 4.1. Summarizing from [11], we have the impedance integral equation

$$\begin{aligned}
\overleftrightarrow{E}_{\mathrm{t}}^{(\mathrm{inc})}(\vec{r}_{\mathrm{s}}, s) &= \left\langle \overleftrightarrow{Z}_{\mathrm{t}}(\vec{r}_{\mathrm{s}}, \vec{r}_{\mathrm{s}}'; s)\,;\ \overleftrightarrow{J}_{\mathrm{s}}(\vec{r}_{\mathrm{s}}', s) \right\rangle \\
&= \overleftrightarrow{1}_{\mathrm{S}} \cdot \overleftrightarrow{E}^{(\mathrm{inc})}(\vec{r}_{\mathrm{s}}, s) \\
\overleftrightarrow{1}_{\mathrm{S}}(\vec{r}_{\mathrm{s}}) &= \overleftrightarrow{1} - \vec{1}_{\mathrm{S}}(\vec{r}_{\mathrm{s}})\,\vec{1}_{\mathrm{S}}(\vec{r}_{\mathrm{s}}) \quad \text{(transverse dyad to S at } \vec{r}_{\mathrm{s}}) \\
\overleftrightarrow{J}_{\mathrm{s}}(\vec{r}_{\mathrm{s}}, s) &= \left\langle \overleftrightarrow{Z}_{\mathrm{t}}^{-1}(\vec{r}_{\mathrm{s}}, \vec{r}_{\mathrm{s}}'; s)\,;\ \overleftrightarrow{E}(\vec{r}_{\mathrm{s}}', s) \right\rangle \\
\vec{r}_{\mathrm{s}},\ \vec{r}_{\mathrm{s}}' &\in \mathrm{S} \ \text{(restricted choices of } \vec{\mathrm{r}})
\end{aligned} \tag{4.1}$$

The inverse kernel can be written in SEM form as

$$\begin{aligned}
\overleftrightarrow{Z}_{\mathrm{t}}^{-1}(\vec{r}_{\mathrm{s}}, \vec{r}_{\mathrm{s}}'; s) &= \sum_{\alpha} \frac{\mathrm{e}^{-(s-s_\alpha)t_{\mathrm{i}}}}{s - s_\alpha}\, U_\alpha\, \vec{j}_{s_\alpha}(\vec{r}_{\mathrm{s}})\, \vec{j}_{s_\alpha}(\vec{r}_{\mathrm{s}}') \\
U_\alpha &= \left\langle \vec{j}_{s_\alpha}(\vec{r}_{\mathrm{s}})\,;\ \frac{\partial}{\partial s}\, \overleftrightarrow{Z}_{\mathrm{t}}(\vec{r}_{\mathrm{s}}, \vec{r}_{\mathrm{s}}'; s)\Big|_{s = s_\alpha}\ ;\ \vec{j}_{s_\alpha}(\vec{r}_{\mathrm{s}}') \right\rangle^{-1} \\
\left\langle \overleftrightarrow{Z}_{\mathrm{t}}(\vec{r}_{\mathrm{s}}, \vec{r}_{\mathrm{s}}'; s_\alpha)\,;\ \vec{j}_{s_\alpha}(\vec{r}_{\mathrm{s}}') \right\rangle &= \vec{0} = \left\langle \vec{j}_{s_\alpha}(\vec{r}_{\mathrm{s}})\,;\ \overleftrightarrow{Z}_{\mathrm{t}}(\vec{r}_{\mathrm{s}}, \vec{r}_{\mathrm{s}}'; s_\alpha) \right\rangle
\end{aligned} \tag{4.2}$$

with t_{i} taken as zero if desired, but in general

$$0 \geq t_{\mathrm{i}} \geq -t_0 = \frac{-L_0}{c}, \quad c = \sqrt{\frac{\mu_0}{\epsilon_0}} \equiv \text{speed of light} \tag{4.3}$$

and with due care to summing over the poles by eigenterms where

$$\begin{aligned}
\alpha &\equiv (\beta, \beta') \equiv \text{natural mode index} \\
\beta &\equiv \text{eigenmode index} \\
\beta' &\equiv \text{index for zeros of } \beta\text{th eigenvalue}
\end{aligned} \tag{4.4}$$

As illustrated in fig. 4.1, we have characteristic dimensions and times for the scatterer

$$\begin{aligned}
t_{\mathrm{f}} &\equiv \frac{L_{\mathrm{f}}}{c} \equiv \text{front time (negative)} \\
t_{\mathrm{b}} &\equiv \frac{L_{\mathrm{b}}}{c} \equiv \text{back time (positive)} \\
L_0 &\equiv ct_0 \equiv \text{maximum liner dimension}
\end{aligned} \tag{4.5}$$

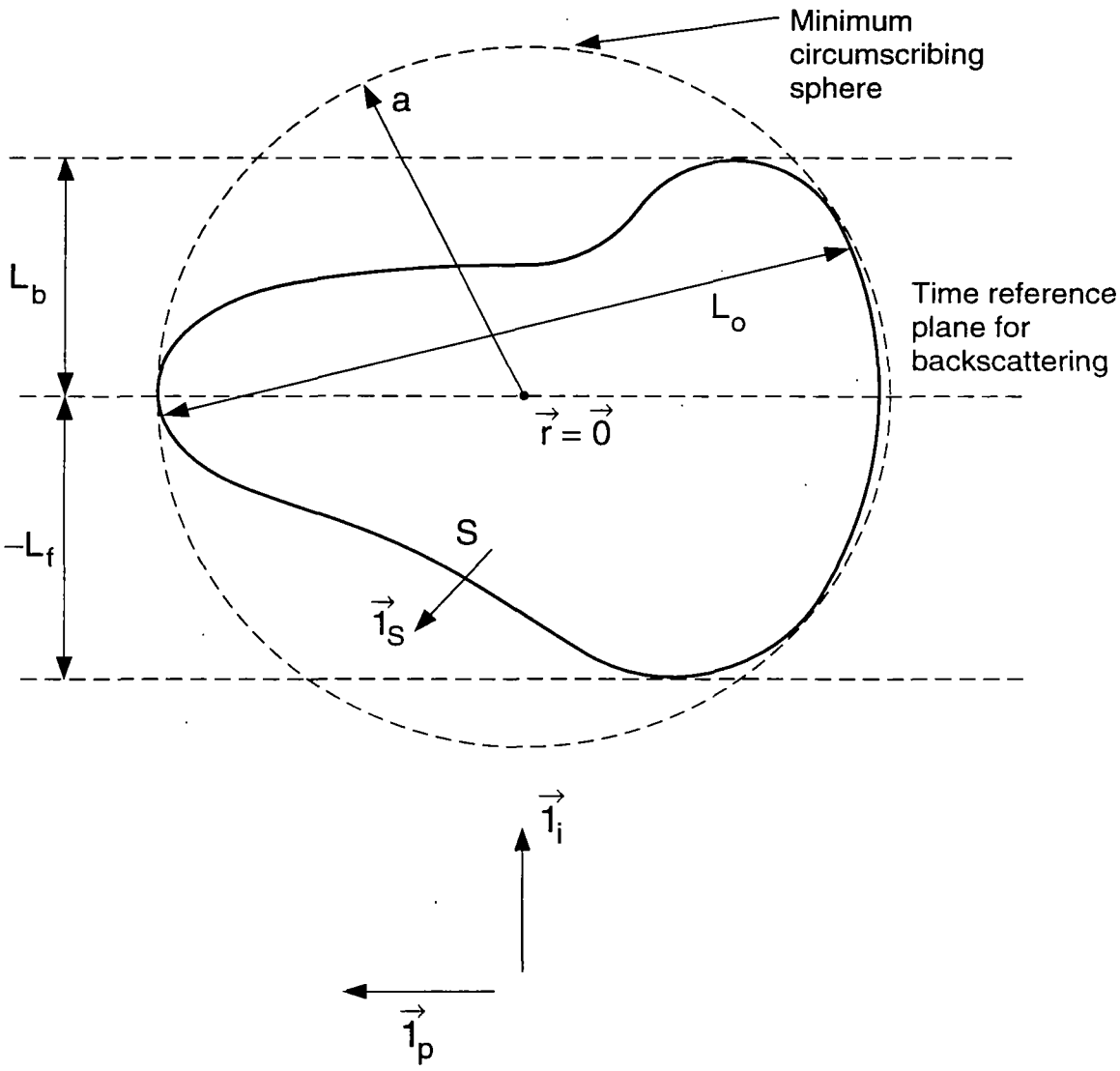

Figure 4.1. Finite-size scatterer in free space illuminated by a plane wave.

The surface current density can be written in class-1 form as [11]

$$\begin{aligned}
\overset{\simeq}{\vec{J}}_{\rm s}(\vec{r}_{\rm s},s) &= E_0\tilde{f}(s)\sum_\alpha \frac{{\rm e}^{-(s-s_\alpha)t_{\rm i}}}{s-s_\alpha}\eta_\alpha(\vec{1}_{\rm i},\vec{1}_{\rm p})\vec{j}_{s_\alpha}(\vec{r}_{\rm s}) \\
\eta_\alpha(\vec{1}_{\rm i},\vec{1}_{\rm p}) &= U_\alpha\vec{1}_{\rm p}\cdot\left\langle {\rm e}^{-\gamma_\alpha\vec{1}_{\rm i}\cdot\vec{r}\,'_{\rm s}}\,,\ \vec{j}_{s_\alpha}(\vec{r}\,'_{\rm s})\right\rangle \\
&\equiv \text{coupling coefficient} \\
\overset{\simeq}{\vec{E}}^{\rm (inc)}(\vec{r},s) &= E_0\,\tilde{f}(s)\vec{1}_{\rm p}\,{\rm e}^{-\gamma\vec{1}_{\rm i}\cdot\vec{r}} \\
&\equiv \text{incident plane wave} \qquad (4.6)\\
\vec{1}_{\rm i} &\equiv \text{direction of incidence} \\
\overset{\leftrightarrow}{1}_{\rm i} &\equiv \overset{\leftrightarrow}{1}-\vec{1}_{\rm i}\vec{1}_{\rm i},\quad \overset{\leftrightarrow}{1}=\vec{1}_{\rm x}\vec{1}_{\rm x}+\vec{1}_{\rm y}\vec{1}_{\rm y}+\vec{1}_{\rm z}\vec{1}_{\rm z}\equiv\text{identity} \\
\vec{1}_{\rm p} &\equiv \text{polarization } (\perp\vec{1}_{\rm i}) \\
\gamma &\equiv \frac{s}{c}\equiv\text{propagation constant}
\end{aligned}$$

where now $t_{\rm i}$ is constrained by

$$t_{\rm i}-t_{\rm f}>-t_{\rm f}+t_{\rm b}-t_0\equiv -t_{\rm s}\le 0 \qquad (4.7)$$

and should be no larger than when currents first begin at the observer at $\vec{r}_{\rm s}$. Often a convenient choice for the is time is when the wave first reaches the objective

$$t_{\rm i}=t_{\rm f} \qquad (4.8)$$

At zero frequency, the surface current density can be found in principle from the integral equation (4.1). However, this is not the most efficient approach due to the singularity of the kernel. By various techniques (including the H-field integral equation), one can establish the surface current density as [4]

$$\overset{\simeq}{\vec{J}}_{\rm s}(\vec{r}_{\rm s},0)=\overset{\leftrightarrow}{\vec{j}}{}^{(0)}_{\rm S}(\vec{r}_{\rm s})\cdot\overset{\simeq}{\vec{H}}^{\rm (inc)}(\vec{0},0) \qquad (4.9)$$

where for plane-wave incidence

$$\overset{\simeq}{\vec{H}}^{\rm (inc)}(\vec{r},s)=\frac{1}{Z_0}\vec{1}_{\rm i}\times\overset{\simeq}{\vec{E}}^{\rm (inc)}(\vec{r},s)=\frac{E_0}{Z_0}\tilde{f}(s)\vec{1}_{\rm i}\times\vec{1}_{\rm p}\,{\rm e}^{-\gamma\vec{1}_{\rm i}\cdot\vec{r}} \qquad (4.10)$$

The dyadic magnetostatic mode is

$$\overset{\leftrightarrow}{\vec{j}}{}^{(0)}_{\rm s}(\vec{r}_{\rm s})=\vec{j}^{(0)}_{\rm s_x}(\vec{r}_{\rm s})\vec{1}_{\rm x}+\vec{j}^{(0)}_{\rm s_y}(\vec{r}_{\rm s})\vec{1}_{\rm y}+\vec{j}^{(0)}_{\rm s_z}(\vec{r}_{\rm s})\vec{1}_{\rm z} \qquad (4.11)$$

where the three vector surface-current-density modes correspond to the response to a unit incident magnetic

field in each of the three orthogonal coordinate directions. Of course, one can normalize these any way one wishes. Note, however, that this response is not proportional to the incident electric field at $\vec{r}=\vec{0}$, but rather to its curl, the incident magnetic field. Note that these modes have the property

$$\begin{aligned} \nabla_S \cdot \vec{j}^{(0)}_{s_\ell}(\vec{r}_s) &= 0 \text{ for } \ell = x,y,z \\ \nabla_S \cdot \overleftrightarrow{j}^{(0)}_S(\vec{r}_s) &= \vec{0} \end{aligned} \tag{4.12}$$

For later convenience, we have the magnetic moment associated with each mode as

$$\vec{m}^{(0)}_\ell = \frac{1}{2}\left\langle \vec{r}_s \times \vec{j}^{(0)}_{s_\ell}(\vec{r}_s) \right\rangle \tag{4.13}$$

and we assume that the coordinates are oriented (rotated) such that

$$\begin{aligned} &\vec{1}_\ell \parallel \vec{m}^{(0)}_\ell \quad , \quad \vec{m}^{(0)}_\ell = m^{(0)}_\ell \vec{1}_\ell \ , \ m^{(0)}_\ell \le 0 \qquad \text{for } \ell = x,y,z \\ &\vec{1}_\ell \cdot \vec{m}^{(0)}_{\ell'} = 0 \qquad \text{for } \ell \neq \ell' \end{aligned} \tag{4.14}$$

Effectively, this means that the magnetic polarizability dyadic (symmetric and real) has been diagonalized with real eigenvalues and real eigenvectors (our unit vectors) [30] as

$$\begin{aligned} \overleftrightarrow{M} &= (M_{n,m}) \\ M_{n,m} &= 0 \qquad \text{for } m \neq n \\ \tilde{\vec{m}}(s) &= \overleftrightarrow{M} \cdot \tilde{\vec{H}}^{(inc)}(\vec{0}, s) \qquad \text{as } s \to 0 \end{aligned} \tag{4.15}$$

There is a non-zero divergence term corresponding to $s = 0$, but via the equation of continuity

$$\nabla_S \cdot \tilde{\vec{J}}_s(\vec{r}_s, s) = -s\,\tilde{\rho}_S(\vec{r}_s, s) \tag{4.16}$$

this is a higher-order term. The surface charge density can be similarly written for zero frequency in terms of the incident electric field

$$\tilde{\rho}_S(\vec{r}_s, 0) = \epsilon_0 \ \tilde{\vec{E}}^{(inc)}(\vec{0}, s) \cdot \vec{\rho}^{(1)}_S(\vec{r}) \tag{4.17}$$

The vector electrostatic mode is

$$\vec{\rho}^{(1)}_S(\vec{r}_s) = \vec{\rho}^{(1)}_{s_{x'}}(\vec{r}_s)\vec{1}_{x'} + \vec{\rho}^{(1)}_{s_{y'}}(\vec{r}_s)\vec{1}_{y'} + \vec{\rho}^{(1)}_{s_{z'}}(\vec{r}_s)\vec{1}_{z'} \tag{4.18}$$

where the three scalar surface-charge-density modes correspond to the response to a unit incident electric

displacement ($\vec{D}$, so as to make the modes dimensionless). Note that x', y', z' indicate coordinate directions which may or may not correspond with x, y, z as convenient.

For later use, we have the electric-dipole moment associated with each mode as

$$\begin{aligned} \vec{p}_\ell^{(1)} &= \left\langle \vec{r}_{\rm s}' \, , \, \rho_{{\rm S}_\ell}^{(1)}(\vec{r}_{\rm s}') \right\rangle \\ &= \frac{1}{s}\int_{\rm S} \vec{j}_{{\rm s}_\ell}^{(1)}(\vec{r}_{\rm s}', s)\, d{\rm S}' \qquad \text{for } \ell = {\rm x}',{\rm y}',{\rm z}' \end{aligned} \tag{4.19}$$

with the usual integration by parts with the current confined to a domain of finite linear dimensions [1,26]. Noting that

$$\nabla_{\rm S} \cdot \vec{j}_{{\rm s}_\ell}^{(1)}(\vec{r}_{\rm s}, s) = -s\,\rho_{{\rm S}_\ell}^{(1)}(\vec{r}_{\rm s}) \tag{4.20}$$

These surface-current-density modes are electrostatic and go to zero as $s \to 0$, so interpret this in a limiting sense. These are not the same as the previous (magnetostatic) modes which have zero divergence. Again, we assume that the coordinates (say x', y', z') are chosen (rotated) such that

$$\begin{aligned} &\vec{1}_\ell \parallel \vec{p}_\ell^{(1)} \quad , \quad \vec{p}_\ell^{(1)} = p_\ell^{(1)}\,\vec{1}_\ell \, , \; p_\ell^{(1)} \geq 0 \qquad \text{for } \ell = {\rm x}',{\rm y}',{\rm z}' \\ &\vec{1}_\ell \cdot \vec{p}_{\ell'}^{(1)} = 0 \qquad \text{for } \ell \neq \ell' \end{aligned} \tag{4.21}$$

This corresponds to the diagonalization of the electric polarizability tensor with real eigenvalues and real eigenvectors [30] as

$$\begin{aligned} \overleftrightarrow{P} &= (P_{\rm n,m}) \\ P_{\rm n,m} &= 0 \qquad \text{for } m \neq n \\ \tilde{\vec{p}}(s) &= \epsilon_0\, \overleftrightarrow{P} \cdot \tilde{\vec{E}}^{(\rm inc)}(\vec{0}, s) \qquad \text{as } s \to 0 \end{aligned} \tag{4.22}$$

Applying the results of sections 2 and 3 to the class-1 form of the surface current density gives a $p = 1$ representation for plane-wave incidence as

$$\begin{aligned} \tilde{\vec{J}}_{\rm s}(\vec{r}_{\rm s}, s) &= E_0 \tilde{f}(s) \sum_\alpha {\rm e}^{-(s-s_\alpha)t_{\rm i}} \frac{s}{s_\alpha} [s - s_\alpha]^{-1}\, \eta_\alpha(\vec{1}_{\rm i}, \vec{1}_{\rm p})\, \vec{j}_{s_\alpha}(\vec{r}_{\rm s}) \\ &\quad + \frac{E_0}{Z_0} \tilde{f}(s)\, {\rm e}^{-st_{\rm i}}\, \overleftrightarrow{j}_{\rm S}^{(0)}(\vec{r}_{\rm s}) \cdot \left[\vec{1}_{\rm i} \times \vec{1}_{\rm p}\right] \\ Z_0 &\equiv \left[\frac{\mu_0}{\epsilon_0}\right]^{1/2} \equiv \text{ wave impedance of free space} \end{aligned} \tag{4.23}$$

One can also form a similar representation for the surface charge density using (4.4) and the surface-charge-density natural modes via the equation of continuity.

In class-2 form, we have [11]

$$\begin{aligned}\overleftrightarrow{J}_{\rm s}(\vec{r}_{\rm s},s) &= E_0\tilde{f}(s)\sum_\alpha U_\alpha\,[s-s_\alpha]^{-1}\;\vec{1}_{\rm p}\cdot\;\overleftrightarrow{C}_\alpha(\vec{1}_{\rm i},s)\;\vec{j}_{{\rm s}_\alpha}(\vec{r}_{\rm s})\\ \overleftrightarrow{C}_\alpha(\vec{1}_{\rm i},s) &\equiv \left\langle \overleftrightarrow{1}_{\rm i}\,{\rm e}^{-\gamma\vec{1}_{\rm i}\cdot\vec{r}'_{\rm s}}\;;\;\vec{j}_{{\rm s}_\alpha}(\vec{r}'_{\rm s})\right\rangle\end{aligned} \tag{4.24}$$

where the coupling coefficients now take the well-known frequency dependent form. In order to form a $p=1$ representation, we can go back to find a class-1 form of the inverse kernel as

$$\overleftrightarrow{Z}_{\rm t}^{-1}(\vec{r}_{\rm s},\vec{r}'_{\rm s};s)=\sum_\alpha {\rm e}^{-(s-s_\alpha)t_{\rm i}}\,\frac{s}{s_\alpha}\,[s-s_\alpha]^{-1}\,U_\alpha\;\vec{j}_{{\rm s}_\alpha}(\vec{r}_{\rm s})\,\vec{j}_{{\rm s}_\alpha}(\vec{r}'_{\rm s})\;+\;{\rm e}^{-st_{\rm i}}\;\overleftrightarrow{Z}_{\rm t}^{-1}(\vec{r}_{\rm s},\vec{r}'_{\rm s};0) \tag{4.25}$$

where the term for $s=0$ is interpreted in a formal sense as that thing which when operating on the incident electric field gives the current density for $s=0$. In particular, it can be taken in a limiting sense along with the electric field as $s\to 0$.

For an incident plane wave,

$$\overleftrightarrow{E}^{(\rm inc)}(\vec{r}_{\rm s},s)\;=\;E_0\tilde{f}(s)\,\vec{1}_{\rm p}\left[1-\gamma\vec{1}_{\rm i}\cdot\vec{r}_{\rm s}+O(s^2)\right]\qquad\text{as } s\to 0 \tag{4.26}$$

since $\vec{r}_{\rm s}$ is bounded. If one were to integrate the first term (a constant) over a magnetostatic mode, the result would be zero due to the fact that these have zero divergence and give no electric-dipole contribution [1,26]. So if we attempt to expand the inverse kernel in terms of the magnetostatic modes, we need the next term proportional to s. This is consistent with the kernel being $O(s^{-1})$ as $s\to 0$ [11]. So expand the inverse kernel in the symmetrical form

$$\overleftrightarrow{Z}_{\rm t}^{-1}(\vec{r}_{\rm s},\vec{r}'_{\rm s};s)=\sum_{\ell=x,y,z} Y_\ell\;\vec{j}^{\,(0)}_{{\rm s}_\ell}(\vec{r}_{\rm s})\;\vec{j}^{\,(0)}_{{\rm s}_\ell}(\vec{r}'_{\rm s})\qquad\text{as } s\to 0 \tag{4.27}$$

with the notion of taking a limit as $s\to 0$ when operating on the incident field.

Consider the ℓth term in (4.27). Integrating over the second term in (4.26) gives an integral of the form [26,29]

$$\begin{aligned}\left\langle\vec{1}_{\rm i}\cdot\vec{r}'_{\rm s}\,,\;\vec{j}^{\,(0)}_{{\rm s}_\ell}(\vec{r}'_{\rm s})\right\rangle &= \vec{1}_{\rm i}\cdot\left\langle\vec{r}'_{\rm s}\,,\;\vec{j}^{\,(0)}_{{\rm s}_\ell}(\vec{r}'_{\rm s})\right\rangle\\ &= -\frac{1}{2}\vec{1}_{\rm i}\times\left\langle\vec{r}'_{\rm s}\times\vec{j}^{\,(0)}_{{\rm s}_\ell}(\vec{r}'_{\rm s})\right\rangle\\ &= -\vec{1}_{\rm i}\times\vec{\rm m}^{(0)}_\ell\end{aligned} \tag{4.28}$$

This last term is a normalized magnetic dipole moment as in (4.13). Then equating the low frequency forms

in (4.9) and (4.27) with (4.26) gives

$$\begin{aligned}\overleftrightarrow{J}_{\rm s}(\vec{r}_{\rm s},0) &= \overleftrightarrow{j}^{(0)}_{\rm S}(\vec{r}_{\rm s})\cdot\overleftrightarrow{H}^{(\rm inc)}(\vec{0},0) = \frac{1}{Z_0}\overleftrightarrow{j}^{(0)}_{\rm S}(\vec{r}_{\rm s})\cdot\left[\vec{1}_{\rm i}\times\overleftrightarrow{E}^{(\rm inc)}(\vec{0},0)\right] \\ &= E_0\,\tilde{f}(s)\,\gamma\sum_{\ell={\rm x,y,z}} Y_\ell\,\vec{j}^{(0)}_{{\rm s}_\ell}(\vec{r}_{\rm s})\,\vec{1}_{\rm p}\cdot\left[\vec{1}_{\rm i}\times\vec{\rm m}^{(0)}_\ell\right] \end{aligned} \tag{4.29}$$

The coefficient of the ℓth magnetostatic mode gives

$$\begin{aligned}\frac{1}{Z_0}\left[\vec{1}_{\rm i}\times\vec{1}_{\rm p}\right]\cdot\vec{1}_\ell &= \gamma Y_\ell\,\vec{1}_{\rm p}\cdot\left[\vec{1}_{\rm i}\times\vec{\rm m}^{(0)}_\ell\right] \\ &= -\gamma Y_\ell\,\vec{\rm m}^{(0)}_\ell\cdot\left[\vec{1}_{\rm i}\times\vec{1}_{\rm p}\right] \end{aligned} \tag{4.30}$$

or, varying $\vec{1}_{\rm i}$ and $\vec{1}_{\rm p}$,

$$\begin{aligned} Y_\ell\,\vec{\rm m}^{(0)}_\ell &= -\frac{1}{\gamma Z_0}\,\vec{1}_\ell \\ Y_\ell &= -\left[\gamma\, m^{(0)}_\ell Z_0\right]^{-1} \end{aligned} \tag{4.31}$$

due to the assumed diagonal form. So now we have

$$\overleftrightarrow{Z}^{-1}_{\rm t}(\vec{r}_{\rm s},\vec{r}\,'_{\rm s};s) = -\sum_{\ell={\rm x,y,z}}\left[\gamma\, m^{(0)}_\ell Z_0\right]^{-1}\vec{j}^{(0)}_{{\rm s}_\ell}(\vec{r}_{\rm s})\,\vec{j}^{(0)}_{{\rm s}_\ell}(\vec{r}\,'_{\rm s}) \qquad \text{as } s\to 0 \tag{4.32}$$

to include in (4.25). Interpreting this as a limit of $s\to 0$ gives the $p=1$, class-1 form in (4.23). Viewed another way, look at (4.25) as a pole expansion for $s^{-1}\overleftrightarrow{Z}_{\rm t}$ picking up what is effectively a first order pole at $s=0$. Combining terms, we have

$$\begin{aligned}\overleftrightarrow{Z}^{-1}_{\rm t}(\vec{r}_{\rm s},\vec{r}\,'_{\rm s};s) &= \sum_\alpha {\rm e}^{-(s-s_\alpha)t_{\rm i}}\,\frac{s}{s_\alpha}\,[s-s_\alpha]^{-1}\,U_\alpha\,\vec{j}_{{\rm s}_\alpha}(\vec{r}_{\rm s})\,\vec{j}_{{\rm s}_\alpha}(\vec{r}\,'_{\rm s}) \\ &\quad -{\rm e}^{-st_{\rm i}}\sum_{\ell={\rm x,y,z}}\left[\gamma\, m^{(0)}_\ell Z_0\right]^{-1}\vec{j}^{(0)}_{{\rm s}_\ell}(\vec{r}_{\rm s})\,\vec{j}^{(0)}_{{\rm s}_\ell}(\vec{r}\,'_{\rm s}) \end{aligned} \tag{4.33}$$

as the $p=1$, class-1 form of the inverse kernel.

Now we have the $p=1$, class-2 form of the surface current density by setting $t_{\rm i}=0$ and operating on the incident electric field to obtain

$$\begin{aligned}\overleftrightarrow{J}_{\rm s}(\vec{r}_{\rm s},s) &= E_0\tilde{f}(s)\left\{\sum_\alpha\frac{s}{s_\alpha}[s-s_\alpha]^{-1}\,\vec{1}_{\rm p}\cdot\,\overleftrightarrow{C}_\alpha(\vec{1}_{\rm i},s)\,\vec{j}_{{\rm s}_\alpha}(\vec{r}_{\rm s})\right. \\ &\quad \left. -\sum_{\ell={\rm x,y,z}}\left[\gamma\, m^{(0)}_\ell Z_0\right]^{-1}\vec{1}_{\rm p}\cdot\,\overleftrightarrow{C}^{(0)}_\ell(\vec{1}_{\rm i},s)\,\vec{j}^{(0)}_{{\rm s}_\ell}(\vec{r}_{\rm s})\right\} \end{aligned} \tag{4.34}$$

$$\overset{\approx}{\vec{C}}{}^{(0)}_{\ell}(\vec{1}_i, s) = \frac{1}{\gamma}\left\langle \overset{\leftrightarrow}{1}_i e^{-\gamma \vec{1}_i \cdot \vec{r}'_s}\ ,\ \vec{j}^{(0)}_{s_\ell}(\vec{r}'_s)\right\rangle$$

$$= \frac{1}{\gamma}\left\langle \overset{\leftrightarrow}{1}_i e^{-\gamma \vec{1}_i \cdot \vec{r}'_s} - 1\ ,\ \vec{j}^{(0)}_{s_\ell}(\vec{r}'_s)\right\rangle$$

The last form uses the fact that the integral over the magnetostatic modes is zero (no contribution to the electric dipole moment).

The forms of the kernel developed in this section have been for the purpose of representing the surface current density on the scatterer. The dominant term as $s \to 0$ are those associated with the induced magnetic-dipole moment (and higher order magnetic moments) of the scatterer. The present form is suitable for a perfectly conducting scatterer for which the $\vec{j}^{(0)}_{s_\ell}(\vec{r}'_s)$ are non-zero. The surface charge density (involving a divergence) contributes to the induced electric dipole moment and is discussed in the next section in the context of the far scattered fields.

5. Far Scattering

As discussed in [11], the far scattered field takes the from

$$\begin{aligned} \overset{\simeq}{E}_{\rm f}(\vec{r},s) &= \frac{e^{-\gamma r}}{4\pi r}\ \overset{\leftrightarrow}{\Lambda}(\vec{1}_{\rm o},\vec{1}_{\rm i};s)\cdot\ \overset{\simeq}{E}^{(\rm inc)}(\vec{0},s) \\ &= E_0\tilde{f}(s)\,\frac{e^{-\gamma r}}{4\pi r}\ \overset{\leftrightarrow}{\Lambda}(\vec{1}_{\rm o},\vec{1}_{\rm i};s)\cdot\vec{1}_{\rm p} \end{aligned} \tag{5.1}$$

where $\vec{1}_{\rm o}$ is the direction to the observer (at $\vec{r}$). The scattering dyadic (2×2 in terms of the transverse components of incident and far-scattered fields) is

$$\overset{\leftrightarrow}{\Lambda}(\vec{1}_{\rm o},\vec{1}_{\rm i};s) = -s\mu_0\left\langle \overset{\leftrightarrow}{1}_{\rm o}\,e^{\gamma\vec{1}_{\rm o}\cdot\vec{r}_{\rm s}}\ ;\ \overset{\simeq}{Z}_{\rm t}^{-1}(\vec{r}_{\rm s},\vec{r}\,'_{\rm s};s)\ ;\ \overset{\leftrightarrow}{1}_{\rm i}\,e^{-\gamma\vec{1}_{\rm i}\cdot\vec{r}\,'_{\rm s}}\right\rangle \tag{5.2}$$

$$\overset{\leftrightarrow}{1}_{\rm i} = \overset{\leftrightarrow}{1} - \vec{1}_{\rm i}\vec{1}_{\rm i} \equiv \text{incidence transverse dyadic}$$

$$\overset{\leftrightarrow}{1}_{\rm o} = \overset{\leftrightarrow}{1} - \vec{1}_{\rm o}\vec{1}_{\rm o};\equiv \text{scattering transverse dyadic}$$

For monostatic or backscattering, this reduces to the symmetric dyadic

$$\begin{aligned} \overset{\simeq}{\Lambda}_{\rm b}(\vec{1}_{\rm i},s) &\equiv \overset{\simeq}{\Lambda}(-\vec{1}_{\rm i},\vec{1}_{\rm i},;s) \\ &= -s\mu_0\left\langle \overset{\leftrightarrow}{1}_{\rm i}\,e^{-\gamma\vec{1}_{\rm i}\cdot\vec{r}_{\rm s}}\ ;\ \overset{\simeq}{Z}_{\rm t}^{-1}(\vec{r}_{\rm s},\vec{r}\,'_{\rm s};s)\ ;\ \overset{\leftrightarrow}{1}_{\rm i}\,e^{-\gamma\vec{1}_{\rm i}\cdot\vec{r}\,'_{\rm s}}\right\rangle \end{aligned} \tag{5.3}$$

At low frequencies, the scattering is dominated by the induced electric and magnetic dipole moments which give far fields [1] as

$$\overset{\simeq}{E}_{\rm f}(\vec{r},s) = \frac{e^{-\gamma r}}{4\pi r}\mu_0 s^2\ \overset{\leftrightarrow}{1}_{\rm o}\cdot\left[-\overset{\simeq}{p}(s) + \frac{1}{c}\vec{1}_{\rm o}\times\overset{\simeq}{m}(s)\right] \qquad \text{as } s\to 0 \tag{5.4}$$

These induced dipole moments are described in terms of polarizability dyadics as in (4.15) and (4.22). Thus, for low frequencies, the scattering dyadic is

$$\overset{\leftrightarrow}{\Lambda}(\vec{1}_{\rm o},\vec{1}_{\rm i};s) = \gamma^2\left[-\overset{\leftrightarrow}{1}_{\rm o}\cdot\overset{\leftrightarrow}{P}\cdot\overset{\leftrightarrow}{1}_{\rm i} + \vec{1}_{\rm o}\times\overset{\leftrightarrow}{M}\times\vec{1}_{\rm i}\right] \qquad \text{as } s\to 0 \tag{5.5}$$

For backscattering, this reduces to

$$\overset{\leftrightarrow}{\Lambda}_{\rm b}(\vec{1}_{\rm i};s) = -\gamma^2\left[\overset{\leftrightarrow}{1}_{\rm i}\cdot\overset{\leftrightarrow}{P}\cdot\overset{\leftrightarrow}{1}_{\rm i} + \vec{1}_{\rm i}\times\overset{\leftrightarrow}{M}\times\vec{1}_{\rm i}\right] \qquad \text{as } s\to 0 \tag{5.6}$$

The class-1 form of the backscattering dyadic [11] is

$$\begin{aligned}
\overleftrightarrow{\Lambda}_b(\vec{1}_i\,;s) &= \sum_\alpha \frac{e^{-(s-s_\alpha)t_i}}{s-s_\alpha}\,\vec{c}_\alpha(\vec{1}_i)\,\vec{c}_\alpha(\vec{1}_i) + \text{possible entire function} \\
\vec{c}_\alpha(\vec{1}_i) &= w_\alpha\,\vec{C}_\alpha(\vec{1}_i) \\
\vec{C}_\alpha(\vec{1}_i) &= \left\langle \overleftrightarrow{1}_i\, e^{-\gamma_\alpha \vec{1}_i\cdot\vec{r}'_s}\,;\ \vec{j}_{s_\alpha}(\vec{r}'_s)\right\rangle \\
W_\alpha &= w_\alpha^2 = -s_\alpha\,\mu_0\,U_\alpha \\
&= -s_\alpha\mu_0\left\langle \vec{j}_{s_\alpha}(\vec{r}_s);\ \frac{\partial}{\partial s}\,\overleftrightarrow{Z}_t(\vec{r}_s,\vec{r}'_s;s)\Big|_{s=s_\alpha}\ ;\ \vec{j}_{s_\alpha}(\vec{r}'_s)\right\rangle^{-1}
\end{aligned} \tag{5.7}$$

There is a requirement on t_i for series convergence as

$$t_i - 2t_f > 2[-t_f + t_b] - t_0 = -t_{bs} \tag{5.8}$$

where the various times are in (4.5) and fig. 4.1. If the backscatter time window t_{bs} is positive, then t_i can be chosen as earlier (less) than $2t_f$, the time of the first backscatter signal. Under this condition, the Bromwich contour can be closed in both half planes around $t = t_i$ with the result that there is no entire function. This occurs for "flat" or "thin" scatterers with near-broadside illumination.

For the class-1 representation, we have a modified pole series

$$\begin{aligned}
\overleftrightarrow{\Lambda}_b(\vec{1}_i\,;s) &= \sum_\alpha e^{-(s-s_\alpha)t_i}\left(\frac{s}{s_\alpha}\right)^p [s-s_\alpha]^{-1}\,\vec{c}_\alpha(\vec{1}_i)\,\vec{c}_\alpha(\vec{1}_i) + \text{possible entire function} \\
&\quad \text{for } p = 0,1,2
\end{aligned} \tag{5.9}$$

where again the entire function is zero within the above restrictions. Even with a negative t_{bs} (requiring an entire function), the above entire function goes to zero at $s = 0$ at least as $0(s^p)$. For $p = 3$, we have

$$\begin{aligned}
\overleftrightarrow{\Lambda}_b(\vec{1}_i\,;s) &= \sum_\alpha e^{-(s-s_\alpha)t_i}\left(\frac{s}{s_\alpha}\right)^3 [s-s_\alpha]^{-1}\,\vec{c}_\alpha(\vec{1}_i)\,\vec{c}_\alpha(\vec{1}_i) \\
&\quad - e^{-st_i}\,\gamma^2\left[\overleftrightarrow{1}_i\cdot\overleftrightarrow{P}\cdot\overleftrightarrow{1}_i + \vec{1}_i\times\overleftrightarrow{M}\times\vec{1}_i\right] \\
&\quad + \text{possible entire function}
\end{aligned} \tag{5.10}$$

Now the entire function is $O(s^3)$ as $s \to 0$, and zero under the previous restrictions. These can be extended to bistatic cases by replacing [9,10,32]

$$\begin{aligned}
\vec{c}_\alpha(\vec{1}_i) &\to \vec{c}_{r\alpha}(\vec{1}_o) = w_\alpha\,\vec{C}_{r\alpha}(\vec{1}_r) = \vec{c}_\alpha(-\vec{1}_o) \\
\vec{1}_i &\to -\vec{1}_o
\end{aligned} \tag{5.11}$$

$$\vec{C}_{r\alpha}(\vec{1}_o) = \left\langle \overleftrightarrow{1}_o e^{-\gamma_\alpha \vec{1}_o \cdot \vec{r}'_s} ; \vec{j}_{s\alpha}(\vec{r}'_s) \right\rangle = \vec{C}_\alpha(-\vec{1}_o)$$

for the first term in each dyad. However, this will change the convergence criterion in (5.8), along with the conditions for a positive time window for t_i for closure in both the RHP and LHP.

For a class-2 form, we have but to integrate the incident wave over the class-2 form of the surface current density as in (4.24) and (4.33), giving

$$\overleftrightarrow{\Lambda}(\vec{1}_o, \vec{1}_i, ; s) = \sum_\alpha \left(\frac{s}{s_\alpha}\right)^p [s - s_\alpha]^{-1} W_\alpha \; \overleftrightarrow{C}_\alpha(-\vec{1}_o, s) \; \overleftrightarrow{C}_\alpha(\vec{1}_i, s) \qquad \text{for } p = 0, 1, 2 \tag{5.12}$$

Using [11] and with t_i taken as zero, this has no additional entire function.

For $p = 3$, note the pole of $s^{-3} \overleftrightarrow{\Lambda}$ at $s = 0$ which comes from the induced dipoles. In section 4, only the magnetostatic modes and associated magnetic-dipole coefficients appeared at $s = 0$ in the current density. Here, however, we need the electric dipole as well. For this purpose, take the electrostatic modes denoted by superscript 1. Now, since the surface charge density goes to zero as $s \to 0$, then from (4.20) we have

$$\vec{j}^{(1)}_{s_\ell}(\vec{r}_s, s) = s \, \vec{j}^{(1)'}_{s_\ell}(\vec{r}_s) = O(s) \qquad \text{as } s \to 0 \tag{5.13}$$

and we note that these have zero curl (due to describing electrostatic response). The electric dipole moment is

$$\begin{aligned}
\overleftrightarrow{p}(s) &= \epsilon_0 \overleftrightarrow{P} \cdot \overleftrightarrow{E}^{(\text{inc})}(\vec{0}, s) = \overleftrightarrow{P} \cdot \overleftrightarrow{D}^{(\text{inc})}(\vec{0}, s) \\
&= \left\{ \sum_{\ell=x',y',z'} \left\langle \vec{r}'_s \, , \, \rho^{(1)}_{S_\ell}(\vec{r}'_s) \right\rangle \vec{1}_\ell \right\} \cdot \overleftrightarrow{D}^{(\text{inc})}(\vec{0}, s) \\
&= \left\{ \sum_{\ell=x',y',z'} \frac{1}{s} \int_S \vec{j}^{(1)}_{s_\ell}(\vec{r}'_s, s) \, dS' \, \vec{1}_\ell \right\} \cdot \overleftrightarrow{D}^{(\text{inc})}(\vec{0}, s) \\
&= \left\{ \sum_{\ell=x',y',z'} \int_S \vec{j}^{(1)'}_{s_\ell}(\vec{r}'_s, s) \, dS' \, \vec{1}_\ell \right\} \cdot \overleftrightarrow{D}^{(\text{inc})}(\vec{0}, s) \qquad \text{as } s \to 0
\end{aligned} \tag{5.14}$$

where the coordinates are those which diagonalize the electric polarizability dyadic. Noting the symmetric form of this dyadic and (4.21), we have

$$\begin{aligned}
\overleftrightarrow{P} &= \sum_{\ell=x',y',z'} \vec{p}^{(1)}_\ell \vec{1}_\ell = \sum_{\ell=x',y',z'} p^{(1)^{-1}}_\ell \vec{p}^{(1)}_\ell \vec{p}^{(1)}_\ell \\
&= \sum_{\ell=x',y',z'} s^{-2} p^{(1)^{-1}}_\ell \left[\int_S \vec{j}^{(1)}_{s_\ell}(\vec{r}_s, s) \, dS \right] \left[\int_S \vec{j}^{(1)}_{s_\ell}(\vec{r}'_s, s) \, dS' \right]
\end{aligned}$$

$$= \sum_{\ell=x',y',z'} p_\ell^{(1)^{-1}} \left[\int_S \vec{j}_{s_\ell}^{(1)'}(\vec{r}_s)\, dS\right] \left[\int_S \vec{j}_{s_\ell}^{(1)'}(\vec{r}_s')\, dS'\right] \qquad \text{as } s \to 0 \tag{5.15}$$

In this form, both the incident and scattered field can be integrated over the domain of the scatterer in a manner consistent with (5.12). Removing the integral signs, we can define

$$\overleftrightarrow{P}(\vec{r}_s, \vec{r}_s') \equiv \sum_{\ell=x',y',z'} p_\ell^{(1)^{-1}}\, \vec{j}_{s_\ell}^{(1)'}(\vec{r}_s)\, \vec{j}_{s_\ell}^{(1)'}(\vec{r}_s') \tag{5.16}$$

as the appropriate polarizability kernel.

The corresponding magnetic-dipole moment from (4.15) gives

$$\begin{aligned} \tilde{\vec{m}}(s) &= \overleftrightarrow{M} \cdot \tilde{\vec{H}}^{(\text{inc})}(\vec{0}, s) \\ \overleftrightarrow{M} &= \sum_{\ell=x,y,z} \vec{m}_\ell^{(0)}\, \vec{1}_\ell = \sum_{\ell=x,y,z} m_\ell^{(0)^{-1}}\, \vec{m}_\ell^{(0)}\, \vec{m}_\ell^{(0)} \end{aligned} \tag{5.17}$$

For use in a class-2 representation, one can use the surface current density in (4.29) or the inverse kernel as in (4.33) as $s \to 0$ to obtain the representation of the magnetic polarizability kernel. From (5.5), we have

$$\vec{1}_o \times \overleftrightarrow{M} \times \vec{1}_i = \sum_{\ell=x,y,z} \gamma^{-2}\, m_\ell^{(0)^{-1}} \left\langle \overleftrightarrow{1}_o\, e^{\gamma\, \vec{1}_o \cdot \vec{r}_s}\, ;\, \vec{j}_{s_\ell}^{(0)}(\vec{r}_s) \right\rangle \left\langle \overleftrightarrow{1}_o\, e^{-\gamma\, \vec{1}_i \cdot \vec{r}_s'}\, ;\, \vec{j}_{s_\ell}^{(0)}(\vec{r}_s') \right\rangle \qquad \text{as } s \to 0 \tag{5.18}$$

noting from before that this is really not a pole since the integral of the magnetostatic modes is zero. So define a kernel to be used with the class-2 form as

$$\overleftrightarrow{M}'(\vec{r}_s, \vec{r}_s') \equiv \sum_{\ell=x,y,z} \gamma^{-2}\, m_\ell^{(0)^{-1}}\, \vec{j}_{s_\ell}^{(0)}(\vec{r}_s)\, \vec{j}_{s_\ell}^{(0)}(\vec{r}_s') \tag{5.19}$$

The $p = 3$ class-2 representation is now

$$\begin{aligned} \tilde{\overleftrightarrow{\Lambda}}(\vec{1}_o, \vec{1}_i; s) &= \sum_\alpha \left(\frac{s}{s_\alpha}\right)^3 [s - s_\alpha]^{-1}\, W_\alpha\, \tilde{\vec{C}}_\alpha(-\vec{1}_o, s)\, \tilde{\vec{c}}_\alpha(\vec{1}_i, s) \\ &\quad + \gamma^2 \left\{ - \sum_{\ell=x',y',z'} p_\ell^{(1)^{-1}}\, \tilde{\vec{C}}_\ell^{(1)}(-\vec{1}_o, s)\, \tilde{\vec{C}}_\ell^{(1)}(\vec{1}_i, s) \right. \\ &\quad \left. + \sum_{\ell=x,y,z} m_\ell^{(0)^{-1}}\, \tilde{\vec{C}}_\ell^{(0)}(-\vec{1}_o, s)\, \tilde{\vec{C}}_\ell^{(0)}(\vec{1}_i, s) \right\} \\ \tilde{\vec{C}}_\ell^{(1)}(\vec{1}_i, s) &= \left\langle \vec{1}_\ell\, e^{-\gamma\, \vec{1}_\ell \cdot \vec{r}_s'}\, ;\, \vec{j}_{s_\ell}^{(1)'}(\vec{r}_s') \right\rangle \end{aligned} \tag{5.20}$$

$$\overrightarrow{\overrightarrow{C}}^{(0)}_{\ell}(\vec{1}_{\rm i}, s) \;=\; \gamma^{-1}\left\langle \overleftrightarrow{1}_{\ell}\; e^{-\gamma\,\vec{1}_{\ell}\cdot\vec{r}'_{\rm s}}\;;\; \vec{j}^{\,(0)}_{{\rm s}\ell}\;(\vec{r}'_{\rm s})\right\rangle$$

For backscattering, merely replace $-\vec{1}_{\rm o}$ by $\vec{1}_{\rm i}$ in the above.

6. Concluding Remarks

This paper has generalized the concept of modified pole series to arbitrary non-negative integer powers of s times $[s - s_\alpha]^{-1}$, applicable to scalar, vector, and dyadic functions of s. Incorporating this with the SEM leads to various forms of pole series for currents on a target and for scattering. This is especially useful for low frequencies (below first resonance) and can be combined with electric- and magnetic-dipole terms for most accurate results.

Differences between the results for class-1 and class-2 forms have been observed. Class-1 is the simplest because no spatial convolutions over the target are required. However, there is a restricted domain of incidence directions for which the series converges at early-time in the case of far-field scattering. Class-2 requires much more extensive computations, but avoids this convergence issue in the scattering sense. However, as we have seen, there is a problem when the target inverse kernel contains a pole at $s = 0$. This can be eventually remedied, at least in part, by a more careful treatment of this pole term which is actually not a true pole in the scattered field, the scattering behaving as s^2 here.

The extensive cases illustrated here may lead the reader to perhaps new questions for resolution concerning both analytical and numerical aspects.

Appendix A. Backscattering from a Thin Wire

As indicated in fig. A.1, let there be a plane wave incident on a thin wire of length $\ell = 2h$, radius b, aligned along the z axis, and centered on the origin. Due to the rotational symmetry ($C_{\infty a}$), let us take

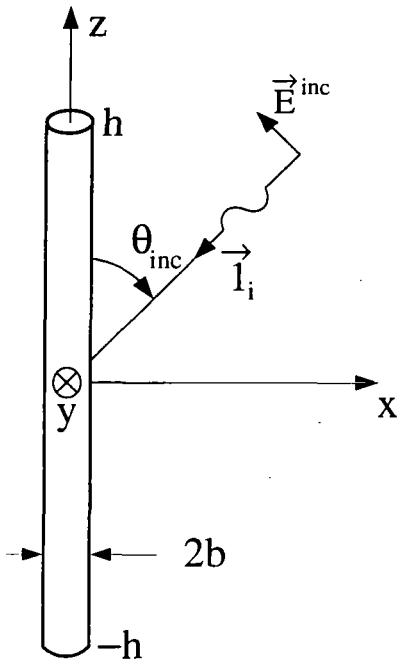

Figure A.1. A thin wire of length $2h$ and radius b.

the x,z plane as the plane of incidence. Furthermore, let the incident (and backscattered) electric field be parallel to the x,z plane (E wave), since the orthogonal polarization produces only small scattering. So the incident field is described by

$$
\begin{aligned}
&\vec{\tilde{E}}^{(inc)}(\vec{r}, s) = E_0 \tilde{f}(s) \vec{1}_e e^{-\gamma \vec{1}_i \cdot \vec{r}} \\
&\vec{\tilde{E}}^{(inc)}(z\vec{1}_z, s) = E_0 \tilde{f}(s) \vec{1}_e e^{-\gamma z \cos(\theta_{inc})} \\
&\vec{1}_e = -\cos(\theta_{inc})\vec{1}_x + \sin(\theta_{inc})\vec{1}_z \\
&\vec{1}_i = -\vec{1}_o = -\sin(\theta_{inc})\vec{1}_x - \cos(\theta_{inc})\vec{1}_z \\
&\overleftrightarrow{1}_i = \overleftrightarrow{1}_i - \vec{1}_i\vec{1}_i \quad , \quad \overleftrightarrow{1}_i \cdot \vec{1}_e = \vec{1}_e
\end{aligned}
\tag{A.1}
$$

A.1 Polarizability

Since the important current is parallel to the z axis, the electric dipole moment is in the z direction, and the electric polarizability tensor (dyad) is

$$\overleftrightarrow{P} = P_{z,z}\,\vec{1}_z\,\vec{1}_z \quad , \quad P_{z,z} = p_z^{(1)} \tag{A.2}$$

and the magnetic polarizability tensor is negligible. Identifying θ_{inc} as θ in what is to follow, the electric-dipole term in the backscattering dyad (in (5.10)) takes the form

$$\overleftrightarrow{1}_i \cdot \overleftrightarrow{P} \cdot \overleftrightarrow{1}_i = \sin^2(\theta) P_{z,z}\,\vec{1}_\theta\,\vec{1}_\theta \tag{A.3}$$

The backscattering dyad takes the form

$$\overleftrightarrow{\Lambda}_b(\vec{1}_i, s) = \tilde{\Lambda}_{b_{\theta,\theta}}\,\vec{1}_\theta\,\vec{1}_\theta = \tilde{\Lambda}_{b_{ee}}\,\vec{1}_e\,\vec{1}_e \tag{A.4}$$

From [2] we have (based on a prolate spheroid of semi-major axis h and semi-minor axis b)

$$\begin{aligned} P_{z,z} &= \frac{4}{3}\pi h b^2 \frac{1-\left(\frac{b}{h}\right)^2}{\left(\frac{b}{h}\right)^2} \left\{ \frac{1}{2}\left[1-\left(\frac{b}{h}\right)^2\right]^{-1/2} \ell n \left[\frac{1+\left[1-\left(\frac{b}{h}\right)^2\right]^{1/2}}{1-\left[1-\left(\frac{b}{h}\right)^2\right]^{1/2}} \right] - 1 \right\}^{-1} \\ &= \frac{4}{3}\pi h^3 \left[1-\left(\frac{b}{h}\right)^2\right] \left\{ \frac{1}{2}\left[1-\left(\frac{b}{h}\right)^2\right]^{-1/2} \ell n \left[\frac{1+\left[1-\left(\frac{b}{h}\right)^2\right]^{1/2}}{1-\left[1-\left(\frac{b}{h}\right)^2\right]^{1/2}} \right] - 1 \right\}^{-1} \\ &= \frac{4}{3}\pi h^3 \left[\ell n\left(\frac{2h}{b}\right) - 1 \right]^{-1} \quad \text{as} \quad \frac{b}{h} \to 0 \quad \text{(thin wire)} \end{aligned} \tag{A.5}$$

Substituting these results in (5.10) with

$$t_i = -h\cos(\theta) \tag{A.6}$$

gives the results for class-1 backscattering for $p = 3$.

For class-2 backscattering as in (5.20) with $p = 3$, we need to evaluate the integrals associated with electric-dipole term. Noting that only ℓ =z gives a significant contribution, we have

$$\begin{aligned} p_z^{(1)} &= P_{z,z} \\ \overleftrightarrow{C}_z^{(1)}(\vec{1}_i, s) &= \overleftrightarrow{C}_z(-\vec{1}_o, s) \quad \text{(backscattering)} \end{aligned} \tag{A.7}$$

$$= \left\langle \overleftrightarrow{1}_{\rm i}\, e^{-\gamma\, \vec{1}_{\rm i}\cdot\vec{r}'_{\rm s}} \; ; \; \vec{j}^{\,(1)'}_{s_z}\,(\vec{r}'_{\rm s}) \right\rangle$$

For a thin wire, the low-frequency current is a line current proportional to $\cos(\pi z/\ell)$. Noting the frequency dependence of low frequencies in (5.13) we have

$$\begin{aligned} \overrightarrow{\overrightarrow{C}}{}^{(1)}_{z}(\vec{1}_{\rm i}, s) &= -\vec{1}_\theta\, C_0\, \sin(\theta) \int_{-h}^{h} e^{-\gamma z' \cos(\theta)} \cos\left(\frac{\pi z'}{2h}\right) dz' \\ &= -\vec{1}_\theta\, C_0\, \sin(\theta) \int_{-h}^{h} \cosh(\gamma z' \cos(\theta)) \cos\left(\frac{\pi z'}{2h}\right) dz' \end{aligned} \tag{A.8}$$

Evaluating the constant, let $s \to 0$ and obtain,

$$\begin{aligned} \overrightarrow{\overrightarrow{C}}{}^{(1)}_{z}(\vec{1}_{\rm i}, 0) &= -\vec{1}_\theta\, C_0\, \sin(\theta) \int_{-h}^{h} \cos\left(\frac{\pi z'}{2h}\right) dz' \\ &= -\vec{1}_\theta\, C_0\, \frac{4h}{\pi} \sin(\theta) \end{aligned} \tag{A.9}$$

Now equate the results for $s \to 0$ from (5.10) with (A.3) (class-1) to that from (5.2) with (A.6) and (A.8) (class-2) giving

$$\begin{aligned} \overleftrightarrow{1}_{\rm i}\cdot\overleftrightarrow{P}\cdot\overleftrightarrow{1}_{\rm i} &= P_{z,z} \sin^2(\theta)\, \vec{1}_\theta \vec{1}_\theta = P^{-1}_{z,z}\, C_0^2 \left(\frac{4h}{\pi}\right)^2 \sin^2(\theta)\, \vec{1}_\theta \vec{1}_\theta \\ C_0 &= \frac{\pi}{4h} P_{z,z} \end{aligned} \tag{A.10}$$

So define

$$\tilde{f}_0(s) = \frac{\pi}{4h} \int_{-h}^{h} \cosh(\gamma z' \cos(\theta)) \cos\left(\frac{\pi z'}{2h}\right) dz' \tag{A.11}$$

and the class-2 form in (5.20) becomes

$$-\gamma^2\, p_z^{(1)^{-1}}\; \overrightarrow{\overrightarrow{C}}{}^{(1)}_{z}(\vec{1}_{\rm i}, s)\; \overrightarrow{\overrightarrow{C}}{}^{(1)}_{z}(\vec{1}_{\rm i}, s) = -\gamma^2\, P_{z,z} \sin^2(\theta)\, \tilde{f}_0^2(s)\, \vec{1}_\theta \vec{1}_\theta \tag{A.12}$$

So the effect of going from class-1 to class-2 is to modify the electric-dipole term by the removal of $e^{-st_{\rm i}}$ in (5.10) and multiplication by $\tilde{f}_0^2(s)$.

So now, let us evaluate $\tilde{f}_0(s)$ as

$$\begin{aligned} \tilde{f}_0(s) &= \frac{\pi}{4h} \int_{-h}^{h} e^{\gamma z' \cos(\theta)} \cos\left(\frac{\pi z'}{2h}\right) dz' \\ &= \frac{\pi}{8h} \int_{-h}^{h} \left[e^{\gamma z' \cos(\theta) + j\frac{\pi z'}{2h}} + e^{\gamma z' \cos(\theta) - j\frac{\pi z'}{2h}} \right] dz' \\ &= \frac{\pi}{8h} \left[\left[\gamma \cos(\theta) + j\frac{\pi}{2h}\right]^{-1} e^{\gamma z' \cos(\theta) + j\frac{\pi z'}{2h}} + \left[\gamma \cos(\theta) - j\frac{\pi}{2h}\right]^{-1} e^{\gamma z' \cos(\theta) - j\frac{\pi z'}{2h}} \right] \Bigg|_{-h}^{h} \end{aligned}$$

$$
\begin{aligned}
&= \frac{\pi}{8h}\left[\left[\gamma\cos(\theta) + j\frac{\pi}{2h}\right]^{-1}\left[je^{\gamma h\cos(\theta)} + je^{-\gamma h\cos(\theta)}\right]\right. \\
&\quad \left. + \left[\gamma\cos(\theta) - j\frac{\pi}{2h}\right]^{-1}\left[-je^{\gamma h\cos(\theta)} - je^{-\gamma h\cos(\theta)}\right]\right] \\
&= \frac{\pi}{4h}\left[j\left[\gamma\cos(\theta) + j\frac{\pi}{2h}\right]^{-1} - j\left[\gamma\cos(\theta) - j\frac{\pi}{2h}\right]^{-1}\right]\cosh(\gamma h\cos(\theta)) \\
&= \frac{1}{2}\left[\left[1 - j\frac{2\gamma h}{\pi}\cos(\theta)\right]^{-1} + \left[1 + j\frac{2\gamma h}{\pi}\cos(\theta)\right]^{-1}\right]\cosh(\gamma h\cos(\theta)) \\
&= \left[1 + \left[\frac{2\gamma h}{\pi}\cos(\theta)\right]^{2}\right]^{-1}\cosh(\gamma h\cos(\theta)) \qquad \text{(A.13)}
\end{aligned}
$$

For $s = j\omega$, this becomes

$$
\tilde{f}_0(j\omega) = \left[1 - \left[\frac{2\omega h}{\pi c}\cos(\theta)\right]^{2}\right]^{-1}\cos\left(\frac{\omega h}{c}\cos(\theta)\right) \qquad \text{(A.14)}
$$

Note that this is not singular at $\omega\, h\cos(\theta) = \pm\pi/2$ since the following cosine function also has zeros that cancel the first order poles.

A.2 Numerical Results

In this section, numerical results depicting the backscattering dyadic from a thin straight wire are presented. The backscattering dyadic is computed using both the class-1 and class-2 forms of the SEM modified pole series. These results are compared to the backscattering dyadic computed using a frequency domain method of moments approach. In the following text, this solution of the backscattering dyadic will be referred to as the direct solution. Furthermore, unless otherwise stated, the direct solution will be considered correct, and the performance of the SEM modified pole series will be based upon the agreement of this solution with the direct solution.

Before examining the results, a brief explanation of the numerical procedures used in obtaining the SEM results is pertinent. Because the straight wire here is considered thin, the SEM can easily be cast into numerical form via the method of moments. Specifically, this involves representing the surface current $\overrightarrow{\overrightarrow{J}}_s$ in a series of N basis functions, and then testing the impedance integral equation (EFIE) (4.1) with a set of N testing functions. The result of this process is a linear matrix equation where the kernel $\overleftrightarrow{Z}_t$ is now represented by a matrix of size N $\times$ N. For the results presented here, a pulse expansion of the surface current density and and pulse testing of the integral equation are used.

Now that the impedance integral equation has been cast into matrix form, all of the essential components of the singularity expansion method such as the natural frequencies (poles), modes, and coupling

coefficients can be computed numerically. Once these parameters have been determined, the application of (5.9) and (5.12) to compute the class-1 and class-2 forms of the backscattering dyadic is straightforward. A variety of numerical methods for computing these parameters have been developed and are discussed in variety of sources [13-16].

The direct solution of the backscattering dyadic, which will be used to evaluate the performance of the SEM results, is also determined numerically via the method of moments. The direct solution involves transforming the same integral equation into matrix form; however, unlike the SEM, the integral equation and resulting matrix equation are in terms of $s = j\omega$ (ω real). Furthermore, the surface current is obtained by directly inverting the kernel of the integral equation. The backscattering dyadic is then computed by applying standard potential theory.

The straight wire considered here as a length-to-radius ($2h/b$) ratio of 200, and it has been subdivided into 51 moment method zones. A total of 27 poles, including conjugate pairs, were used in computing the SEM results. Figure A.2 shows the location of these poles. In the figure, the poles have been grouped according to their eigenset [7]. Each eigenset is represented by an arc, and the poles belonging to each eigenset lie on the arc. By an eigenset, we mean all the terms associated with one matrix eigenvalue λ_n (the natural frequencies being the zeros of these eigenvalues.)

The parameters in the following figures are chosen with an eye to test the convergence properties of the series in both class-1 and class-2 forms . As discussed in section 5 and [11], there is a backscattering time window for convergence of the class-1 series. In (5.8), this requires that $t_{bs} \geq 0$, so that t_i can be chosen without having the series diverge for early time. In our thin-wire example, the symmetry of the geometry has

$$\begin{aligned} L_0 &= L = 2h \\ t_0 &= \frac{L_0}{c} = \frac{2h}{c} \\ t_b &= -t_f = \frac{h}{c}\cos(\theta_{inc}) \\ t_{bs} &= t_0 + 2[t_f - t_b] = t_0[1 - 2\cos(\theta_{inc})] \\ &\equiv \text{backscatter time window} \end{aligned} \tag{A.15}$$

This says that there is a range of θ_{inc} given by

$$60^\circ \leq \theta_{inc} \leq 90^\circ \quad \text{for } t_{bs} \geq 0 \tag{A.16}$$

In this range t_i, chosen per (4.8), gives series convergence, a *necessary* condition for lack of an additional entire function. In the illustrations, then $\theta_{inc} = 45^\circ$ violates this condition, while $\theta_{inc} = 90^\circ$ satisfies this

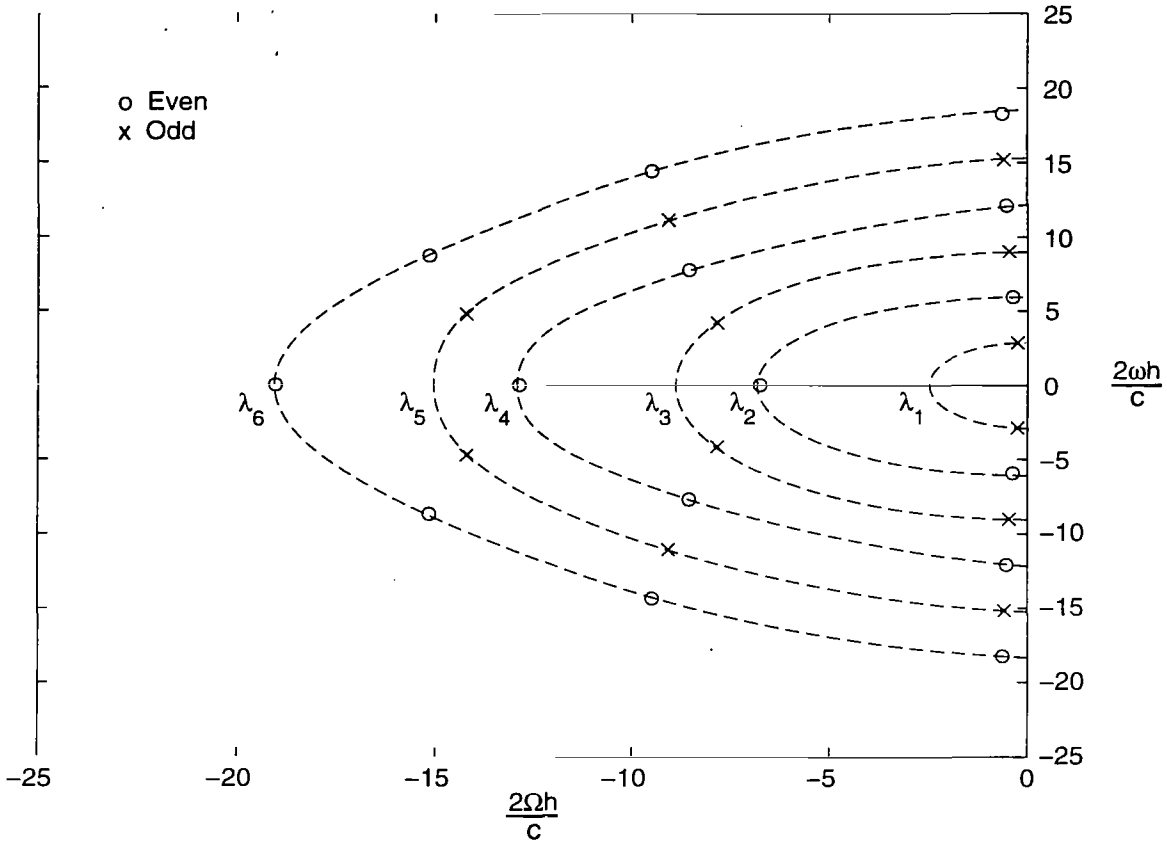

Figure A.2. The pole locations of the thin straight wire, $2h/b = 200$. The poles are grouped into eigensets.

condition.

The thin-wire has no magnetic dipole term. The electric-dipole term is contributed to by only odd n in the λ_n eigensets. This can be seen from the symmetry of the currents about the center of the wire. For even n, the volume integral of the current is exactly zero. So for low frequencies, adding an even n in the sum to the previous sum ending in odd n contributes very little below first resonance.

Figures A.3 through A.8 illustrate the magnitude of the backscattering dyadic $\tilde{\Lambda}_b$ for the straight wire as a function of frequency for the two orientations mentioned above. The incident electric field is oriented in the x,z plane (E wave polarization) as illustrated in fig. A.1. For each orientation, both the class-1 and class-2 forms of the SEM modified pole series are used to compute the backscattering dyadic $\tilde{\Lambda}_{b_{ee}}$ where the e denotes that the incident and scattered fields are E-waves. In each case, solutions of $\tilde{\Lambda}_{b_{ee}}$ for powers $p = 0$, 1, 2, and 3 of the modified pole series are given.

Figure A.3 shows the magnitude of $\tilde{\Lambda}_{b_{ee}}$ for an incident angle of 45°. The SEM solutions were

obtained using a class-1 coupling coefficient. The upper plot of fig. A.3 shows the scattering dyadic on a log-log scale. The lower plot depicts the scattering dyadic on a linear scale. The log scale plot is useful for examining the performance of the SEM solution in the lower frequency region whereas the linear scale plot emphasizes the resonance region. By inspecting the log scale plot, it is apparent that as the power of the modified pole series is increased, the low frequency agreement of the SEM solutions with the direct solutions progressively improves. This result is expected since at low frequencies, the scattering dyadic is proportional to s^2. In the low frequency region, there is a slight discrepancy between the $p = 3$ solution and the direct solution. This discrepancy appears to be constant up to the resonance region. At low frequencies, the polarizability term in (5.10) dominates the $p = 3$ solution. Since the polarizability term (A.3) accurately describes the quasi-static behavior of the straight wire, the $p = 3$ solution is considered correct. The error in the direct solution could be attributed to the choice of basis and testing functions. Although this hypothesis was not investigated, choosing a set of smoother functions other than pulses could possibly improve the direct solution in the low frequency region.

In the resonance region, the modified pole series solutions presented in fig. A.3 perform fairly well. In particular, the $p = 0$ solution agrees extremely well with the direct solution. This result is surprising since such nice agreement is usually not expected with a class-1 coupling coefficient. The $p = 1$ solution does well in capturing the peaks of the resonances; however, its performance in capturing the nulls is suspect (small differences of large numbers). This behavior may be attributed to the class-1 coupling coefficient. The class-1 coupling coefficient does not contribute critical phase information like the class-2 coupling coefficient. The $p = 2$ and $p = 3$ solutions do well in capturing the first and second resonances. Beyond the second resonance, these solutions begin to diverge from the direct solution. The behavior of the $p = 3$ solution can, at least partially, be explained by the influence of the polarizability term. The class-1 polarizability term increases quadratically with frequency. Thus, at frequencies beyond the first couple of resonances, the polarizability term is large and begins to dominate the $p = 3$ solution.

Figure A.4 shows the class-1, $p = 3$ modified pole series solutions of $\tilde{\Lambda}_{\mathrm{bee}}$ for various pole contributions. As in fig. A.3, the magnitude of $\tilde{\Lambda}_{\mathrm{bee}}$ is plotted for an incident angle of 45°. The various pole contributions used in the modified pole series solutions correspond to the various combinations of the eigensets shown in fig. A.2. Three different $p = 3$ solutions of $\tilde{\Lambda}_{\mathrm{bee}}$ were obtained by using 2, 4, and 6 eigensets (or arcs). Referring to fig. A.2, the solution obtained by using 2 arcs signifies that the poles belonging to the eigensets for eigenvalues λ_1 and λ_2 were used. Similarly, the solution obtained by using 4 arcs denotes that the eigensets for eigenvalues λ_1 through λ_4 were used.

Returning to fig. A.4, one can see that the various $p = 3$ solutions converge in the low frequency region. This is expected since the higher order pole terms have very little influence on the response at low frequencies. Furthermore, as was indicated earlier, the class-1 polarizability term in (5.10) dominates the

response at low frequencies. In the resonance region, all of the $p = 3$ solutions do well in the area around the the first resonance. However, beyond the first resonance, these solutions begin to diverge from the direct solution. In particular, the solutions obtained using 2 and 4 arcs begin to track the polarizability term around the second resonance. The solution using 6 arcs captures the first and second resonances fairly well. After the second resonance, the agreement of this solution with the direct solution deteriorates. One can observe the peaks of the third and fourth resonances in this solution, but because of the influence of the polarizability term, the amplitudes are incorrect.

Figures A.5 and A.6 are similar in format to figs. A.3 and A.4, respectively. In both figures, the modified pole series is employed to compute $\tilde{\Lambda}_{\mathsf{b_{ee}}}$ for broadside incidence ($\theta = 90°$). The class of the SEM solution is not an issue here since both the class-1 and class-2 forms of the solutions are equivalent for broadside incidence. In fig. A.5, we see that the $p = 2$ and $p = 3$ solutions produced the best results in the low frequency region as expected. Although the $p = 2$ solution coincides with the direct solution, the $p = 3$ solution is considered to be the correct response in the low frequency region. Observe that the difference between the direct solution and the $p = 3$ solution remains constant up to the resonance region. This same characteristic was noticed in figs. A.3 and A.4 which may indicate the source of error in the direct solution is independent of incidence angle. This observation seems to give plausibility to the hypothesis that the source of error is related to the choice of basis and testing functions.

In the resonance region, the modified pole series solutions are varied. The $p = 2$ solution agrees extremely well with the direct solution. It appears that the agreement of the modified pole series solutions with the direct solution improve with increasing power up to $p = 2$. The $p = 0$, 1, and 3 solutions capture the first resonance well, but then begin to diverge thereafter. The $p = 1$ solution lags slightly behind that of the $p = 2$ solution although it appears that the margin of error is increasing with frequency. After the first resonance, the $p = 3$ result begins to follow the polarizability term . As explained earlier, this behavior is attributed to the quadratic nature of the polarizability term. The $p = 3$ solutions of fig. A.6 provide further evidence of this characteristic. All of the SEM results presented in fig. A.6 are accurate up through the first resonance. Beyond this point, the $p = 3$ solutions begin to be dominated by the polarizability term. Note that the third resonance (there being no second resonance due to the symmetry of the excitation) is not contained in the result obtained using 2 eigensets. This suggests that the first two eigensets contain very little spectral information related to the third and higher order resonances, as one should expect, since natural frequencies are zeros of particular eigenvalues [7].

Figures A.7 and A.8 are the class-2 equivalents of figs. A.3 and A.4, respectively. In these figures, the class-2 form of the modified pole series is used to compute $\tilde{\Lambda}_{\mathsf{b_{ee}}}$ for an incident angle of 45°. In similar fashion to fig. A.3, fig. A.7 shows the magnitude of $\tilde{\Lambda}_{\mathsf{b_{ee}}}$ for various powers of the modified pole series. By comparing fig. A.3 with A.7, it is apparent that the class-2 coupling coefficient significantly changes the

various solutions. In the low frequency region, the class-2, $p = 0$ solution is similar to the class-1, $p = 0$ result. However, in the resonance region, the class-1 result actually agrees better with the direct solution than the class-2 result. This is an interesting result since the class-2 solution is expected to give better agreement. However, excellent agreement of the $p = 1$ and $p = 2$ solutions with the direct solution are observed in fig. A.7. The performance of the class-2, $p = 1$ result in the low frequency is improved in comparison to the class-1 result. Both the $p = 2$ and $p = 3$ results continue to give excellent results at low frequencies. Note that the constant offset between the direct solution and the $p = 3$ result has not changed. A very significant result in fig. A.7 is the performance of the $p = 3$ solution in the resonance region. Except for a large deviation in the null between the second and third resonances, the class-2 $p = 3$ solution agrees very well with the direct solution. The class-2 polarizability term peaks in the area between the second and third resonances resulting in the aforementioned deviation. Beyond the third resonance, the magnitude of the polarizability term begins to rapidly decline. As this occurs, the performance of the $p = 3$ solution improves.

In fig. A.8, the excellent performance of the class-2, $p = 3$ solution is further validated. Regardless of the number of eigensets used, the low frequency agreement of $p = 3$ solution is maintained. Only in the resonance region does the number of eigensets become an issue. The solution using two arcs nicely captures the first two resonances and then rolls off. This result is expected since the first two arcs contain mainly information regarding the first two resonances. There is not much difference between the solutions using four and six arcs in the frequency range of interest. Again, this result is anticipated since the frequency range of interest spans only the first four resonances. The solution using six arcs actually contains more spectral information than is necessary to obtain an accurate result over the desired frequency range.

The limited data presented here show that numerical convergence in the resonance region (beyond first resonance) appears to better for the class-2 form. This should not be surprising since the spatial convolution with the incident wave suppresses high frequencies as compared to class 1. This becomes important for the larger values of p which emphasize high frequencies in this region. In both classes, the larger p give more accurate results than the direct solution for low frequencies. Furthermore, the direct solution appears more accurate than that with the moment-method poles, indicating some additional errors of unknown source. The results for $\theta_{\text{inc}} = 90°$ also appear better than for $\theta_{\text{inc}} = 45°$, consistent with (A.16), but the absence of the second pole also contributes to this result.

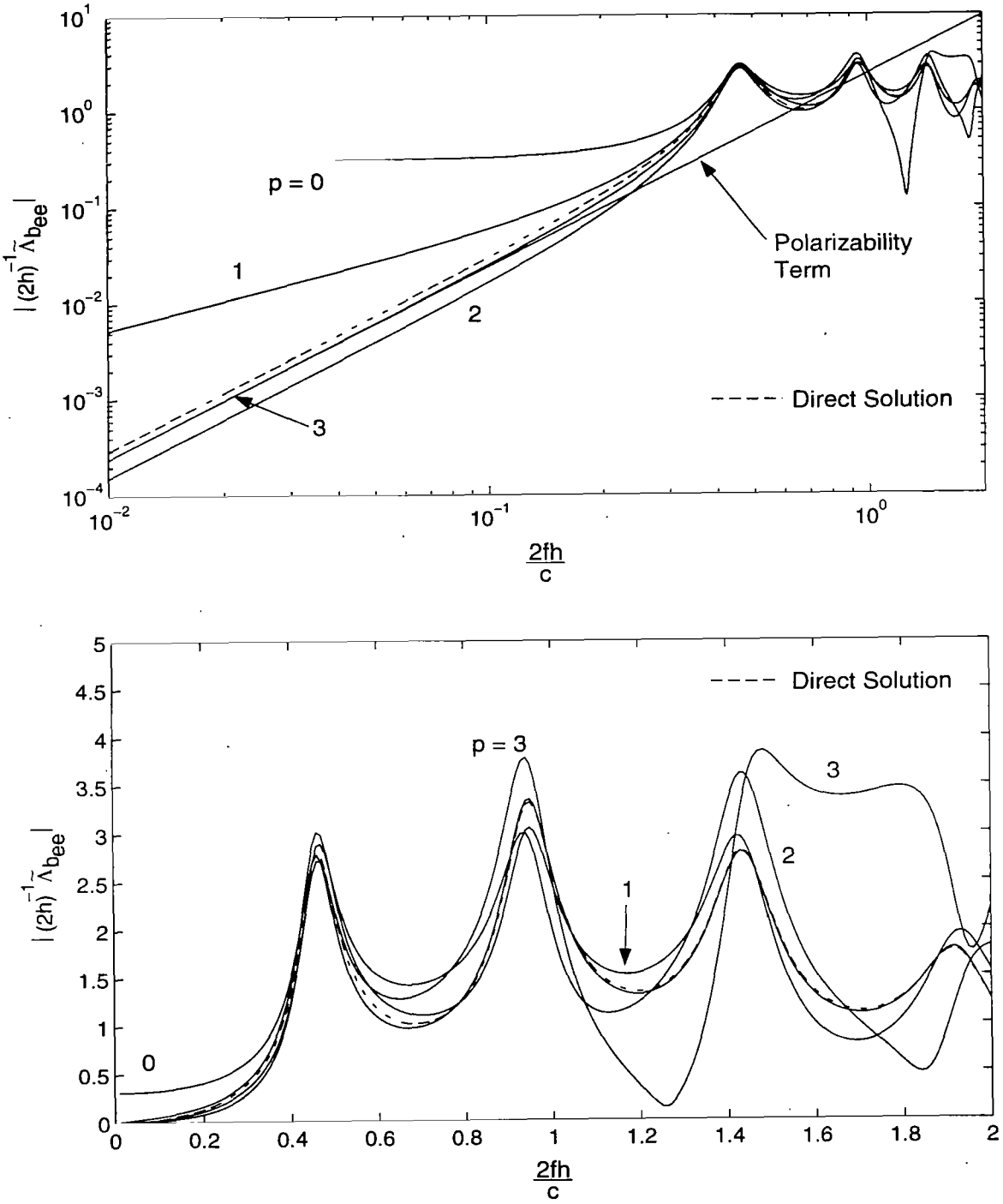

Figure A.3. Magnitude of the backscattering dyadic from a straight wire, calculated using the class-1 SEM modified pole series (p=0,1,2,3) for $\theta_{inc} = 45°$. The frequency domain/method of moments solution (direct solution) is provided for comparison.

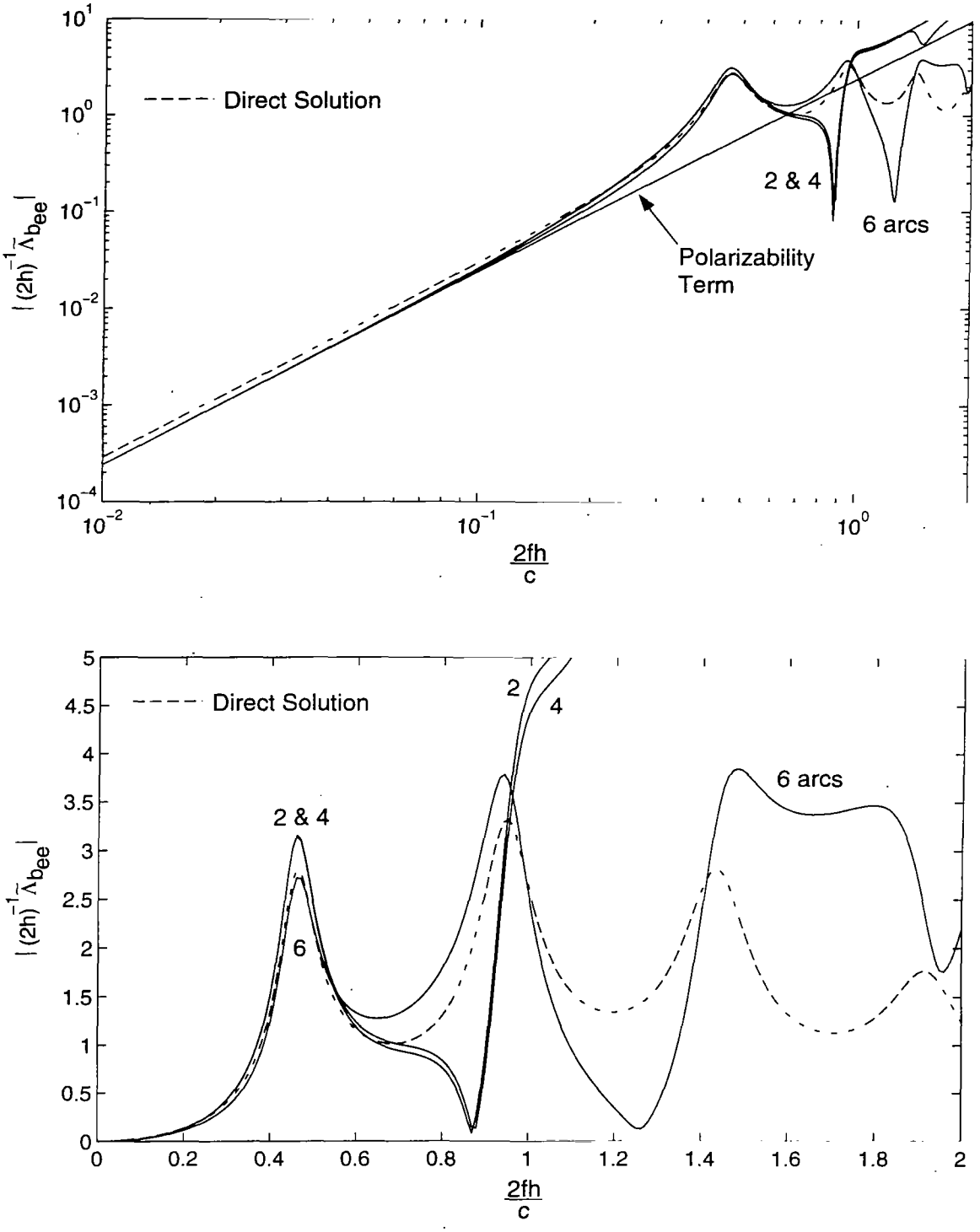

Figure A.4. Magnitude of the backscattering dyadic from a straight wire for $\theta_{inc} = 45°$, calculated using the p=3, class-1 SEM representation with 2, 4, and 6 eigensets and compared to the frequency domain result.

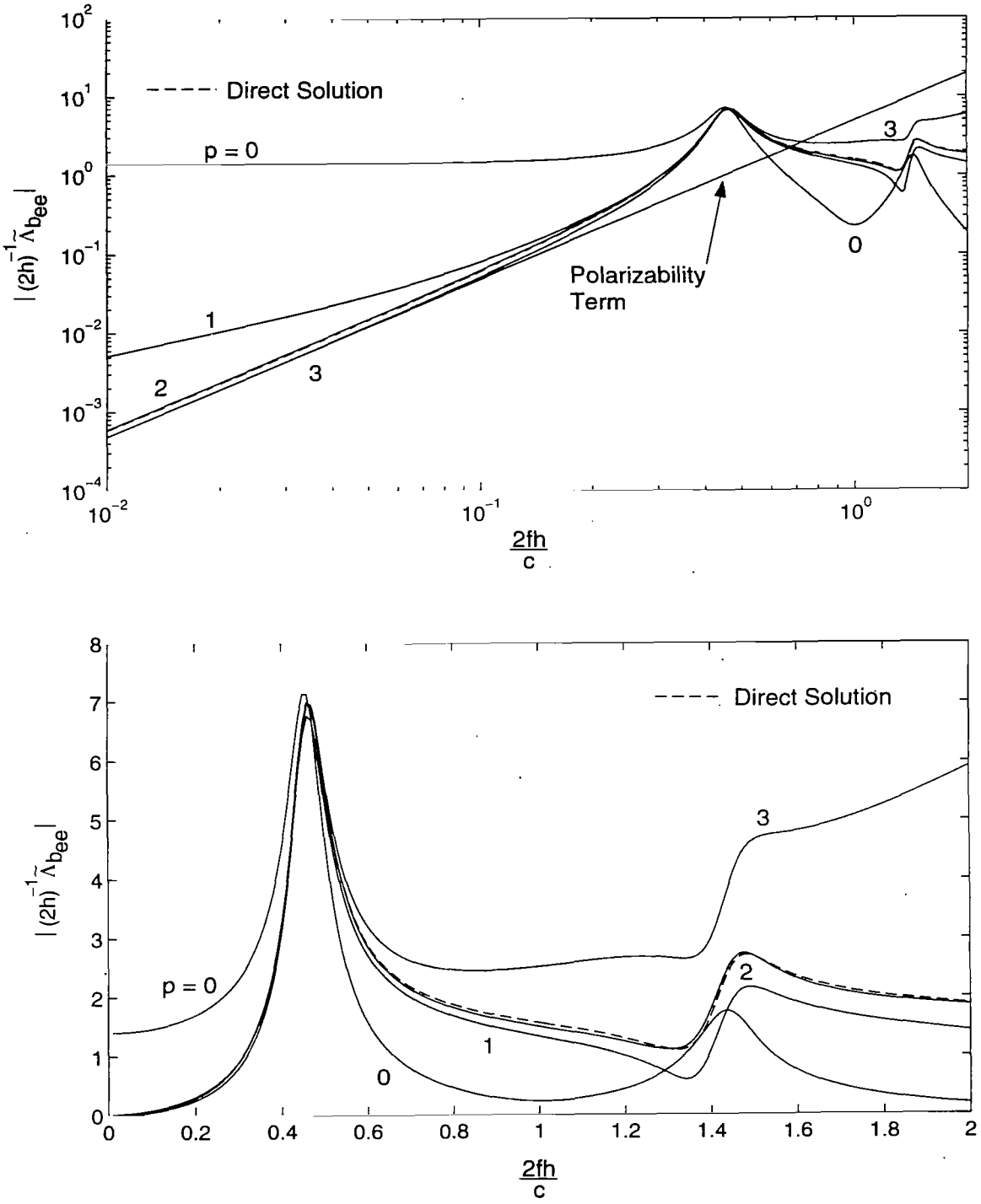

Figure A.5. Magnitude of the backscattering dyadic from a straight wire, calculated using the SEM modified pole series (class-1 $\equiv$ class-2) (p=0,1,2,3) for $\theta_{inc} = 90°$. The frequency domain/method of moments solution (direct solution) is provided for comparison.

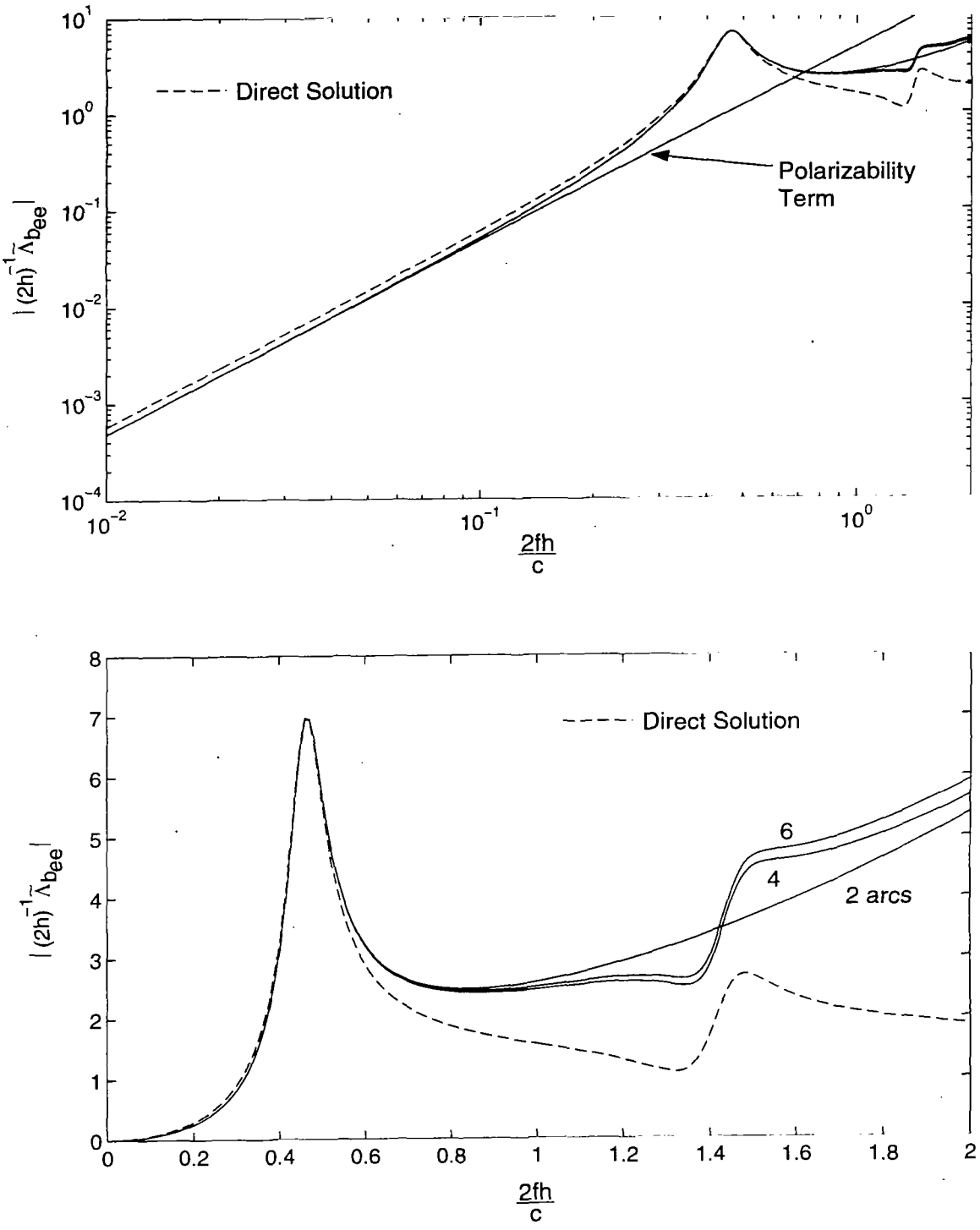

Figure A.6. Magnitude of the backscattering dyadic from a straight wire for $\theta_{inc} = 90°$, calculated using the p=3 SEM representation (class-1 $\equiv$ class-2) with 2, 4, and 6 eigensets and compared to the frequency domain result.

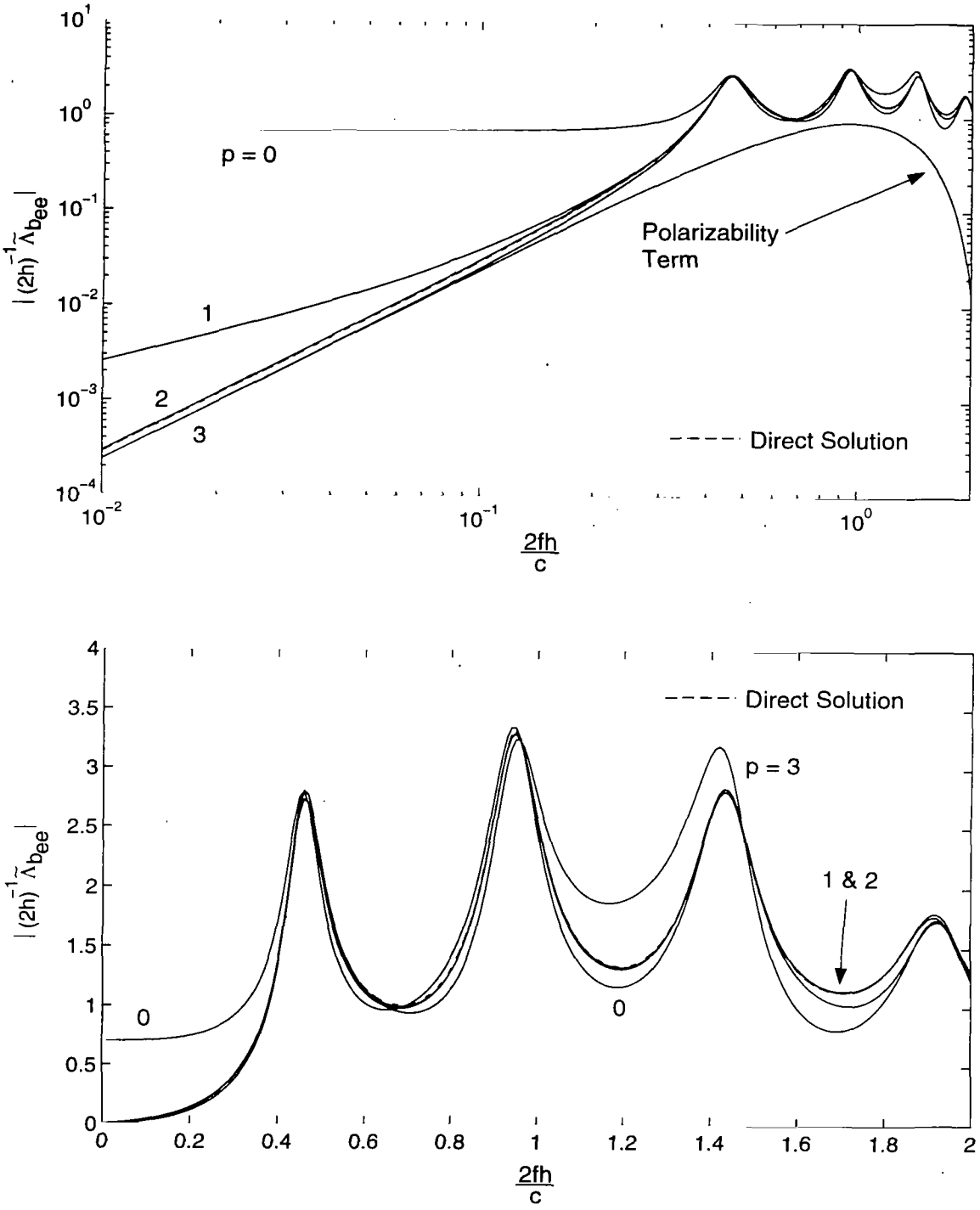

Figure A.7. Magnitude of the backscattering dyadic from a straight wire, calculated using the class-2 SEM modified pole series (p=0,1,2,3) for $\theta_{inc} = 45°$. The frequency domain/method of moments solution (direct solution) is provided for comparison.

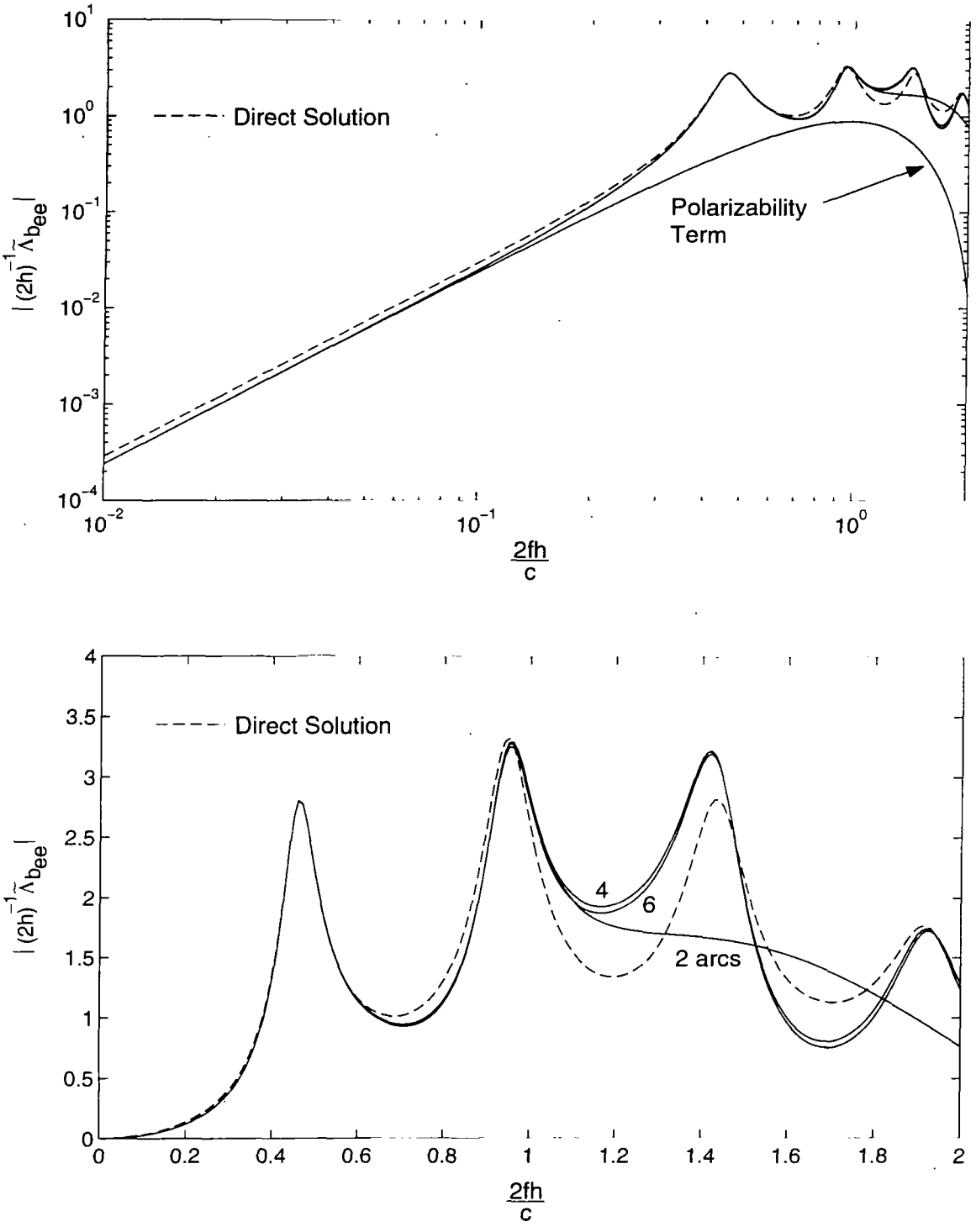

Figure A.8. Magnitude of the backscattering dyadic from a straight wire for $\theta_{inc} = 45°$, calculated using the p=3, class-2 SEM representation with 2, 4, and 6 eigensets and compared to the frequency domain result.

Appendix B. Backscattering from a Thin Circular Loop

As indicated in fig. B.1, let there be a plane wave incident on a thin circular loop of major radius a and minor radius b, with the z axis as an axis of rotational symmetry ($C_{\infty a}$). As in appendix A, let the x,z plane be the plane of incidence. Now there are two polarizations of interest.

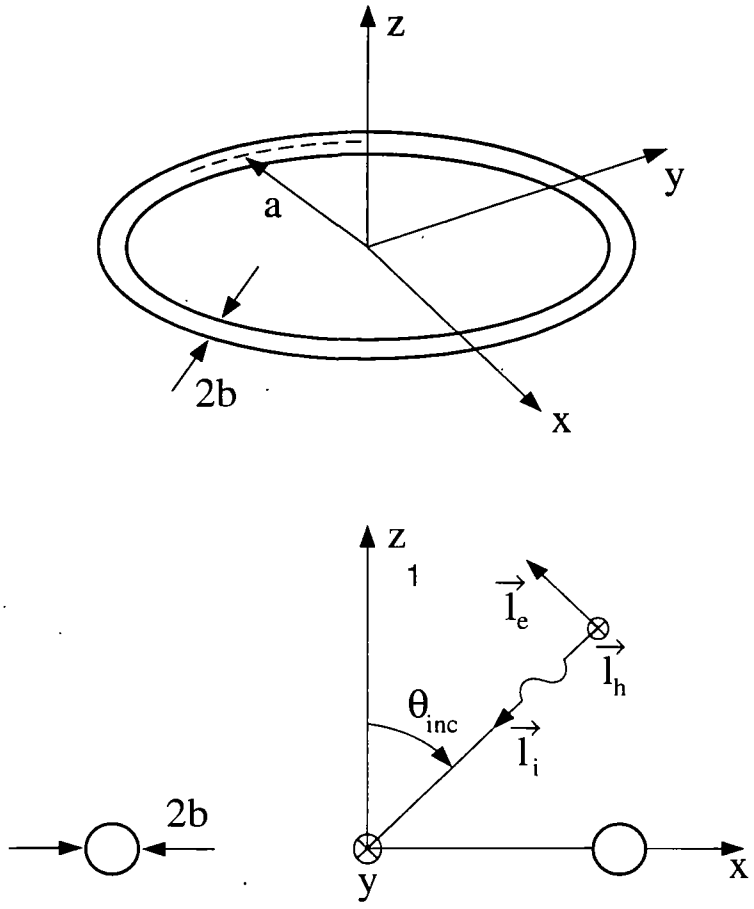

Figure B.1. A thin wire loop with a loop radius a and a wire radius b.

An E wave has the incident electric field parallel to the plane of incidence with

$$\begin{aligned}
&\vec{\tilde{E}}_e^{(inc)}(\vec{r},s) = E_0\,\tilde{f}(s)\,\vec{l}_e\,e^{-\gamma\vec{l}_i\cdot\vec{r}} \\
&\vec{l}_e = -\cos(\theta_{inc})\,\vec{l}_x + \sin(\theta_{inc})\,\vec{l}_z \\
&\vec{l}_i = -\vec{l}_o = -\sin(\theta_{inc})\,\vec{l}_x - \cos(\theta_{inc})\,\vec{l}_z \\
&\overleftrightarrow{l}_i = \overleftrightarrow{l}_i - \vec{l}_i\vec{l}_i = \vec{l}_e\vec{l}_e + \vec{l}_h\vec{l}_h
\end{aligned} \tag{B.1}$$

where the incident field tangential to the thin wire is

$$\begin{aligned}
\vec{1}_\phi \cdot \overset{\sim}{\vec{E}}{}_e^{(inc)}(a\vec{1}_\Psi, s) &= E_0\, \tilde{f}(s)\, \vec{1}_e \cdot \vec{1}_\phi\, e^{-\gamma a \vec{1}_i \cdot \vec{1}_\Psi} \\
\vec{1}_e \cdot \vec{1}_\phi &= -\cos(\theta_{inc})\, \vec{1}_x \cdot \vec{1}_\phi = \cos(\theta_{inc}) \sin(\phi) \\
\vec{1}_i \cdot \vec{1}_\Psi &= -\sin(\theta_{inc})\, \vec{1}_x \cdot \vec{1}_\Psi = -\sin(\theta_{inc}) \cos(\phi)
\end{aligned} \tag{B.2}$$

An H wave has the electric field perpendicular to the plane of incidence with

$$\begin{aligned}
\overset{\sim}{\vec{E}}{}_h^{(inc)}(\vec{r}, s) &= E_0\, \tilde{f}(s)\, \vec{1}_h\, e^{-\gamma \vec{1}_i \cdot \vec{r}} \\
\vec{1}_h &= \vec{1}_y
\end{aligned} \tag{B.3}$$

The incident electric field tangential to the thin wire is

$$\begin{aligned}
\vec{1}_\phi \cdot \overset{\sim}{\vec{E}}{}_h^{(inc)}(a\vec{1}_\Psi, s) &= E_0\, \tilde{f}(s)\, \vec{1}_h \cdot \vec{1}_\phi\, e^{-\gamma a \vec{1}_i \cdot \vec{1}_\Psi} \\
\vec{1}_h \cdot \vec{1}_\phi &= \cos(\phi)
\end{aligned} \tag{B.4}$$

B.1 Polarizability

For this problem, the important dipole moments (not negligible due to the thin wire) give polarizability tensors (dyads)

$$\begin{aligned}
\overleftrightarrow{P} &= P_{x,x}\, \vec{1}_x \vec{1}_x + P_{y,y}\, \vec{1}_y \vec{1}_y \\
\overleftrightarrow{M} &= M_{z,z}\, \vec{1}_z \vec{1}_z
\end{aligned} \tag{B.5}$$

Identifying θ_{inc} as θ in what is to follow, the dipole terms in the backscattering dyad (in (5.10)) take the form

$$\begin{aligned}
\vec{1}_i \cdot \overleftrightarrow{P} \cdot \vec{1}_i &= \cos^2(\theta)\, P_{x,x}\, \vec{1}_e \vec{1}_e + P_{y,y}\, \vec{1}_h \vec{1}_h \\
\vec{1}_i \times \overleftrightarrow{M} \times \vec{1}_i &= -\sin^2(\theta)\, M_{z,z}\, \vec{1}_h \vec{1}_h
\end{aligned} \tag{B.6}$$

The backscattering dyad takes the form

$$\overset{\simeq}{\Lambda}_b(\vec{1}_i, s) = \tilde{\Lambda}_{e,e}\, \vec{1}_e \vec{1}_e + \tilde{\Lambda}_{h,h}\, \vec{1}_h \vec{1}_h \tag{B.7}$$

The symmetry with respect to the x,z plane leads to this diagonal representation. Note that ϕ is used as a coordinate on the loop for our later integration, so e,h gives better coordinates for the backscattering (equivalent to v,h (vertical,horizontal) radar coordinates) than θ, ϕ.

Perfectly conducting bodies of revolution have the general property for the components of the polarizability tensors [30].

$$P_{x,x} = P_{y,y} = -2M_{z,z} \tag{B.8}$$

The single component required is [30]

$$M_{z,z} = -\pi^2 a^3 \left[\ell n \left(\frac{8a}{b} \right) - 2 \right]^{-1} \tag{B.9}$$

This can be found from formulas for a circular slot aperture, or by a first-principles derivation. The inductance of the perfectly conducting loop [31] is

$$L \simeq \mu_0 a \left[\ell n \left(\frac{8a}{b} \right) - 2 \right]^{-1} \quad \text{for} \quad b \ll a \tag{B.10}$$

Using a reciprocity approach, if the loop is driven (at low frequencies) by a current I, the enclosed magnetic flux is LI and the magnetic moment is $\pi a^2 I$. Equate this to the induced dipole moment $M_{z,z} H_z^{(inc)}$ with the negative of the excluded magnetic flux $\mu_0 \pi a^2 H_z^{(inc)}$ giving

$$M_{z,z} = \frac{-\mu_0}{L} (\pi a^2)^2 \quad \text{for} \quad b \ll a \tag{B.11}$$

in agreement with (B.9).

For class-1 backscattering, we have

$$t_i = -a \sin(\theta) \tag{B.12}$$

for use in (5.10). For an incident E wave, we have the dipole part

$$\left[\overleftrightarrow{1}_i \cdot \overleftrightarrow{P} \cdot \overleftrightarrow{1}_i + \vec{1}_i \times \overleftrightarrow{M} \times \vec{1}_i \right] \cdot \vec{1}_e \vec{1}_e = \cos^2(\theta) P_{x,x} \vec{1}_e \vec{1}_e = -2 \cos^2(\theta) M_{z,z} \vec{1}_e \vec{1}_e \tag{B.13}$$

while for an incident H wave we have the dipole part

$$\begin{aligned} \left[\overleftrightarrow{1}_i \cdot \overleftrightarrow{P} \cdot \overleftrightarrow{1}_i + \vec{1}_i \times \overleftrightarrow{M} \times \vec{1}_i \right] \cdot \vec{1}_h \vec{1}_h &= \left[P_{y,y} - \sin^2(\theta) M_{z,z} \right] \vec{1}_h \vec{1}_h \\ &= -\left[2 + \sin^2(\theta) \right] M_{z,z} \vec{1}_h \vec{1}_h \end{aligned} \tag{B.14}$$

giving the requisite terms for the $p = 3$ representation.

It can be noted at this point that the natural modes have analytic representations. For this body of revolution ($C_{\infty a}$ symmetry [33]) these modes are frequency independent, the same as the eigenmodes, and can be written as [3,6,8]

$$
\begin{aligned}
i_\beta(\phi) &= \begin{cases} [\pi a]^{-1/2}\sin(n\phi) & \text{for fields symmetric with respect to the xz plane (E wave)} \\ \left[\pi a\left[1+1_{n,0}\right]\right]^{-1/2}\cos(n\phi) & \text{for fields antisymmetric with respect to the xz plane (H wave)} \end{cases} \\
\beta &= \begin{pmatrix} sy \\ as \end{pmatrix}, n \\
\alpha &= (\beta, n') \qquad\qquad (B.15) \\
n' &\equiv \text{index of natural frequency for given } \beta \text{ or } n \\
\int_{\text{loop}} i_\beta(\phi)\, i_{\beta'}(\phi) d\ell &= \int_0^{2\pi} i_\beta(\phi)\, i_{\beta'}(\phi) a d\phi \\
&= 1_{\beta,\beta'} \quad \text{(orthonormalization)}
\end{aligned}
$$

where current is taken positive in the ϕ direction, and the modes are orthonormalized as in [7]. Note that, except for $n = 0$, there are two eigenmodes for each n, and two natural modes for each natural frequency s_α. However, they separate neatly according to the two different kinds of incident wave. Furthermore, $n = 0$ gives the uniform loop current for the magnetic-dipole term, and $n = 1$ gives the currents for the two electric-dipole terms. The normalization in (B.15) is appropriate for eigenmodes, but can be changed as desired (e.g. to peak value unity) for natural modes and quasi-static modes.

Consider now the class-2 backscattering for an E-wave. For $p = 3$, we need to evaluate the integral associated with $P_{x,x}$ in (5.20). Noting that only $\ell = x$ gives a significant contribution, we have

$$
\begin{aligned}
p_x^{(1)} &= P_{x,x} \\
\overset{\simeq}{\vec{C}}{}_x^{(1)}(\vec{1}_i, s) &= \overset{\simeq}{\vec{C}}{}_x^{(1)}(-\vec{1}_o, s) \quad \text{(backscattering)} \qquad\qquad (B.16) \\
&= \left\langle \vec{1}_e \vec{1}_e e^{-\gamma \vec{1}_i \cdot \vec{r}_s} \; ; \; \vec{j}{}_{s_x}^{(1)'}(\vec{r}_s') \right\rangle
\end{aligned}
$$

For our thin loop, the surface current density reduces to a line current proportional to $\sin(\phi)\vec{1}_\phi$. Noting the frequency dependence at low frequencies in (5.13), we have

$$
\begin{aligned}
\overset{\simeq}{\vec{C}}{}_x^{(1)}(\vec{1}_i, s) &= C_1 \int_0^{2\pi} \vec{1}_e \vec{1}_e e^{\gamma a \sin(\theta)\cos(\phi)} \cdot \vec{1}_\phi \sin(\phi)\, a d\phi \\
&= aC_1 \cos(\theta)\vec{1}_e \int_0^{2\pi} e^{\gamma a \sin(\theta)\cos(\phi)} \sin^2(\phi) d\phi \\
&= 2aC_1 \cos(\theta)\vec{1}_e \int_0^{\pi} e^{\gamma a \sin(\theta)\cos(\phi)} \sin^2(\phi) d\phi \\
&= 2aC_1 \cos(\theta)\vec{1}_e \pi^{1/2}\Gamma\left(\frac{3}{2}\right)\frac{2}{\gamma a \sin(\theta)} I_1(\gamma a \sin(\theta))
\end{aligned}
$$

$$= \quad 2\pi a C_1 \cos(\theta) \frac{I_1(\gamma a \sin(\theta))}{\gamma a \sin(\theta)} \; \vec{1}_e \tag{B.17}$$

which is given in terms of a modified Bessel function [24]. Letting $s \to 0$ we have

$$\overset{\simeq}{C}{}_x^{(1)}(\vec{1}_i, 0) = \pi a C_1 \cos(\theta) \vec{1}_e \tag{B.18}$$

Equating this to the class-1 results for this dipole term gives

$$\begin{aligned} \overleftrightarrow{1}_i \cdot \overleftrightarrow{P} \cdot \overleftrightarrow{1}_i \cdot \vec{1}_e \vec{1}_e &= \cos^2(\theta) P_{x,x} \vec{1}_e \vec{1}_e = P_{x,x}^{-1} C_1^2 (\pi a)^2 \cos^2(\theta) \vec{1}_e \vec{1}_e \\ C_1 &= \frac{1}{\pi a} P_{x,x} \end{aligned} \tag{B.19}$$

This gives

$$\overset{\simeq}{C}{}_x^{(1)}(\vec{1}_i, s) = 2\pi P_{x,x} \cos(\theta) \frac{I_1(\gamma a \sin(\theta))}{\gamma a \sin(\theta)} \; \vec{1}_e \tag{B.20}$$

and the class-2 form in (5.20) becomes

$$\begin{aligned} -\gamma^2 p_x^{(1)^{-1}} \; \overset{\simeq}{C}{}_x^{(1)}(\vec{1}_i, s) \; \overset{\simeq}{C}{}_x^{(1)}(\vec{1}_i, s) &= -\gamma^2 4 \, P_{x,x} \cos^2(\theta) \left[\frac{I_1(\gamma a \sin(\theta))}{\gamma a \sin(\theta)} \right]^2 \vec{1}_e \vec{1}_e \\ &\to -\gamma^2 \, P_{x,x} \cos^2(\theta) \, \vec{1}_e \vec{1}_e \quad \text{as } s \to 0 \end{aligned} \tag{B.21}$$

An alternate form for $s = j\omega$ has

$$\overset{\simeq}{C}{}_x^{(1)}(\vec{1}_i, j\omega) = 2 \, P_{x,x} \cos(\theta) \, \frac{J_1\left(\frac{\omega a}{c} \sin(\theta)\right)}{\frac{\omega a}{c} \sin(\theta)} \; \vec{1}_e \tag{B.22}$$

which is in terms of the usual Bessel functions.

For an H wave, the class-2 backscattering dyad has both electric and magnetic-dipole terms. First we have for the electric-dipole part

$$\begin{aligned} p_y^{(1)} &= P_{y,y} \\ \overset{\simeq}{C}{}_y^{(1)}(\vec{1}_i, s) &= \overset{\simeq}{C}{}_y^{(1)}(-\vec{1}_o, s) \quad \text{(backscattering)} \\ &= \left\langle \vec{1}_h \vec{1}_h e^{-\gamma \vec{1}_i \cdot \vec{r}'_s} \; ; \; \vec{j}_{s_y}^{(1)'}(\vec{r}'_s) \right\rangle \end{aligned} \tag{B.23}$$

For this term, the surface current density reduces to a line current proportional to $\cos(\phi) \vec{1}_\phi$. Now we have

$$\overset{\simeq}{C}{}_y^{(1)}(\vec{1}_i, s) = C_2 \int_0^{2\pi} \vec{1}_h \vec{1}_h e^{\gamma a \sin(\theta)\cos(\phi)} \cdot \vec{1}_\phi \cos(\phi) \, a d\phi$$

$$
\begin{aligned}
&= aC_2\,\vec{1}_h \int_0^{2\pi} e^{\gamma a \sin(\theta)\cos(\phi)} \cos^2(\phi) d\phi \\
&= 2aC_2\,\vec{1}_h \int_0^{\pi} e^{\gamma a \sin(\theta)\cos(\phi)} \left[1 - \sin^2(\phi)\right] d\phi \\
&= 2aC_2\,\vec{1}_h \left\{ \pi^{1/2}\,\Gamma\left(\frac{1}{2}\right) I_0(\gamma a \sin(\theta)) - \pi^{1/2}\Gamma\left(\frac{3}{2}\right) \frac{I_1(\gamma a \sin(\theta))}{\gamma a \sin(\theta)} \right\} \\
&= 2\pi a C_2\,\vec{1}_h \left\{ I_0(\gamma a \sin(\theta)) - \frac{I_1(\gamma a \sin(\theta))}{\gamma a \sin(\theta)} \right\} \qquad \text{(B.24)}
\end{aligned}
$$

Letting $s \rightarrow 0$ gives

$$
\vec{\tilde{C}}_y^{(1)}(\vec{1}_i, 0) = \pi a C_2\,\vec{1}_h \qquad \text{(B.25)}
$$

Equating this to the class-1 results for this electric-dipole term gives

$$
\begin{aligned}
&\overleftrightarrow{1}_i \cdot \overleftrightarrow{P} \cdot \overleftrightarrow{1}_i \cdot \vec{1}_h\,\vec{1}_h = P_{y,y}\,\vec{1}_h\,\vec{1}_h = P_{y,y}^{-1} C_2^2 (\pi a)^2\,\vec{1}_h\,\vec{1}_h \\
&C_2 = \frac{1}{\pi a} P_{y,y} \qquad \text{(B.26)}
\end{aligned}
$$

This gives

$$
\vec{\tilde{C}}_y^{(1)}(\vec{1}_i, 0) = 2P_{y,y} \left\{ I_0(\gamma a \sin(\theta)) - \frac{I_1(\gamma a \sin(\theta))}{\gamma a \sin(\theta)} \right\} \vec{1}_h \qquad \text{(B.27)}
$$

and the class-2 form in (5.20) becomes

$$
\begin{aligned}
-\gamma^2 p_y^{(1)^{-1}}\ \vec{\tilde{C}}_y^{(1)}(\vec{1}_i, s)\ \vec{\tilde{C}}_y^{(1)}(\vec{1}_i, s) &= -\gamma^2 4\, P_{y,y} \left\{ I_0(\gamma a \sin(\theta)) - \frac{I_1(\gamma a \sin(\theta))}{\gamma a \sin(\theta)} \right\}^2 \vec{1}_h\,\vec{1}_h \\
&\rightarrow -\gamma^2\, P_{y,y}\,\vec{1}_h\,\vec{1}_h \quad \text{as } s \rightarrow 0 \qquad \text{(B.28)}
\end{aligned}
$$

An alternate form for $s = j\omega$

$$
\vec{\tilde{C}}_y^{(1)}(\vec{1}_i, j\omega) = 2\, P_{y,y} \left\{ J_0\left(\frac{\omega a}{c} \sin(\theta)\right) - \frac{J_1\left(\frac{\omega a}{c} \sin(\theta)\right)}{\frac{\omega a}{c} \sin(\theta)} \right\} \vec{1}_h \qquad \text{(B.29)}
$$

The H-wave response also has a magnetic-dipole term in (5.20) for which we have

$$
\begin{aligned}
m_z^{(0)} &= M_{z,z} \\
\vec{\tilde{C}}_z^{(0)}(\vec{1}_i, s) &= \vec{\tilde{C}}_z^{(0)}(-\vec{1}_o, s) \quad \text{(backscattering)} \qquad \text{(B.30)} \\
&= \gamma^{-1} \left\langle \vec{1}_h\,\vec{1}_h\, e^{-\gamma \vec{1}_i \cdot \vec{r}'_s}\ ;\ \vec{j}_{s_z}^{(0)'}(\vec{r}'_s) \right\rangle
\end{aligned}
$$

For this term, the surface current density reduces to a uniform line current in th direction $\vec{1}_\phi$. Now we have

$$\begin{aligned}
\overset{\sim}{\vec{C}}{}_z^{(0)}(\vec{1}_i, s) &= C_3 \gamma^{-1} \int_0^{2\pi} \vec{1}_h \vec{1}_h e^{\gamma a \sin(\theta)\cos(\phi)} \cdot \vec{1}_\phi \, a d\phi \\
&= \frac{a}{\gamma} C_3 \vec{1}_h \int_0^{2\pi} e^{\gamma a \sin(\theta)\cos(\phi)} \cos(\phi) d\phi \\
&= \frac{2a}{\gamma} C_3 \vec{1}_h \int_0^{\pi} e^{\gamma a \sin(\theta)\cos(\phi)} \cos(\phi) d\phi \\
&= \frac{2\pi a}{\gamma} C_3 I_1(\gamma \sin(\theta)) \vec{1}_h
\end{aligned} \tag{B.31}$$

Letting $s \rightarrow 0$ gives

$$\overset{\sim}{\vec{C}}{}_z^{(0)}(\vec{1}_i, 0) = \pi a^2 \sin(\theta) C_3 \vec{1}_h \tag{B.32}$$

Equating this to the class-1 results for this magnetic-dipole term gives

$$\begin{aligned}
-\left[\vec{1}_i \times \overleftrightarrow{M} \times \vec{1}_i\right] \cdot \vec{1}_h \vec{1}_h &= -\sin^2(\theta) M_{z,z} \vec{1}_h \vec{1}_h \\
&= -M_{z,z}^{-1} C_3^2 (\pi a^2)^2 \sin^2(\theta) \vec{1}_h \vec{1}_h \\
C_3 &= \frac{1}{\pi a^2} M_{z,z}
\end{aligned} \tag{B.33}$$

This gives

$$\overset{\sim}{\vec{C}}{}_z^{(0)}(\vec{1}_i, 0) = 2 M_{z,z} \frac{I_1(\gamma a \sin(\theta))}{\gamma a} \vec{1}_h \tag{B.34}$$

and the class-2 form in (5.20) becomes

$$\begin{aligned}
\gamma^2 m_z^{(0)^{-1}} \; \overset{\sim}{\vec{C}}{}_z^{(0)}(\vec{1}_i, s) \; \overset{\sim}{\vec{C}}{}_z^{(0)}(\vec{1}_i, s) &= \gamma^2 4 M_{z,z} \left\{ \frac{I_1(\gamma a \sin(\theta))}{\gamma a} \right\}^2 \vec{1}_h \vec{1}_h \\
&\rightarrow \gamma^2 M_{z,z} \vec{1}_h \vec{1}_h \quad \text{as } s \rightarrow 0
\end{aligned} \tag{B.35}$$

An alternate form for $s = j\omega$ has

$$\overset{\sim}{\vec{C}}{}_z^{(0)}(\vec{1}_i, j\omega) = 2 M_{z,z} \frac{J_1\left(\frac{\omega a}{c} \sin(\theta)\right)}{\frac{\omega a}{c}} \vec{1}_h \tag{B.36}$$

B.2 Numerical results

This section presents numerous results illustrating the backscattering dyadic from a thin circular loop for a variety of polarizations and incident angles. In computing the backscattering dyadic, both the class-1 and class-2 forms of the SEM modified pole series are used. The performance of the various SEM solutions is measured by comparison to a reference frequency domain solution of the backscattering dyadic.

The characteristics of this reference solution and how it is obtained will be addressed in the subsequent text. For the results presented here, the reference solution is considered correct, and the performance of the SEM modified pole series will be evaluated based on the agreement of these solutions with the reference solution.

Unlike the results presented for the straight wire in Appendix A, the numerical results for the circular loop are *not* computed using a method of moments approach. Instead, the rotational symmetry of the loop is utilized to obtain an analytic solution for the current induced on the loop by the incident field. This is accomplished by expanding the current, kernel, and incident field of the EFIE in a spatial Fourier series. Once the current is known, standard potential theory can be applied to find the far backscattered field.

The Fourier series approach for solving the current on a thin circular loop is treated extensively in the literature [17-19,25]. In these sources, the loop antenna is primarily studied, but the extension of the methodology to the scattering case is straightforward. The case of electromagnetic scattering by loaded wire loops has been examined by Harrington [20]. The Fourier series solution to the loop antenna is also investigated from an SEM perspective in several sources [3,6].

As noted earlier, the purpose of this appendix is to present results depicting the backscattering dyadic from a thin circular loop. A detailed theoretical treatment of the loop scatterer is not relevant here. However, in order to provide a basis for the numerical results, a concise summary of the theory is necessary. The following summary relies heavily on the expositions by Wu [19], King and Harrison [25], and Harrington [20] with the only distinct difference being the extension of the theory to the complex plane, or s-domain. Some notational changes have been made in order to avoid conflicts with the notation already established.

B.2.1 Summary of the theory

Due to the thin nature of the loop ($a \gg b$) in fig. B.1, the integral equation in (4.1) can be significantly reduced to

$$a\,\tilde{E}_{\phi}^{(inc)}(a,\phi,0;s) \;=\; \int_0^{2\pi} \tilde{G}(\phi-\phi';s)\,\tilde{I}(\phi';s)d\phi' \tag{B.37}$$

where the various functions have been expressed in terms of cylindrical coordinates and the complex frequency s. The quantity $\tilde{E}_{\phi}^{(inc)}$ denotes the ϕ-component of the incident electric field along the wire at $\rho = a$, $z = 0$. Similarly, the loop current at any angle ϕ on the wire is represented by $\tilde{I}(\phi)$. The current $\tilde{I}(\phi)$ and the ϕ-component of the incident field are related to one another in free space by the function $\tilde{G}(\phi-\phi')$.

As suggested in the introduction, a solution for the loop current can be found by expanding each of the aforementioned functions in a Fourier series as

$$\tilde{I}(\phi;s) \;=\; \frac{E_0}{Z_0}\sum_{n=-\infty}^{\infty} \tilde{a}_n(s)e^{jn\phi},$$

$$\tilde{G}(\phi-\phi';s) = \sum_{n=-\infty}^{\infty} \tilde{G}_n(s)e^{jn(\phi-\phi')}, \tag{B.38}$$

$$\tilde{E}_\phi^{(\mathrm{inc})}(a,\phi,0;s) = E_0 \sum_{n=-\infty}^{\infty} \tilde{e}_n^{(\mathrm{inc})}(s,\vec{1}_\mathrm{i},\vec{1}_\mathrm{p})e^{jn\phi},$$

$$= E_0\,\vec{1}_\mathrm{p}\,e^{-\gamma\vec{1}_\mathrm{i}\cdot\vec{r}}$$

$$\tilde{f}(s)=1,\ \vec{1}_\mathrm{p}=\vec{1}_\mathrm{e}\ \text{or}\ \vec{1}_\mathrm{h}\,.$$

The Fourier coefficient $\tilde{a}_n$ of the current expansion is related to the Fourier coefficients $\tilde{G}_n$ and $\tilde{e}_n^{(\mathrm{inc})}$ by

$$\tilde{a}_n(s) = \frac{a\,\tilde{e}_n^{(\mathrm{inc})}(s,\vec{1}_\mathrm{i},\vec{1}_\mathrm{p})}{2\pi\,\tilde{G}_n(s)}. \tag{B.39}$$

This expression can be obtained by using (B.38) in (B.37) and performing the integration.

Note that here the modes have been defined in complex form $e^{jn\phi}$. For real-valued modes (such as one might measure), one can use $\cos(n\phi)$ and $\sin(n\phi)$, noting the two-fold degeneracy for each n, except $n=0$, due to the symmetry [33]. Furthermore, in the present problem, natural modes and eigenmodes (here frequency independent) are one and the same. In (B.15), the eigenmodes (now also natural modes) are orthonormalized for convenience in the general eigenmode expansion [7]. By combining the $\tilde{a}_n e^{jn\phi}$ with $\tilde{a}_{-n}e^{-jn\phi}$ for $n \geq 1$ in (B.38), one obtains a coefficient times an eigenmode proportional to $\sin(n\phi)$ for E-wave incidence, and proportional to $\cos(n\phi)$ for H-wave incidence. The $n=0$ term differs from the others by a factor of $2^{-1/2}$, which when squared gives $1/2$, as will appear consistent with the later expressions ((B.53) and (B.54)).

The next step in completing the solution for the loop current is to find expressions for $\tilde{G}_n$ and $\tilde{e}_n^{(\mathrm{inc})}$. The development of an expression for $\tilde{G}_n$ can be quite tedious. For completeness, only the final result will be given here. King and Harrison [25] provide a detailed development of this coefficient. The coefficient $\tilde{G}_n$ is given by

$$\tilde{G}_n(s) = \tilde{G}_{-n}(s) = \frac{1}{4\pi}\left[\gamma a\left(\frac{1}{2}\tilde{V}_{n+1}(s) + \frac{1}{2}\tilde{V}_{n-1}(s)\right) + \frac{n^2}{\gamma a}\tilde{V}_n(s)\right]. \tag{B.40}$$

The coefficients $\tilde{V}_n$ have been approximated by Wu [19] to be

$$\tilde{V}_0(s) = \frac{1}{\pi}\left[\ell n\left(\frac{8a}{b}\right) - \frac{\pi}{2}\int_0^{-j2\gamma a}[\Omega_0(x) + jJ_0(x)]\,dx\right]$$

$$\tilde{V}_n(s) = \tilde{V}_{-n}(s) = \frac{1}{\pi}\left[K_0\left(\frac{nb}{a}\right)I_0\left(\frac{nb}{a}\right) + D_n - \frac{\pi}{2}\int_0^{-j2\gamma a}[\Omega_{2n}(x) + jJ_{2n}(x)]\,dx\right]. \tag{B.41}$$

The functions I_0 and K_0 are zeroth order modified Bessel functions of the first and second kind, respectively,

J_{2n} is a Bessel function of order $2n$, Ω_{2n} is a Lommel-Weber function of order $2n$, and

$$D_n = \ell n(4n) + \gamma_{ec} - 2\sum_{m=0}^{n-1} \frac{1}{2m+1} \tag{B.42}$$

where γ_{ec} is Euler's constant [24]. Routines for evaluating the integral of the Bessel and Lommel-Weber functions are given in [12].

Finally, the coefficient $\tilde{e}_n^{(inc)}$ can be determined from the following expression

$$\tilde{e}_n^{(inc)}(s, \vec{1}_i, \vec{1}_p) = \frac{1}{2\pi E_o} \int_0^{2\pi} \vec{1}_\phi \cdot \overset{\simeq}{\vec{E}}^{(inc)} e^{-jn\phi} d\phi. \tag{B.43}$$

This expression represents the usual integral equation for the Fourier coefficient. For E-wave polarization, (B.2) (with $E_o = 1$) can be substituted into (B.43). Upon integration, the expression for the Fourier coefficient of the incident field becomes

$$\tilde{e}_n^{(inc)}(s, \vec{1}_i, \vec{1}_e) = jn\cos(\theta_{inc}) \left[\frac{I_n(\gamma a \sin(\theta_{inc}))}{\gamma a \sin(\theta_{inc})}\right]. \tag{B.44}$$

Similarly, for H-wave polarization, (B.3) can be used in (B.43) to give

$$\tilde{e}_n^{(inc)}(s, \vec{1}_i, \vec{1}_h) = I_n'(\gamma a \sin(\theta_{inc})) \tag{B.45}$$

where the prime $'$ denotes the derivative of the modified Bessel function with respect to its argument. Both (B.44) and (B.45) have physical significance in that they are coupling coefficients. The spatial Fourier modes on the loop are of the form $e^{jn\phi}$. Hence, the integral in (B.43) represents the coupling of the incident electric field to the nth Fourier mode.

Now that a solution for the loop current has been found, the far backscattered field can be computed via standard potential theory [11]. Because the loop is thin, the far-field approximation of the electric field can be expressed as

$$\overset{\simeq}{\vec{E}}_f(s) = \frac{-s\mu}{4\pi r} e^{-\gamma r} \int_0^{2\pi} \tilde{I}(\phi'; s) \cdot \vec{1}_\phi \; e^{\gamma \vec{1}_o \cdot a \vec{1}_\Psi} \, a d\phi. \tag{B.46}$$

Using (B.38) and (B.39), the vector $\vec{1}_p$ component ($\vec{1}_e$ or $\vec{1}_h$) of the backscattered electric field becomes

$$\overset{\simeq}{\vec{E}}_f(s) \cdot \vec{1}_p = \frac{-E_0 \gamma a^2}{4\pi r} e^{-\gamma r} \left\{ \sum_{n=-\infty}^{\infty} \frac{\tilde{e}_n^{(inc)}(s, \vec{1}_i, \vec{1}_p)}{\tilde{G}_n(s)} \left(\frac{1}{2\pi} \int_0^{2\pi} \vec{1}_p \cdot \vec{1}_\phi \, e^{\gamma \vec{1}_o \cdot a \vec{1}_\Psi} e^{jn\phi} d\phi \right) \right\}. \tag{B.47}$$

The term in parentheses of (B.47) has the form of a coupling coefficient and is similar to the expression in (B.43). This coupling coefficient effectively quantifies how much of the nth Fourier mode couples to the radiated field. By denoting this coupling coefficient with the term $\tilde{e}_n^{(r)}$, the expression for the far electric

field becomes

$$\overleftrightarrow{E}_{\mathrm{f}}(s)\cdot\vec{1}_{\mathrm{p}}=\frac{-E_0\gamma a^2}{4\pi r}\mathrm{e}^{-\gamma r}\sum_{n=-\infty}^{\infty}\frac{\tilde{e}_n^{(\mathrm{inc})}(s,\vec{1}_{\mathrm{i}},\vec{1}_{\mathrm{p}})\,\tilde{e}_n^{(\mathrm{r})}(s,\vec{1}_{\mathrm{o}},\vec{1}_{\mathrm{p}})}{\tilde{G}_n(s)} \tag{B.48}$$

where

$$\tilde{e}_n^{(\mathrm{r})}(s,\vec{1}_{\mathrm{o}},\vec{1}_{\mathrm{p}})=\frac{1}{2\pi}\int_0^{2\pi}\vec{1}_{\mathrm{p}}\cdot\vec{1}_{\phi}\,\mathrm{e}^{\gamma\vec{1}_{\mathrm{o}}\cdot a\vec{1}_{\Psi}}e^{jn\phi}\,d\phi. \tag{B.49}$$

For backscattering ($\vec{1}_{\mathrm{o}}=-\vec{1}_{\mathrm{i}}$), where both the transmitter and receiver are located in the x,z plane at an angle θ_{inc} from the z axis, the coefficients $\tilde{e}_n^{(\mathrm{inc})}$ and $\tilde{e}_n^{(\mathrm{r})}$ are equivalent for either E-wave or H-wave polarization. Hence, by using (B.44) and (B.45), we can write the product of these two coefficients as

$$\tilde{e}_n^{(\mathrm{inc})}(s,\vec{1}_{\mathrm{i}},\vec{1}_{\mathrm{e}})\,\tilde{e}_n^{(\mathrm{r})}(s,-\vec{1}_{\mathrm{i}},\vec{1}_{\mathrm{e}})=-n^2\cos^2\theta_{\mathrm{inc}}\left[\frac{I_n(\gamma a\sin(\theta_{\mathrm{inc}}))}{\gamma a\sin(\theta_{\mathrm{inc}})}\right]^2 \tag{B.50}$$

for E-wave polarization, and

$$\tilde{e}_n^{(\mathrm{inc})}(s,\vec{1}_{\mathrm{i}},\vec{1}_{\mathrm{h}})\,\tilde{e}_n^{(\mathrm{r})}(s,-\vec{1}_{\mathrm{i}},\vec{1}_{\mathrm{h}})=\left[I_n'(\gamma a\sin(\theta_{\mathrm{inc}}))\right]^2. \tag{B.51}$$

for H-wave polarization.

Using (B.48), the backscattering dyadic $\overleftrightarrow{\Lambda}_{\mathrm{b}}$ can be written as

$$\overleftrightarrow{\Lambda}_{\mathrm{b}}(s)=-\gamma a^2\sum_{n=-\infty}^{\infty}\frac{\tilde{e}_n^{(\mathrm{inc})}(s,\vec{1}_{\mathrm{i}},\vec{1}_{\mathrm{p}})\,\tilde{e}_n^{(\mathrm{r})}(s,-\vec{1}_{\mathrm{i}},\vec{1}_{\mathrm{p}})}{\tilde{G}_n(s)}\;\vec{1}_{\mathrm{p}}\vec{1}_{\mathrm{p}}\,. \tag{B.52}$$

By using (B.50) and the identity $I_n(x)=I_{-n}(x)$, the expression for the backscattering dyadic in (B.52) can be specialized for E-wave backscattering as

$$\overleftrightarrow{\Lambda}_{\mathrm{b_{ee}}}(s)=2\gamma a^2\cos^2(\theta_{\mathrm{inc}})\sum_{n=1}^{\infty}\frac{n^2}{\tilde{G}_n(s)}\left[\frac{I_n(\gamma a\sin(\theta_{\mathrm{inc}}))}{\gamma a\sin(\theta_{\mathrm{inc}})}\right]^2\vec{1}_{\mathrm{e}}\vec{1}_{\mathrm{e}}\,. \tag{B.53}$$

Similarly, by using (B.51) and the relationship $I_n'(x)=I_{-n}'(x)$ in (B.52), an expression for H-wave backscattering can be written as

$$\overleftrightarrow{\Lambda}_{\mathrm{b_{hh}}}(s)=-\gamma a^2\left[\frac{\left[I_0'(\gamma a\sin(\theta_{\mathrm{inc}}))\right]^2}{G_0(s)}+2\sum_{n=1}^{\infty}\frac{\left[I_n'(\gamma a\sin(\theta_{\mathrm{inc}}))\right]^2}{G_n(s)}\right]\vec{1}_{\mathrm{h}}\vec{1}_{\mathrm{h}}\,. \tag{B.54}$$

The reference solution contained in the numerical results is either (B.53) or (B.54) with s replaced by $j\omega$.

B.2.2 The SEM Solution

To express the backscattering dyadic in terms of the SEM, Umashankar [6] shows that the coefficient $1/\tilde{G}_n(s)$ (referred to as the transfer admittance) can be expressed in a singularity series as

$$\frac{1}{\tilde{G}_n(s)} = \sum_{\alpha} \frac{R_{n\alpha}}{s - s_{n\alpha}} \tag{B.55}$$

where $R_{n\alpha}$ is the residue of $1/\tilde{G}_n(s)$ at the pole $s = s_{n\alpha}$. The SEM representation of the backscattering dyadic can be determined now by substituting (B.55) into (B.52). After some manipulation, the SEM representation of the backscattering dyadic can be written as

$$\overleftrightarrow{\Lambda}_{\mathrm{b}}(s) = a^2 \left\{ \sum_{n=-\infty}^{\infty} \left[\sum_{\alpha} \left(\frac{s}{s_{n\alpha}} \right) \frac{1}{s - s_{n\alpha}} W_{n\alpha} \right] \tilde{e}_n^{(\mathrm{inc})}(s, \vec{1}_{\mathrm{i}}, \vec{1}_{\mathrm{p}}) \, \tilde{e}_n^{(\mathrm{r})}(s, -\vec{1}_{\mathrm{i}}, \vec{1}_{\mathrm{p}}) \right\} \vec{1}_{\mathrm{p}} \vec{1}_{\mathrm{p}} \tag{B.56}$$

$$W_{n\alpha} = \frac{-s_{n\alpha} \mu R_{n\alpha}}{Z_0}.$$

This equation is the $p = 1$ case of the modified pole series for the class-2 representation of the backscattering dyadic. The other cases ($p = 0$, 2, and 3) follow as shown in chapter 5 of the note. By using (B.50), the class-2 form of the E-polarized backscattering dyadic can be written as

$$\overleftrightarrow{\Lambda}_{\mathrm{b_{ee}}}(s) = -2a^2 \cos^2(\theta_{\mathrm{inc}}) \sum_{n=1}^{\infty} \sum_{\alpha} \left(\frac{s}{s_{n\alpha}} \right)^p \frac{W_{n\alpha}}{s - s_{n\alpha}} n^2 \left[\frac{I_n(\gamma a \sin(\theta_{\mathrm{inc}}))}{\gamma a \sin(\theta_{\mathrm{inc}})} \right]^2 \vec{1}_{\mathrm{e}} \vec{1}_{\mathrm{e}}$$
$$\text{for } p = 0, 1, 2, 3. \tag{B.57}$$

We can also use (B.51) to write the class-2 form of the H-polarized backscattering dyadic as

$$\overleftrightarrow{\Lambda}_{\mathrm{b_{hh}}}(s) = a^2 \left\{ \sum_{n=0}^{\infty} [1 + 1_{n,0}] \sum_{\alpha} \left(\frac{s}{s_{n\alpha}} \right)^p \frac{W_{n\alpha}}{s - s_{n\alpha}} [I_n'(\gamma a \sin(\theta_{\mathrm{inc}}))]^2 \right\} \vec{1}_{\mathrm{h}} \vec{1}_{\mathrm{h}}$$
$$\text{for } p = 0, 1, 2, 3. \tag{B.58}$$

Of course, the $p = 3$ form in (B.57) and (B.58) has the additional polarizability term whose functional form has been already been addressed.

Similarly, the class-1 representation of the backscattering dyadic can be expressed as

$$\overleftrightarrow{\Lambda}_{\mathrm{b}}(s) = a^2 \sum_{n=-\infty}^{\infty} \left\{ \sum_{\alpha} \left(\frac{s}{s_{n\alpha}} \right)^p \frac{\mathrm{e}^{-(s - s_{n\alpha}) t_{\mathrm{i}}}}{s - s_{n\alpha}} W_{n\alpha} \, \tilde{e}_n^{(\mathrm{inc})}(s, \vec{1}_{\mathrm{i}}, \vec{1}_{\mathrm{p}}) \, \tilde{e}_n^{(\mathrm{r})}(s, -\vec{1}_{\mathrm{i}}, \vec{1}_{\mathrm{p}}) \right\} \vec{1}_{\mathrm{p}} \vec{1}_{\mathrm{p}}$$
$$\text{for } p = 0, 1, 2, 3 \tag{B.59}$$

where t_{i} has been defined in (B.12). For E-wave polarization, the class-1 form of the backscattering dyadic

can be expressed as

$$\overleftrightarrow{\Lambda}_{b_{ee}}(s) = -2a^2\cos^2(\theta_{inc})\sum_{n=1}^{\infty}\sum_{\alpha}\left(\frac{s}{s_{n\alpha}}\right)^p \frac{e^{-(s-s_{n\alpha})t_i}}{s-s_{n\alpha}} W_{n\alpha}\, n^2 \left[\frac{I_n(\gamma_{n\alpha}a\sin(\theta_{inc}))}{\gamma_{n\alpha}a\sin(\theta_{inc})}\right]^2 \vec{1}_e\vec{1}_e \quad \text{for } p = 0,1,2,3 \tag{B.60}$$

$$\gamma_{n\alpha} = \frac{s_{n\alpha}}{c}.$$

The class-1 modified pole series representation of the backscattering dyadic for H-wave polarization can also be written as

$$\overleftrightarrow{\Lambda}_{b_{hh}}(s) = a^2\left\{\sum_{n=0}^{\infty}[1+1_{0,n}]\sum_{\alpha}\left(\frac{s}{s_{n\alpha}}\right)^p \frac{e^{-(s-s_{n\alpha})t_i}}{s-s_{n\alpha}} W_{n\alpha}\,[I_n'(\gamma_{n\alpha}a\sin(\theta_{inc}))]^2\right\}\vec{1}_h\vec{1}_h \quad \text{for } p = 0,1,2,3. \tag{B.61}$$

The class-1, p =3 solution also has an additional polarizability term which is not shown in (B.60) or (B.61). This polarizability term is given in (B.13) and (B.14) for E-wave and H-wave polarizations, respectively. Note that a distinguishing difference between the class-1 and class-2 representations is that in the case of the class-1 representation, the coefficients $\tilde{e}_n^{(inc)}$ and $\tilde{e}_n^{(r)}$ are now evaluated at the pole locations of the nth Fourier mode.

B.2.3 Results

The results presented below are computed for a circular loop having a loop radius to wire radius $(a/b) = 200$. By choosing a/b to be 200, we are certain that the thin wire approximation used in (B.37) and elsewhere in this appendix is valid. In addition, only the Fourier modes $n = 0$ through $n = 5$ are used in obtaining both the reference solution and the SEM solutions. Using additional modes does not alter the solutions over the frequency range of interest.

The SEM solutions of the backscattering dyadic are constructed with roughly 112 poles including conjugate pairs. The poles of the loop considered here are shown in fig. B.2. The poles locations essentially represent the zeros of $\tilde{G}_n(s)$. Since each Fourier mode n has a corresponding pole distribution, the poles in fig. B.2 have been grouped by their respective modes. Furthermore, in accordance with the works of Umashankar [6] and Blackburn [3], the pole locations for each mode can be divided into the following three categories:

Type I For each mode n, there is a single pole near the $j\omega$ axis at approximately $\omega = n$.

Type II There are $n + 1$ poles (including conjugate pairs) which lie roughly on the left hand side of an

ellipse centered at $s = 0$ and with semi-major axis slightly larger than n.

Type III The poles belonging to this type lie in layers roughly parallel to the $j\omega$ axis. An infinite number of poles is contained in each layer, and they are space approximately $\Delta\omega = \pi a/c$ units apart.

The upper plot of fig. B.2 shows the pole locations for the Type I and Type II poles associated with the first six Fourier modes ($n = 0$ to $n = 5$). A number of the Type III poles associated with these modes (not including conjugate pairs) are shown in the lower plot of fig. B.2.

Before discussing the results, there is one issue that needs to be addressed. This issue concerns the pole at $s = 0$ of the zeroth mode. For E-wave backscattering, this pole does not pose a problem for either the class-1 or class-2 form of the SEM representation since the zeroth mode does not couple to the response. Furthermore, as shown in [5], the natural frequency at $s = 0$ is not a pole of scattering (does not couple to the incident field). Hence, it is automatically excluded from the summation for the class-1 representation. However, for H-wave backscattering, this pole does create a problem for the class-2 form of the modified pole series. By inspecting (B.58), one notices that the expression becomes indeterminate when the pole at the origin is included in the summation. Actually, only the p=2 and p=3 forms of the class-2 representation are indeterminate when this pole is used. In order to be consistent, we have chosen to exclude this pole in all of the SEM solutions presented here. Consequently, the performance of the p=1 solution has been modified. The $p = 0$ solution is not affected by the inclusion of the pole at $s = 0$. This can easily be verified by substituting $s_{0,0} = 0$ into the $p = 0$ form of (B.58). Although the exclusion of the pole at s=0 degrades the p=1 solution, we can still study the relative performance of the various modified pole series solutions without including this pole.

As in the previous case of the thin wire, parameters are again chosen to test the convergence properties of the series. In our thin-wire loop example, the symmetry of the loop has

$$\begin{aligned} L_o &= L = 2a \\ t_o &= \frac{L_o}{c} = \frac{2a}{c} \\ t_b &= -t_f = \frac{a}{c}\sin(\theta_{inc}) \\ t_{bs} &= t_o + 2[t_f - t_b] = t_o[1 - 2\sin(\theta_{inc})] \\ &\equiv \text{backscatter time window} \end{aligned} \tag{B.62}$$

This gives a range of θ_{inc} as

$$0 \leq \theta_{inc} \leq 30^\circ \quad \text{for} \quad t_{bs} \geq 0. \tag{B.63}$$

(Note that this is the complement of the range in (A.16).) Again t_i, chosen per (4.8), gives series convergence, a *necessary* condition for lack of an additional entire function. In the illustrations, $\theta_{inc} = 45^\circ$ and 90° violate

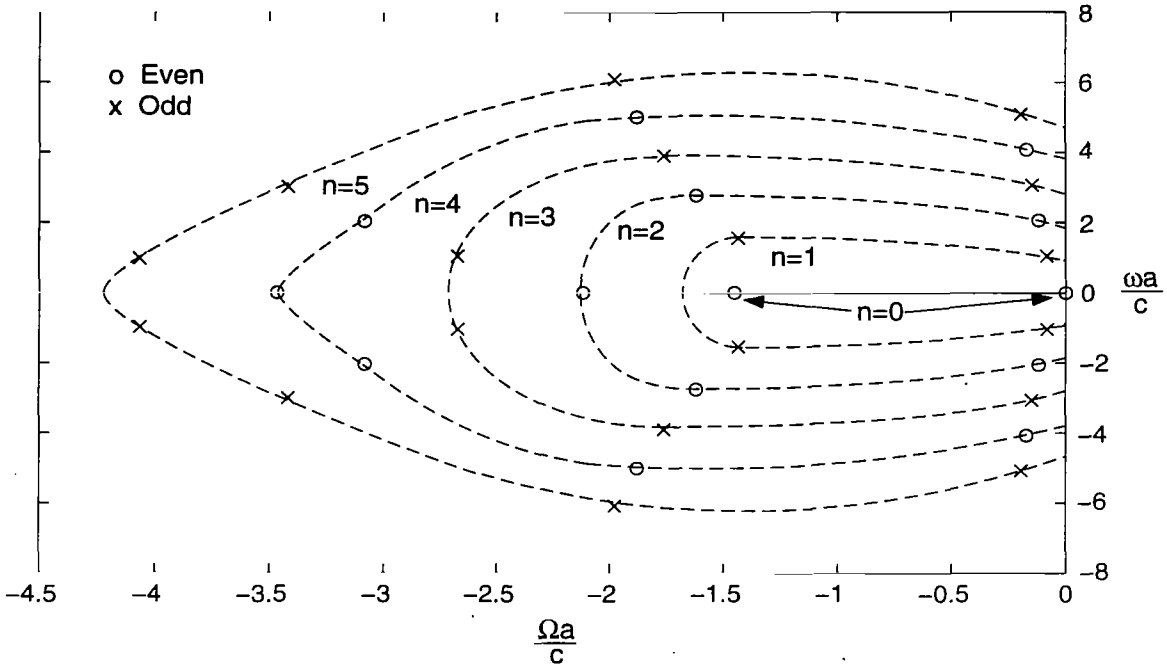

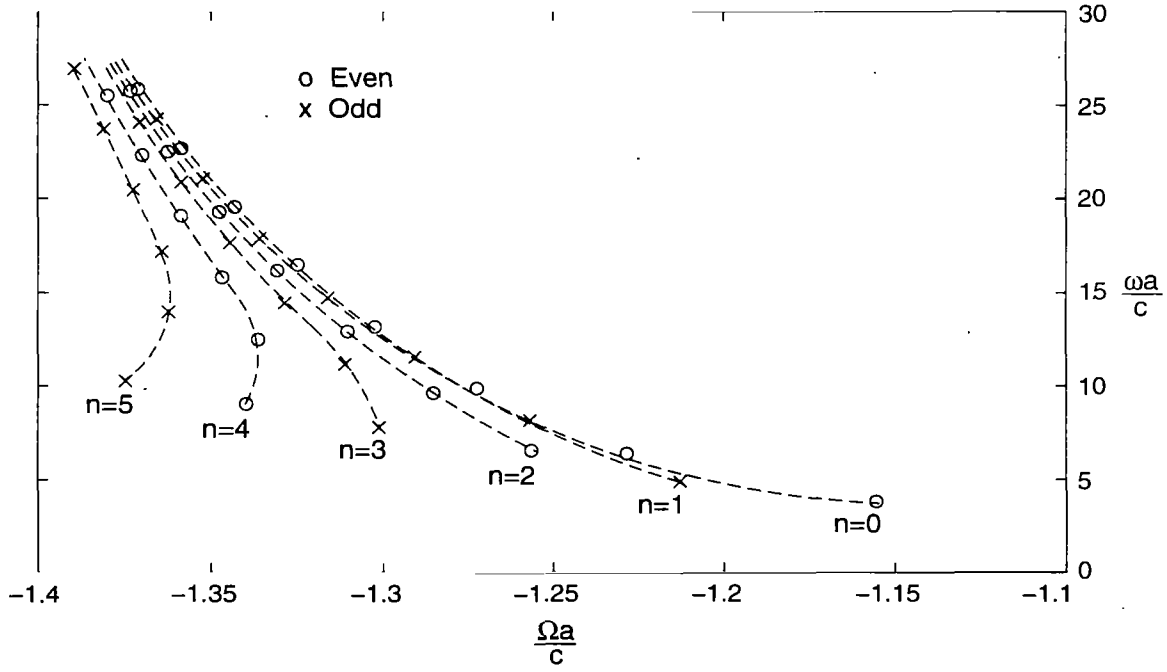

Figure B.2. The pole locations of the thin circular loop, $a/b = 200$. The top figure shows the Type I and II poles grouped by their corresponding Fourier mode. The bottom figure shows the Type III poles.

this condition, while $\theta_{\text{inc}} = 0°$ satisfies condition.

The reader should note that due to the rotational symmetry of the loop, the low frequency response is dominated by the lower n. The magnetic dipole moment is associated exclusively with $n = 0$, and does not appear in any E-wave response. The electric dipole moment is associated exclusively with $n = 1$. Higher order terms give quadrupole, etc. For all E-wave responses, the number of modes used begins with $n = 1$ in the count, while for H-wave responses, the number of modes used begins with $n = 0$. For $\theta_{\text{inc}} = 0°$ (a special case), the incident wave can be labelled as either E-wave or H-wave, but the first mode is $n = 1$.

Figures B.3 through B.16 depict the magnitude of the backscattering dyadic as a function of frequency for the orientations and polarizations mentioned above. In Figures B.3 though B.8, the E-polarized backscattering dyadic $\tilde{\Lambda}_{\text{b}_{\text{ee}}}$ is investigated for $\theta_{\text{inc}} = 0°$ and 45°. Similarly, figs. B.9 and B.16 show the H-polarized backscattering $\tilde{\Lambda}_{\text{b}_{\text{hh}}}$ for $\theta_{\text{inc}} = 45°$ and 90° . For each orientation and polarization, both the class-1 and class-2 forms of the modified pole series are used to compute the backscattering dyadic. As was done in Appendix A, figs. B.3 through B.16 each contain two plots. The upper plot of each figure depicts the scattering dyadic on a log-scale, and the lower plot illustrates the scattering dyadic on a linear scale.

Figure B.3 shows the magnitude of $\tilde{\Lambda}_{\text{b}_{\text{ee}}}$ for an incident angle of 45°. The SEM solutions were obtained using the class-1 form of the modified pole series. As one can see from the upper plot, excellent agreement with the reference solution is obtained in the low frequency region with the $p = 2$ and $p = 3$ solutions. The $p = 1$ solution does converge well for some low frequencies below the resonance region. However, at frequencies below $fa/c = 0.01$, this solution diverges from the reference solution. The $p = 1$ solution is only proportional to s, and therefore, we would expect the convergence of the solution to deteriorate at low frequencies.

Although the $p = 0$ solution does not perform well in the low frequency region, it gives very good results in the resonance region. Similarly, the $p = 1$ and $p = 2$ solutions do well in this region. On the other hand, the $p = 3$ solution does poorly in the resonance region. As was seen in Appendix A, the class-1 polarizability term adversely influences the $p = 3$ solution. The class-1 polarizability term increases with the square of the frequency (see (5.10)). As a result, the polarizability term dominates the $p = 3$ solution in the resonance region.

In fig. B.4, the effect of changing the number of contributing Fourier modes on the $p = 3$, class-1 solution is studied. Three solutions using different number of Fourier modes are shown. One solution utilizes the poles of only the $n = 1$ Fourier mode. The other two solutions are constructed using two and three Fourier modes. The solution obtained using two modes signifies that the poles belonging to the modes $n = 1$ and $n = 2$ were used. Similarly, the solution obtained using three modes denotes that the poles belonging to modes $n = 1, 2$, and 3 were used. As noted previously, the zeroth mode is not considered here since it does

not couple to the response for E-wave backscattering. Like fig. B.3, the solutions shown in fig. B.4 represent the magnitude of $\tilde{A}_{b_{ee}}$ for an incident angle of 45°.

By inspecting fig. B.4, we see that each of the $p = 3$, class-1 solutions do well in predicting the low frequency behavior of the backscattering dyadic. However, in the resonance region, the various $p = 3$ solutions are similar in performance to the $p = 3$ solution shown in fig. B.3. Again, the influence of the class-1 polarizability term is responsible for this performance. Nevertheless, aspects of the correct solution can be observed in the SEM solutions. The $p = 3$ result using 1 mode contains the first resonant peak. Beyond the first peak, this solution essentially follows the polarizability term. This suggests that the $n = 1$ mode corresponds to the first resonance. Likewise, the $p = 3$ solution using 2 and 3 modes contains the first two resonant peaks. In fig. B.3 these solutions appear to be the same. However, if the vertical axis of both plots were enlarged, the third resonant peak would be seen in the solution using 3 modes. Again, this behavior suggest that the poles of the $n = 2$ and $n = 3$ modes are related to the second and third resonances, respectively.

Figures B.5 and B.6 are similar to figs. B.3 and B.4 with the only difference being that the class-2 form of the modified pole series is used to compute the backscattering dyadic for $\theta_{\text{inc}} = 45°$. By observing fig. B.5, we see that the class-2, $p = 2$ solution gives excellent results in both the low frequency and resonance regions. The class-2, $p = 1$ solution also converges well in the resonance region and at some low frequencies. At frequencies below $fa/c = 0.01$, this solution begins to diverge from the reference solution. When comparing the $p = 1$ and $p = 2$, class-2 solutions with their corresponding class-1 solution in fig. B.3, one notices that class-2 representation provides only a marginal improvement in performance. Furthermore, it appears that the class-1, $p = 0$ solution is more accurate than the class-2 results in the resonance region. In the low frequency region, both class-1 and class-2 forms of the $p = 0$ solution perform poorly. This result is anticipated since the $p = 0$ solution is not proportional to s^2.

One noticeable improvement that the class-2 solution has over the class-1 solution can be seen in the $p = 3$ result. Both forms of the solution provide nice results in the low frequency region. However, in the resonance region, the class-2, p=3 result is slightly more accurate. The reason for the improved accuracy can be explained by observing the class-2 polarizability term. Unlike the class-1 polarizability term which increases with frequency, the class-2 polarizability term peaks in the resonance region and then begins to decrease. Consequently, the influence of the class-2 polarizability term on the p=3 solution is reduced in the resonance region.

In similar fashion to fig. B.4, fig. B.6 shows the class-2, $p = 3$ solution of $\tilde{A}_{b_{ee}}$ for a variety of mode contributions. Solutions using 1,2 and 3 Fourier modes are considered. As one can see, all three of the SEM solutions converge very well to the reference solution in the low frequency region. In addition, all three solutions converge to the polarizability term in this region as well. Since the polarizability term is a

part of the $p = 3$ solution, these results indicate that it dominates the solution in the low frequency region. Furthermore, these results show that the variations in the modal content do not change the low frequency response of the $p = 3$ solution. However, in the resonance region, varying the modal content does alter the solutions. The $p = 3$ solution using only the $n = 1$ mode captures the first resonance peak, and then begins to follow the polarizability term. Similarly, the $p = 3$ solution using modes $n = 1$ and $n = 2$ contains two resonant peaks. Up through the first resonant peak, the solution using two modes is identical to the solution using only one mode. Based on this observation, it appears that each mode influences the solution in only localized regions of the response. Further support of this observation can be seen in the solution using three modes.

The results presented thus far considered only the case of $\tilde{\Lambda}_{\mathrm{bee}}$ for $\theta_{\mathrm{inc}} = 45°$. In figs. B.7 and B.8, results of $\tilde{\Lambda}_{\mathrm{bee}}$ are shown for broadside incidence ($\theta_{\mathrm{inc}} = 0°$). Because the excitation is broadside, the class-1 and class-2 forms of the backscattering dyadic are equivalent. Beginning with fig. B.7, we immediately note the excellent performance of the $p = 2$ result in both the low frequency and resonance areas of the response. Regardless of the form of the modified pole series used, the $p = 2$ solution of $\tilde{\Lambda}_{\mathrm{bee}}$ has consistently provided very good results. The performance of the $p = 1$ solution is comparable to the $p = 2$ solution particularly in the resonance region. However, at frequencies below $fa/c = 0.01$, the $p = 1$ solution diverges from the desired result. The performance of $p = 0$ result at low frequencies continues to be poor, although this is expected. In the resonance area, the performance is not much better. After capturing the first resonant peak, the $p = 0$ result quickly diverges from the reference solution One interesting observation in these results is the difference in performance of the $p = 0$ and $p = 1$ solution in the low frequency area. In going from the $p = 0$ form of the modified pole series to the $p = 1$ form, one sees a dramatic improvement in performance. This characteristic has also been observed in the previous results. Note that for $\theta_{\mathrm{inc}} = 0°$ there is a special symmetry in that the incident field, expanded on the loop, contains only an $n = 1$ term. This is associated with the simultaneous arrival of the *uniform* plane wave assumed. Since only the $n = 1$ term appears (also containing the electric dipole term, there being no magnetic dipole term), contributions from any other n would be numerical error. Note also that only poles for $n = 1$ (fig. B.2) can appear in the response, a very special case.

The behavior of the $p = 3$ solution in fig. B.7 is similar to the $p = 3$ result shown in fig. B.3. Because of the polarizability term, the $p = 3$ solution does well at low frequencies, but performs poorly in the resonance region. After capturing the first resonant peak, the solution is dominated by the polarizability term. This identical behavior can be seen in the results of fig. B.8 where the $p = 3$ solution is computed using several different mode contributions. Note that there is essentially no distinguishable features among the three SEM solutions. For broadside incidence only the odd modes contribute to the response. Hence, there should be no difference in the solutions using the $n = 1$ mode and the solution using the $n = 1$ and 2 modes. However, if we were to expand the vertical axis of each plot, we could observe the peak of the third

resonance in the solution using modes $n = 1, 2$, and 3.

Having presented a variety of results illustrating the E-polarized backscattering dyadic, we can now focus our attention on the results depicting the H-polarized backscattering dyadic $\tilde{\Lambda}_{b_{hh}}$. These results are shown in figs. B.9 through B.16. Figures B.9 through B.12 contain solutions of $\tilde{\Lambda}_{b_{hh}}$ for $\theta_{inc} = 45°$, and figs. B.12 through B.16 show $\tilde{\Lambda}_{b_{hh}}$ for $\theta_{inc} = 90°$.

Illustrated in fig. B.9 are the class-1 solutions of $\tilde{\Lambda}_{b_{hh}}$ for $\theta_{inc} = 45°$. By inspecting the upper plot, one observes that the low frequency agreement of the SEM solutions with the reference solution diminish with decreasing power p of the modified pole series. Both the $p = 2$ and $p = 3$ solution provide good results at low frequencies. The $p = 2$ solution gives good results in this region because the form of the solution is proportional to s^2. The $p = 3$ solution does well at low frequencies primarily because it contains the polarizability term. As we have seen in the previous results, the polarizability term accurately describes the low frequency behavior of the backscattering dyadic.

In the resonance region, all of the modified pole series do well. Of particular interest is the $p = 3$ solution. Unlike the class-1, $p = 3$ solutions of $\tilde{\Lambda}_{b_{ee}}$, the class-1, $p = 3$ solution shown in fig. B.9 agrees nicely with the reference solution in the resonance region. Note that the class-1 polarizability term increases with the square of frequency. In the discussion of the results for E-wave backscattering, we suggested that this solution adversely influences the $p = 3$ solution. However, for H-wave backscattering, the s^2 behavior of the polarizability term actually improves the $p = 3$ solution in the frequency range of interest. Without the inclusion of the polarizability term, the convergence of the this solution would be poor at both low and resonant frequencies. At higher resonant frequencies, the $p = 3$ solution does become dominated by the polarizability term. As a result, the solution diverges from the desired result.

Additional results illustrating the performance of the $p = 3$ solution are shown in fig. B.10. These results were constructed by varying the number of mode contributions. Three different $p = 3$ solutions were obtained by using 2, 3, and 4 modes. The solution obtained using 2 modes implies that the poles belonging to modes $n = 0$ and $n = 1$ were used to construct the solution. Recall that the pole at $s = 0$ of the zeroth mode was excluded from the calculations. Similarly, the solution using 3 modes indicates that the poles belonging to modes $n = 0$, 1, and 2 were used in computing the solution.

In fig. B.10, one observes that all three $p = 3$ solutions converge to the reference solution at low frequencies. In the resonance region, the solutions vary depending on the number of modes that were used. For example, the result using 2 modes captures the first resonant peak and then diverges from the reference solution. Similarly, the result using 3 modes captures the first and second resonances. As we observed in the results of $\tilde{\Lambda}_{b_{ee}}$, these results also indicate that the nth mode is related to the nth resonant peak. This relationship suggests that by altering the number of modes in the solution, we can spatially filter the response

of the backscattered field.

The class-2 results of $\tilde{\Lambda}_{b_{hh}}$ for $\theta_{inc} = 45°$ are shown in figs. B.11 and B.12. When comparing the results in fig. B.11 with the class-1 results of fig. B.9, some interesting observations can be made. Perhaps the most interesting aspect is that the class-1 results seem to be be better than their class-2 companions. Normally, we expect the class-2 results to be better than the class-1 results. The convergence of both the class-1 and class-2 forms of the $p = 3$ solution are comparable at low frequencies. However, the class-1, $p = 2$ solution actually converges to better to the reference solution than the class-2, $p = 2$ solution. The same can be said for the class-1, $p = 1$ result. One explanation for these results may be the exclusion of the pole at $s = 0$. Although not shown here, results were obtained for the class-2, $p = 1$ form of $\tilde{\Lambda}_{b_{hh}}$ that included the pole at the origin. These results showed that including the pole at $s = 0$ significantly improved the convergence of the $p = 1$ solution. As noted earlier, evaluating the $p = 2$ and $p = 3$ forms of $\tilde{\Lambda}_{b_{hh}}$ at the pole at $s = 0$ yields an indeterminate expression. Including the pole at $s = 0$ in the $p = 0$ solution yields zero for that term in the summation. Hence, including the pole at the origin has no effect on the $p = 0$ result.

Like fig. B.10, the results shown in fig. B.12 provide additional insight into the class-2, $p = 3$ form of the modified pole series through variation of the modal content. By comparing the class-1 solutions of fig. B.10 with the class-2 solutions, we observe that the solutions are very similar. Both the class-1 and class-2 solutions using two modes are nearly identical. However, the class-2 solutions using 3 and 4 modes do not converge as well to the reference solution as do their class-1 counterparts. The difference in performance of these solutions may in part be attributed to the difference in the class-1 and class-2 polarizability terms.

The last set of results depict $\tilde{\Lambda}_{b_{hh}}$ for an incident angle of $\theta_{inc} = 90°$. In this orientation, the incident and scattered fields are sweeping across the diameter of the loop. In order for the SEM solutions to be accurate, the coupling coefficients involved must be capable of contributing early-time information. The inability of the class-1 solution to contribute this information can be seen in fig. B.13. Nearly all of the SEM solutions shown in fig. B.13 perform poorly, particularly the $p = 0$ and $p = 1$ solutions. The class-1, $p = 3$ solution does well at low frequencies, but this performance is primarily due to the inclusion of the polarizability term. In the resonance region, the $p = 3$ solution converges fairly well to the reference solution up through the second resonant peak. Beyond this peak, the $p = 3$ solution quickly diverges from the reference solution. This behavior of the $p = 3$ solution can also be seen in fig. B.14. Up through the first resonant peak, all three of the $p = 3$ solutions converge well to the reference solution. Beyond this peak, the various solutions rapidly diverge from the desired result. Nevertheless, the difference in the modal content of the solutions is apparent.

When the class-2 form of the modified pole series is used to compute $\tilde{\Lambda}_{b_{hh}}$ for $\theta_{inc} = 90°$, a significant improvement in performance occurs. The solutions shown in fig. B.15 provides evidence of this amelioration. By inspecting fig. B.15, one observes that the convergence of the SEM solutions improves as the power of

the pole series is increased. The class-2, $p = 3$ solution appears to be the superior SEM solution in both the low frequency and resonance regions. Furthermore, there appears to be no distinguishable difference in the $p = 1$ and $p = 2$ solutions in the resonance region. However, as noted earlier, the $p = 1$ solution can be improved if the pole at $s = 0$ were included in the pole series.

In similar fashion to figs. B.12 and B.14, fig. B.16 shows several class-2, $p = 3$ solutions in which the number of contributing modes has been varied. Regardless of the number of modes used, the low frequency agreement of all three solutions remains unchanged. This same result has been observed in all of the previous results. Hence, it appears that the modal content of the $p = 3$ solution does not affect the convergence of the solution in the low frequency region. In this region, the polarizability term dominates the $p = 3$ solution. This should be obvious from the results since, at low frequencies, the $p = 3$ solution not only converges to the reference solution, but also to the polarizability term. Only in the resonance region do we see the effects of changing the modal content of the solution. Furthermore, as the results in fig. B.16 show, there is a relationship between the nth mode and the nth resonant peak. For example, the $p = 3$ solution using three modes utilizes the poles belonging to modes $n = 0$, 1, and 2. As a result, this $p = 3$ solution captures the first two resonant peaks of the reference solution and then diverges.

Comparing the various figures here, several things can be observed. At low frequencies, the reference solution agrees very well with the polarizability term, better than in the case of the thin-wire. This indicates that, at least in this region, the solution technique involving analytic modes is more accurate. We also observe that the class-1 results are generally better for $\theta_{\text{inc}} = 0°$, consistent with (B.63). The comparison of class-1 to class-2 forms is more difficult due to the aforementioned problem with the pole at $s = s_{0,0} = 0$, as it influences the class-2 results. To do this properly, one should consider appropriate asymptotics near $s = 0$. One can let $s_{0,0} \neq 0$ by changing the problem to another passive one by letting there be some resistance uniformly distributed around the loop with $s_{0,0}$=resistance/inductance. Then from (B.56), we see one power of $s_{0,0}$ in $W_{0,0}$. This removes the pole for $p = 0$ in the limit $s_{0,0} \to 0$. For $p = 1$, it can even cancel the $s_{0,0}$ in $(s,\, s_{0,0})^1$, leaving an evaluatable expression. Including resistance modifies (B.40) for $\tilde{G}_0(s)$ so that $R_{0,0}$ in (B.55) is well behaved. For $p = 2, 3$ inclusion of a pole at $s = 0$ in the class-2 form blows up as $s_{0,0} \to 0$. A more detailed evaluation of this phenomena (and especially in the context of more general conducting scatterers per eigenimpedance-synthesis formulae in [7] might improve the handling of the class-2 form.

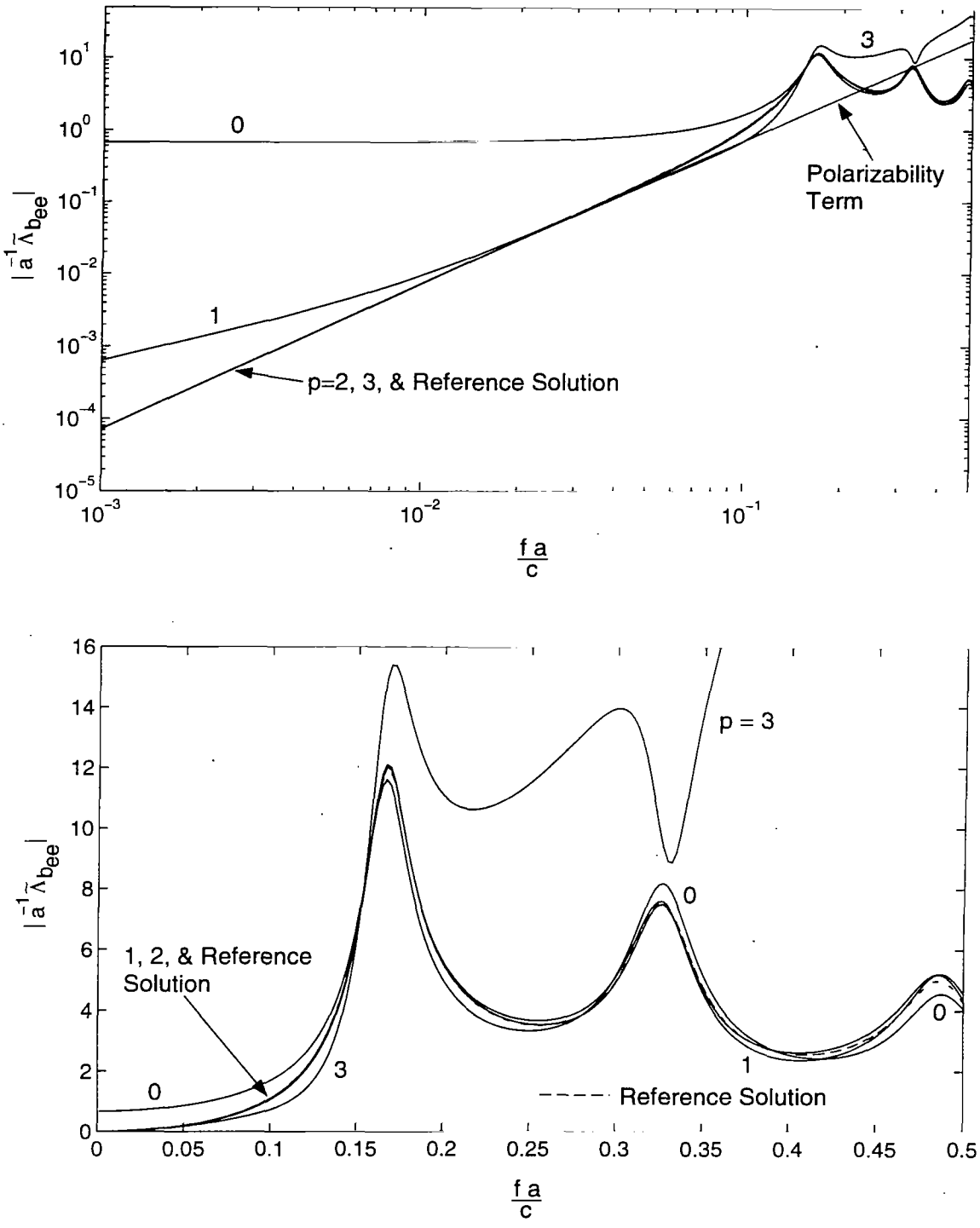

Figure B.3. Magnitude of the backscattering dyadic from a thin circular loop due to an E-polarized plane wave incident from $\theta_{\text{inc}} = 45°$, calculated using the class-1 SEM modified pole series (p=0,1,2,3). The reference solution is provided for comparison.

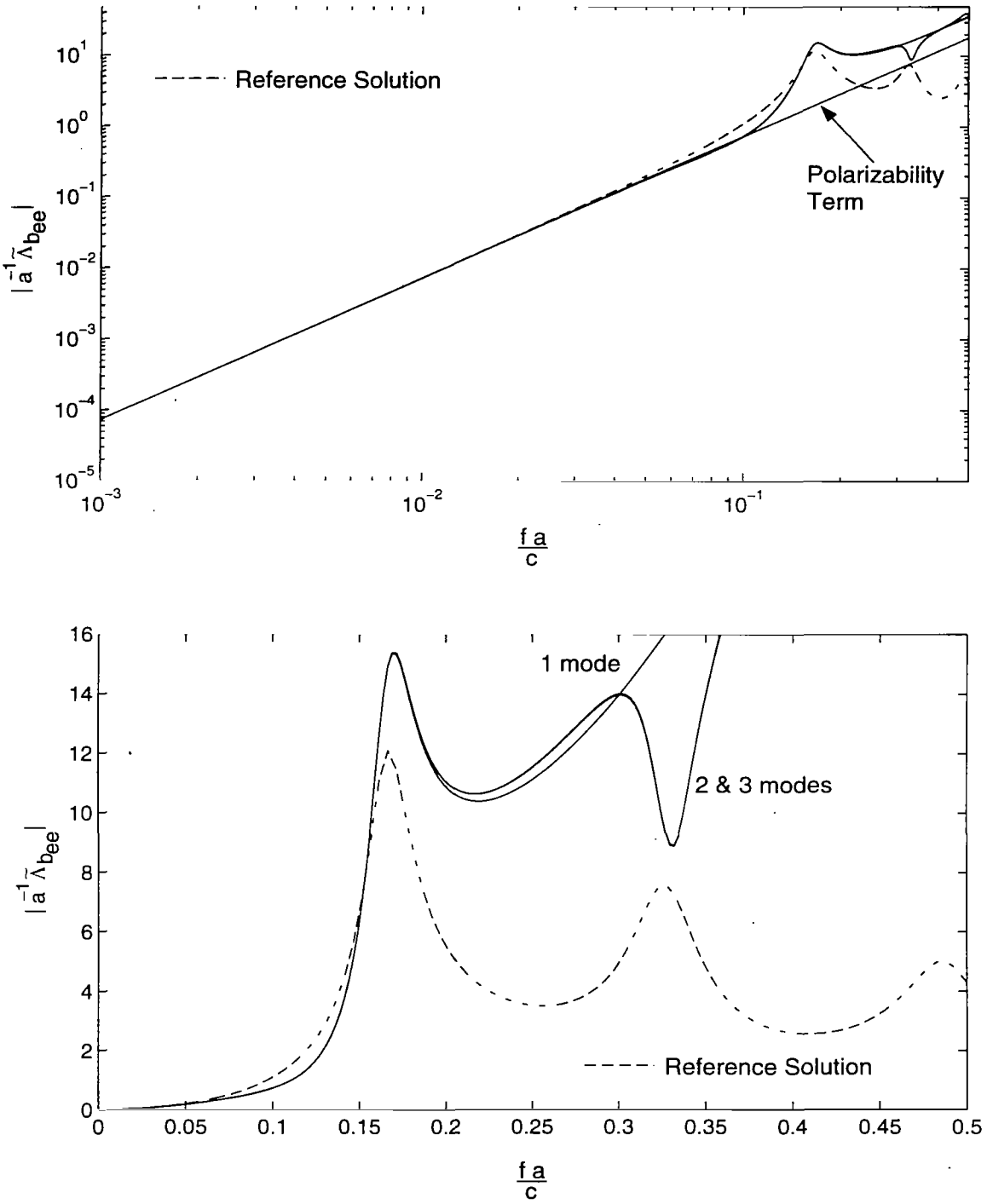

Figure B.4. Magnitude of the backscattering dyadic from a thin circular loop due to an E-polarized plane wave incident from $\theta_{inc} = 45°$, calculated using the p=3, class-1 SEM representation. The SEM solutions were obtained using 1, 2, and 3 modes.

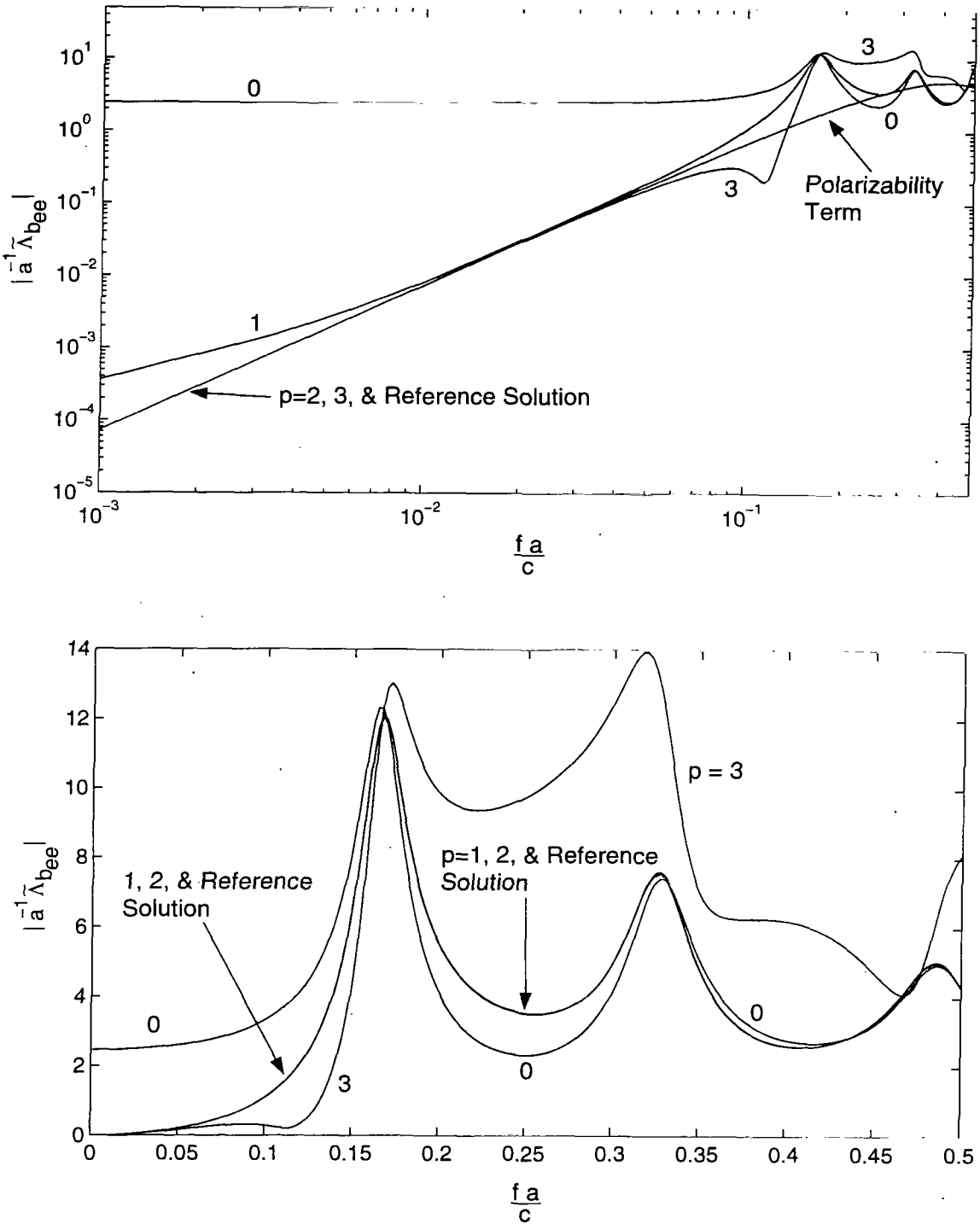

Figure B.5. Magnitude of the backscattering dyadic from a thin circular loop due to an E-polarized plane wave incident from $\theta_{\text{inc}} = 45°$, calculated using the class-2 SEM modified pole series (p=0,1,2,3). The reference solution is provided for comparison.

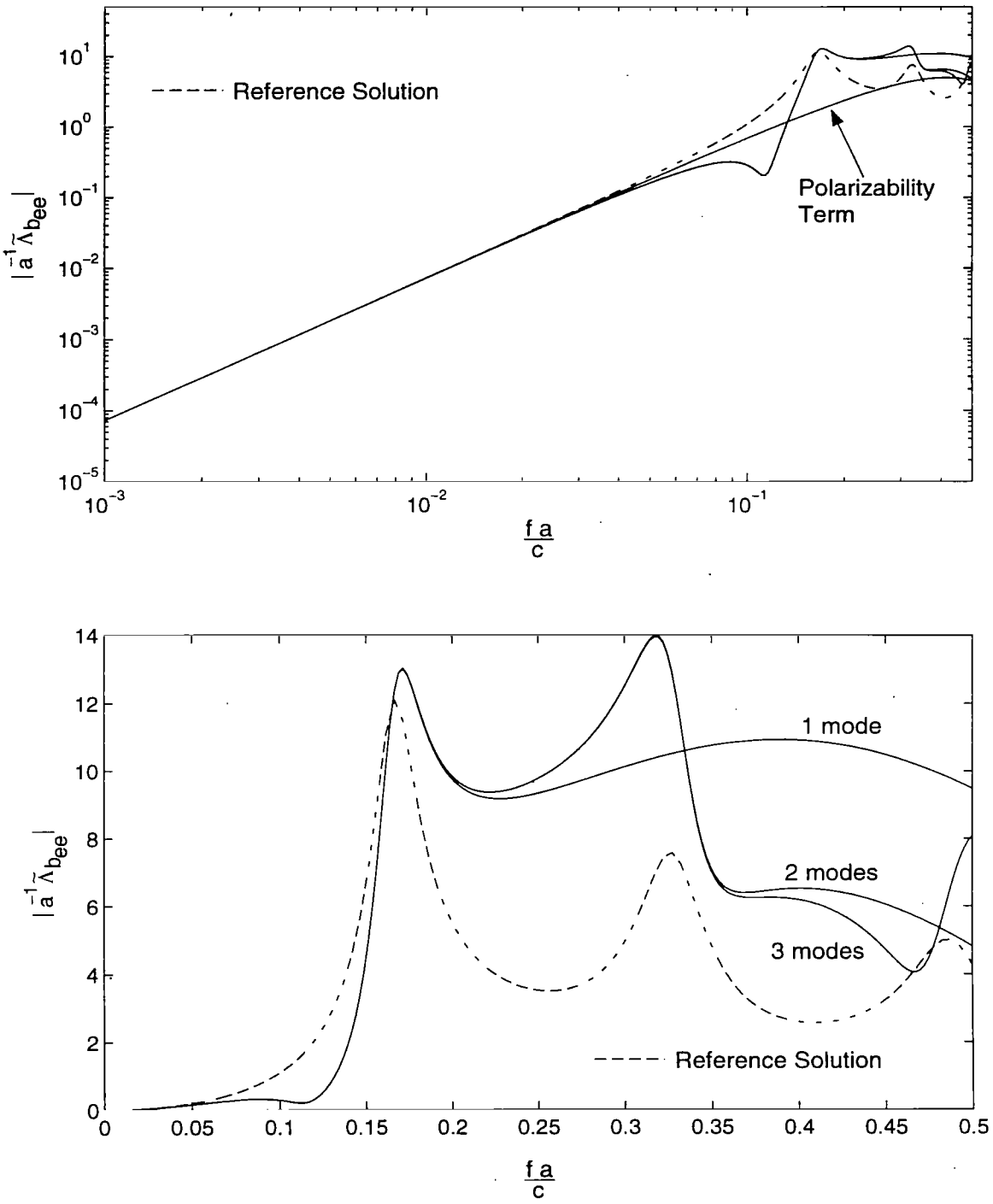

Figure B.6. Magnitude of the backscattering dyadic from a thin circular loop due to an E-polarized plane wave incident from $\theta_{inc} = 45°$, calculated using the p=3, class-2 SEM representation. The SEM solutions were obtained using 1, 2, and 3 modes.

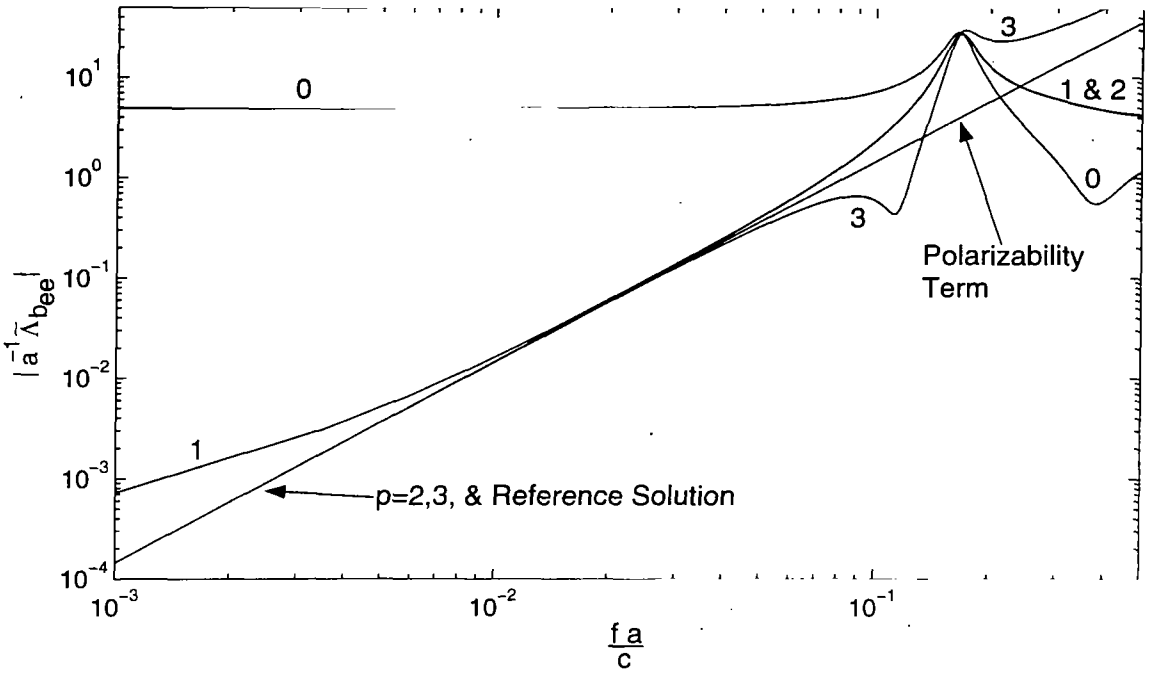

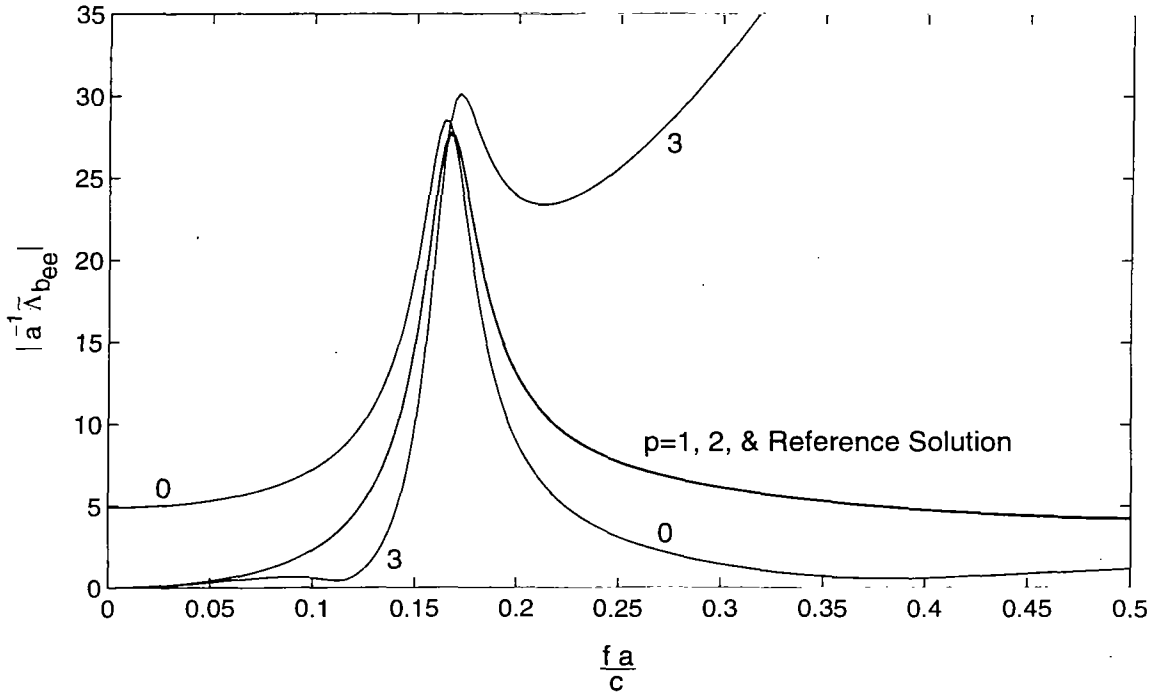

Figure B.7. Magnitude of the backscattering dyadic from a thin circular loop due to an E-polarized (or equivalently H-polarized) plane wave incident from $\theta_{\text{inc}} = 0°$, calculated using the SEM modified pole series (p=0,1,2,3) (class-1 $\equiv$ class-2). The reference solution is provided for comparison.

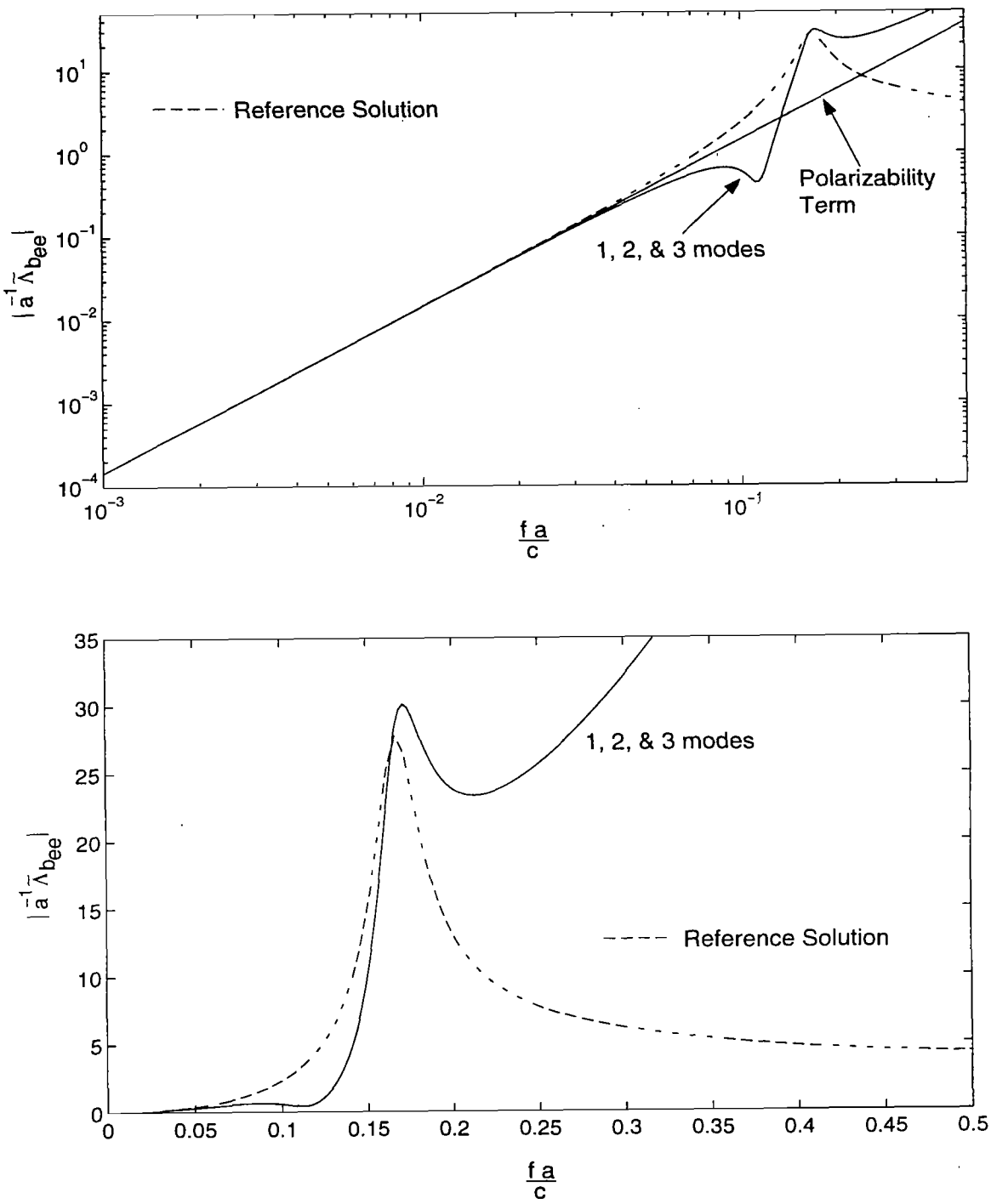

Figure B.8. Magnitude of the backscattering dyadic from a thin circular loop due to an E-polarized (or equivalently H-polarized) plane wave incident from $\theta_{inc} = 0°$, calculated using the p=3 SEM representation (class-1 $\equiv$ class-2). The SEM solutions were obtained using 1, 2, and 3 modes.

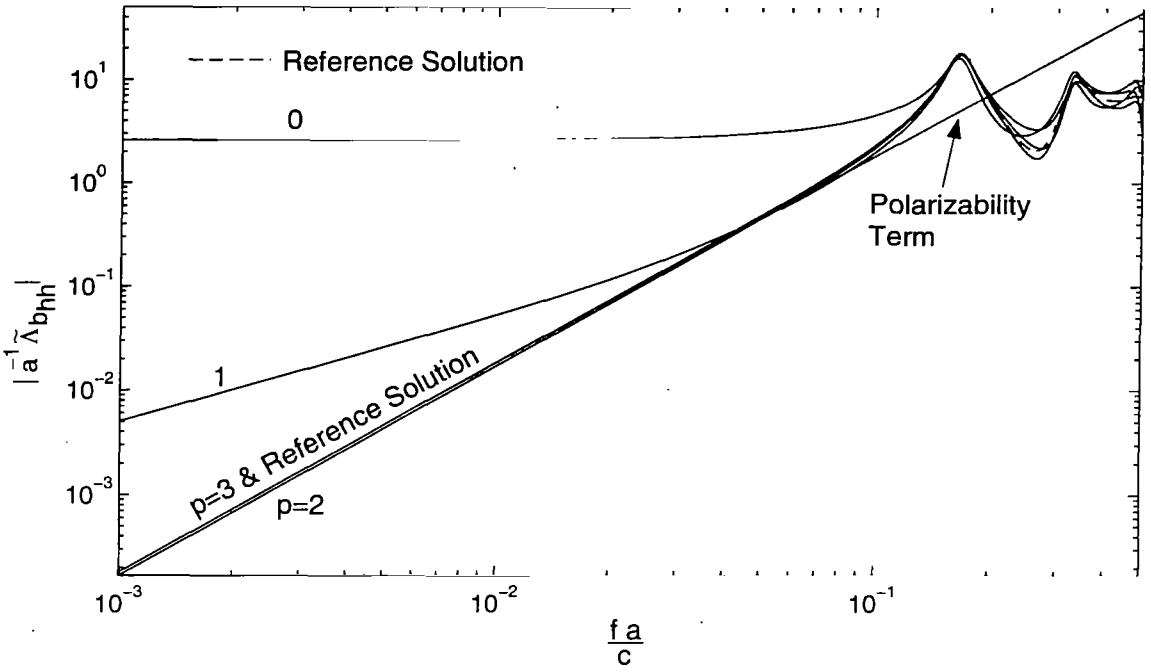

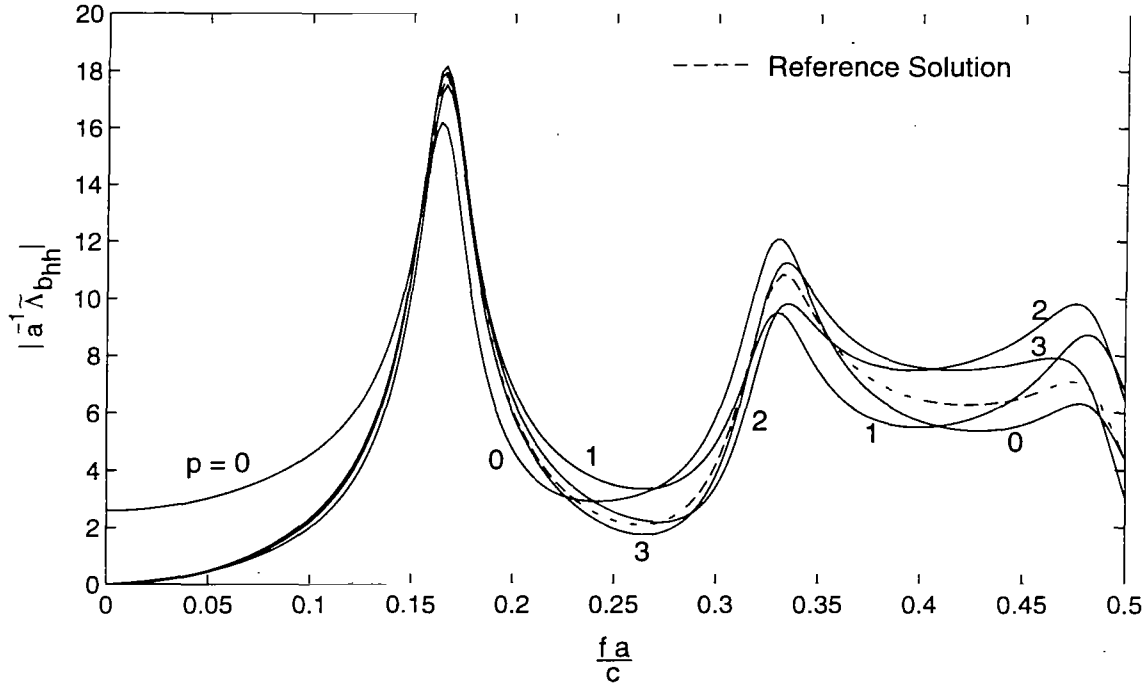

Figure B.9. Magnitude of the backscattering dyadic from a thin circular loop due to an H-polarized plane wave incident from $\theta_{\text{inc}} = 45°$, calculated using the class-1 SEM modified pole series (p=0,1,2,3). The reference solution is provided for comparison.

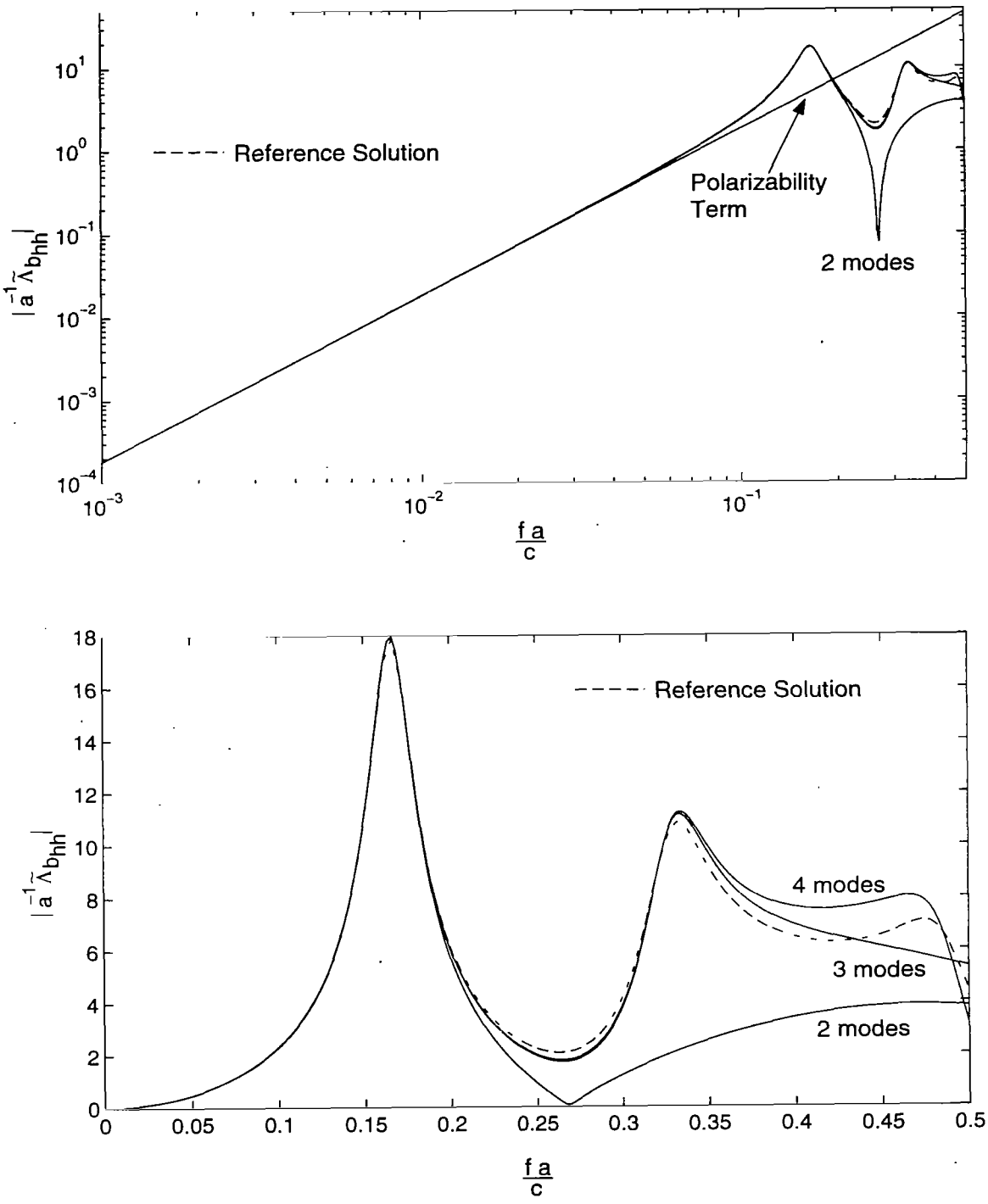

Figure B.10. Magnitude of the backscattering dyadic from a thin circular loop due to an H-polarized plane wave incident from $\theta_{\text{inc}} = 45°$, calculated using the p=3, class-1 SEM representation. The SEM solutions were obtained using 2, 3, and 4 modes.

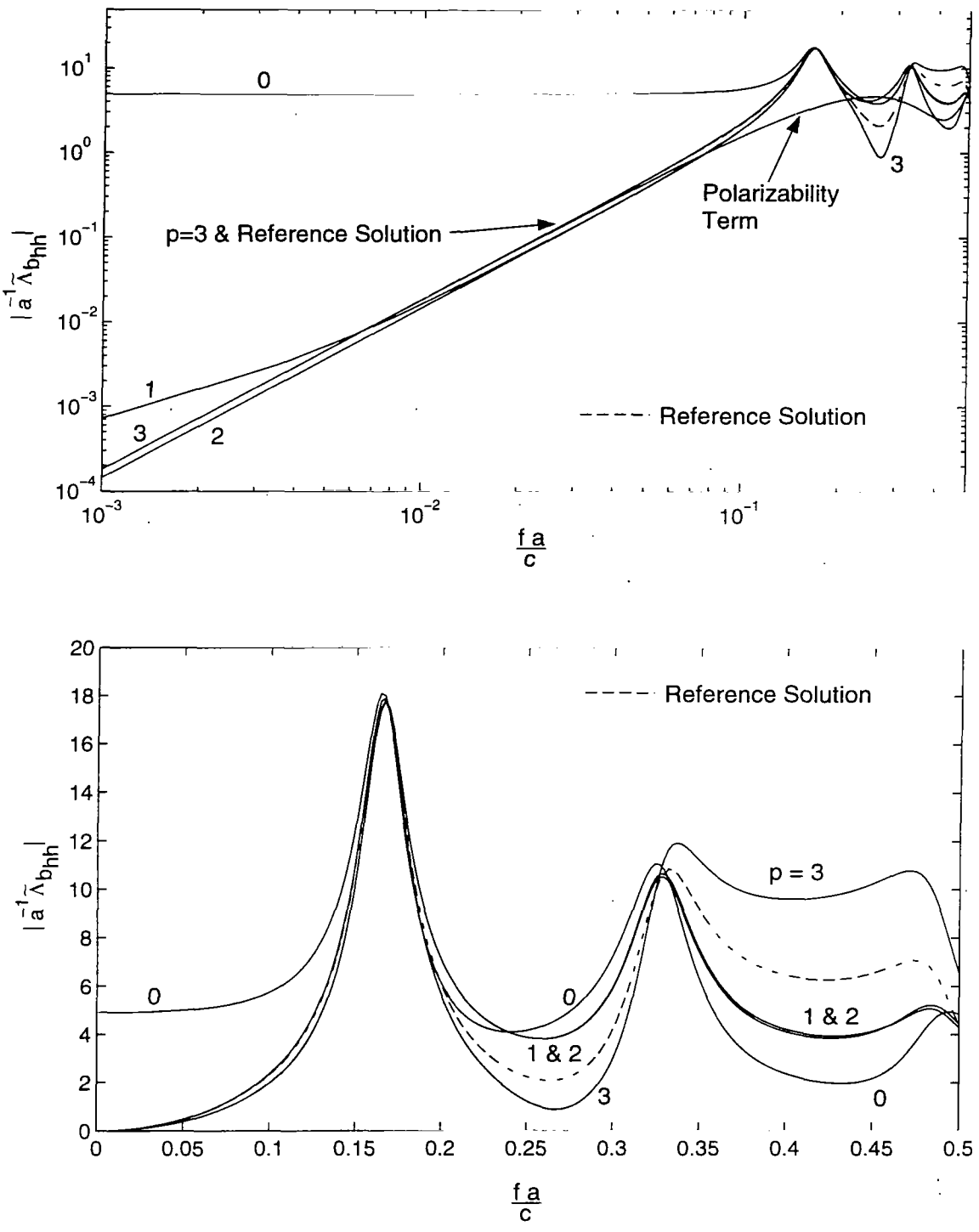

Figure B.11. Magnitude of the backscattering dyadic from a thin circular loop due to an H-polarized plane wave incident from $\theta_{inc} = 45°$, calculated using the class-2 SEM modified pole series (p=0,1,2,3). The reference solution is provided for comparison.

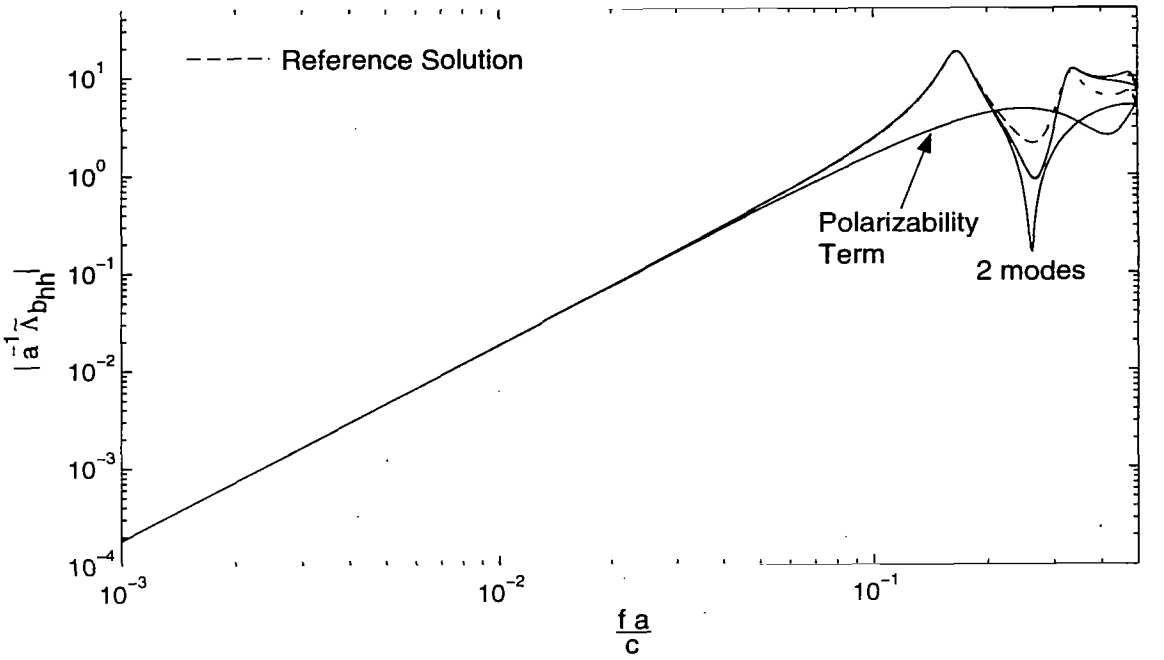

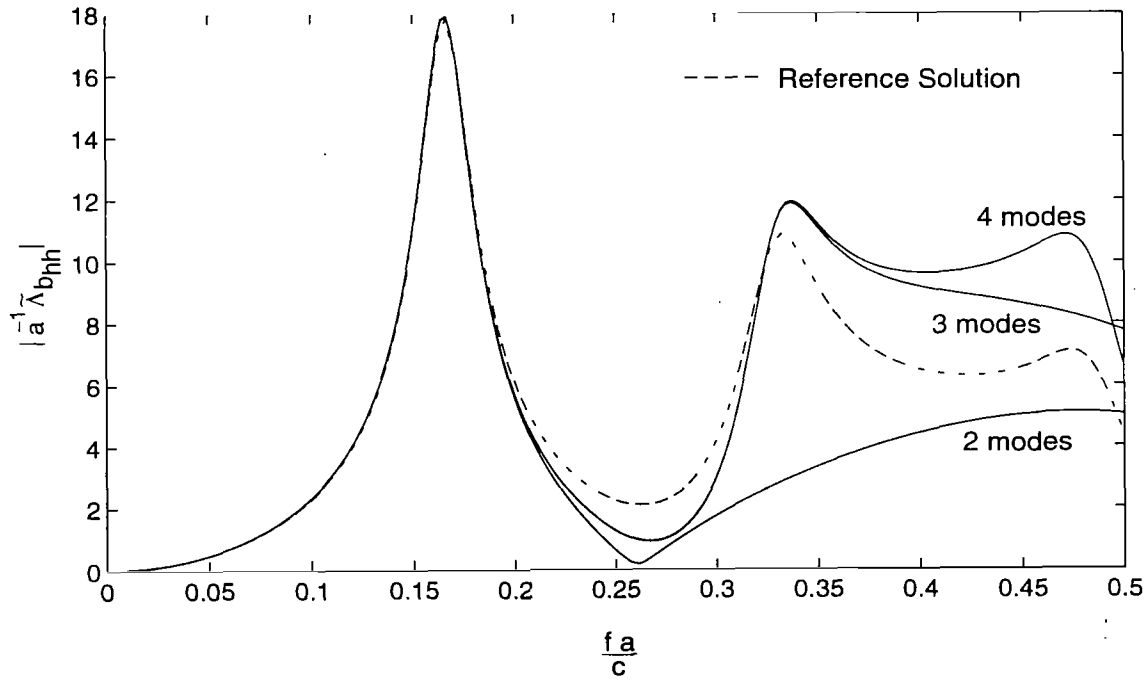

Figure B.12. Magnitude of the backscattering dyadic from a thin circular loop due to an H-polarized plane wave incident from $\theta_{inc} = 45°$, calculated using the p=3, class-2 SEM representation. The SEM solutions were obtained using 2, 3, and 4 modes.

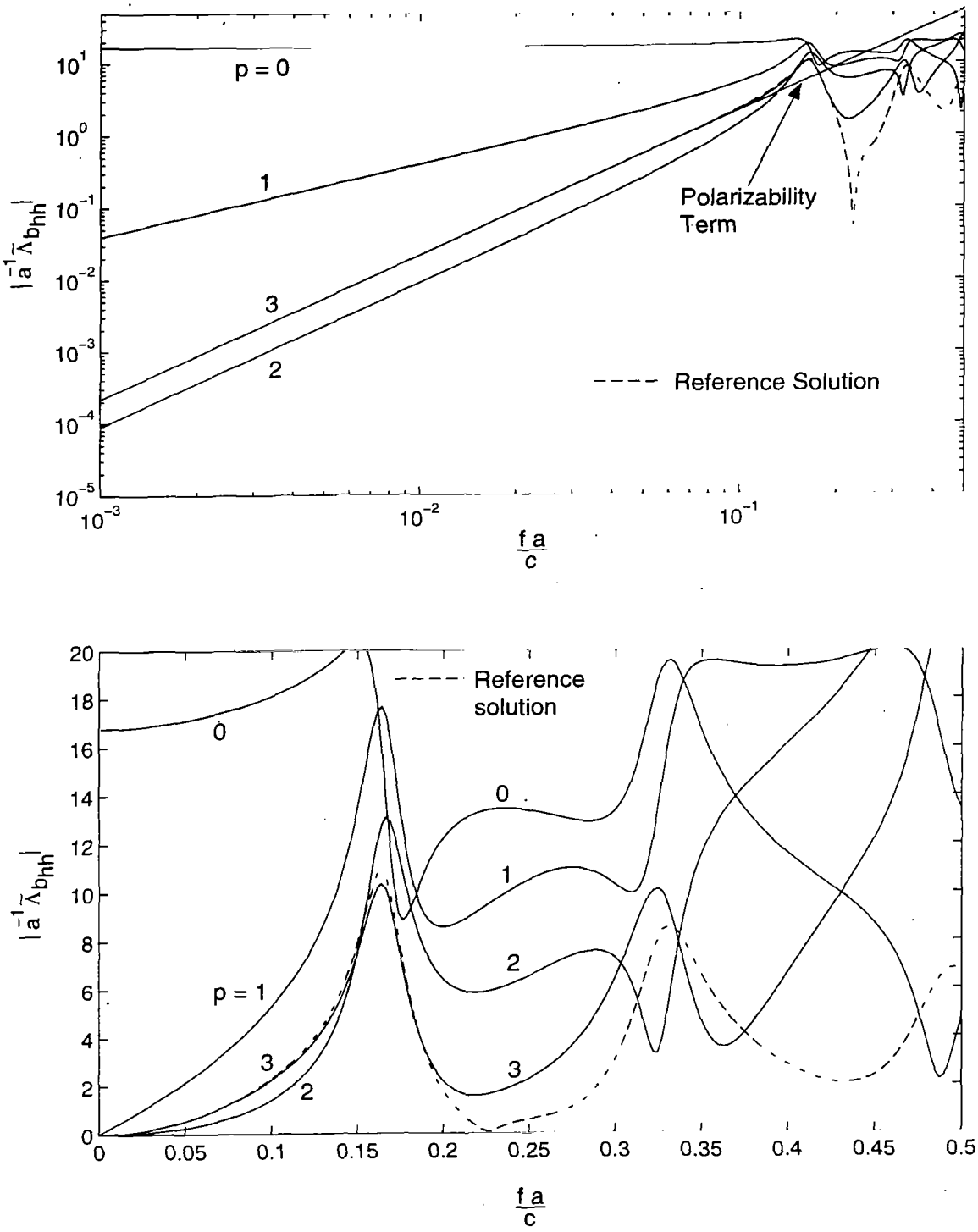

Figure B.13. Magnitude of the backscattering dyadic from a thin circular loop due to an H-polarized plane wave incident from $\theta_{inc} = 90°$, calculated using the class-1 SEM modified pole series (p=0,1,2,3). The reference solution is provided for comparison.

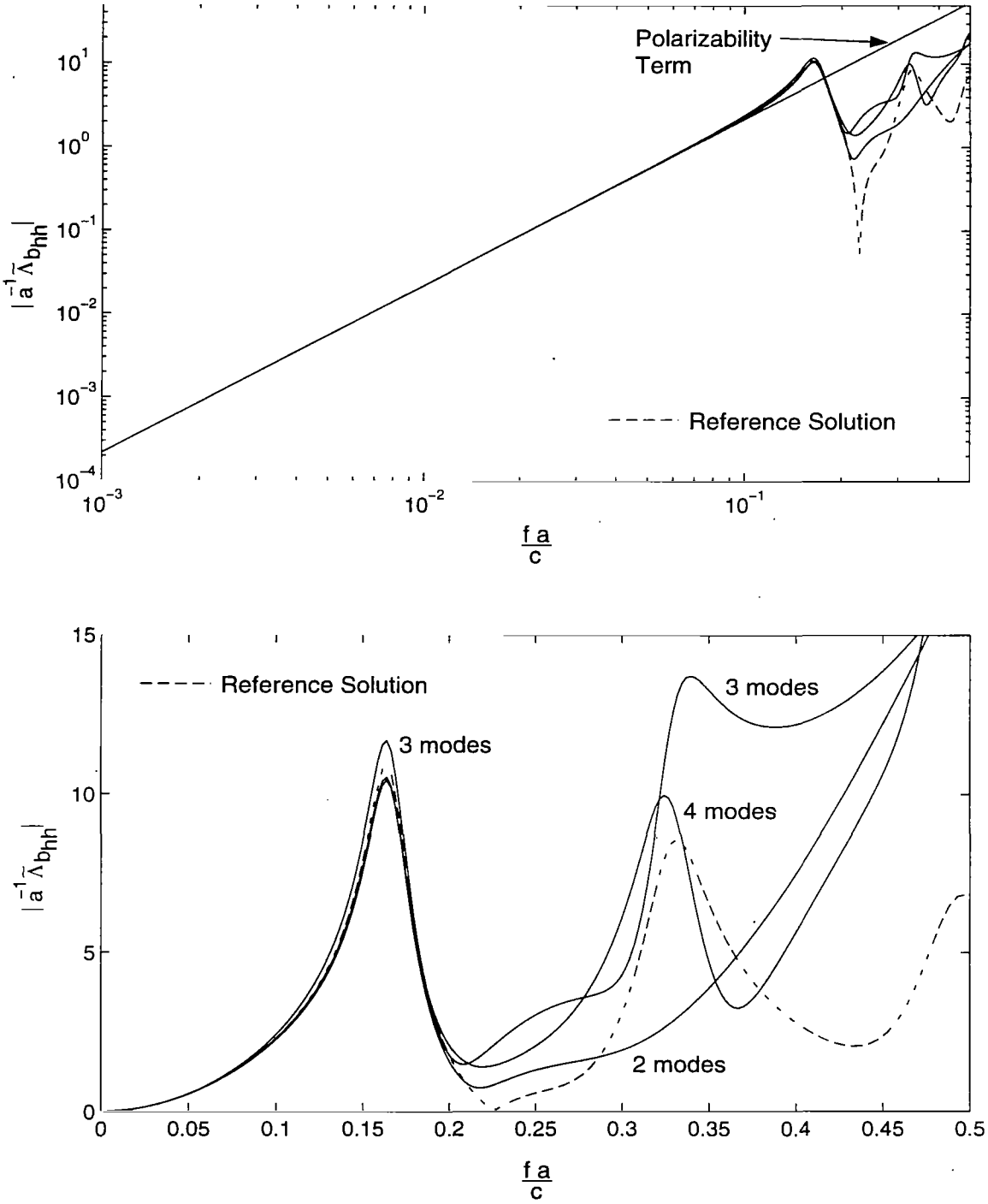

Figure B.14. Magnitude of the backscattering dyadic from a thin circular loop due to an H-polarized plane wave incident from $\theta_{\text{inc}} = 90°$, calculated using the p=3, class-1 SEM representation. The SEM solutions were obtained using 2, 3, and 4 modes.

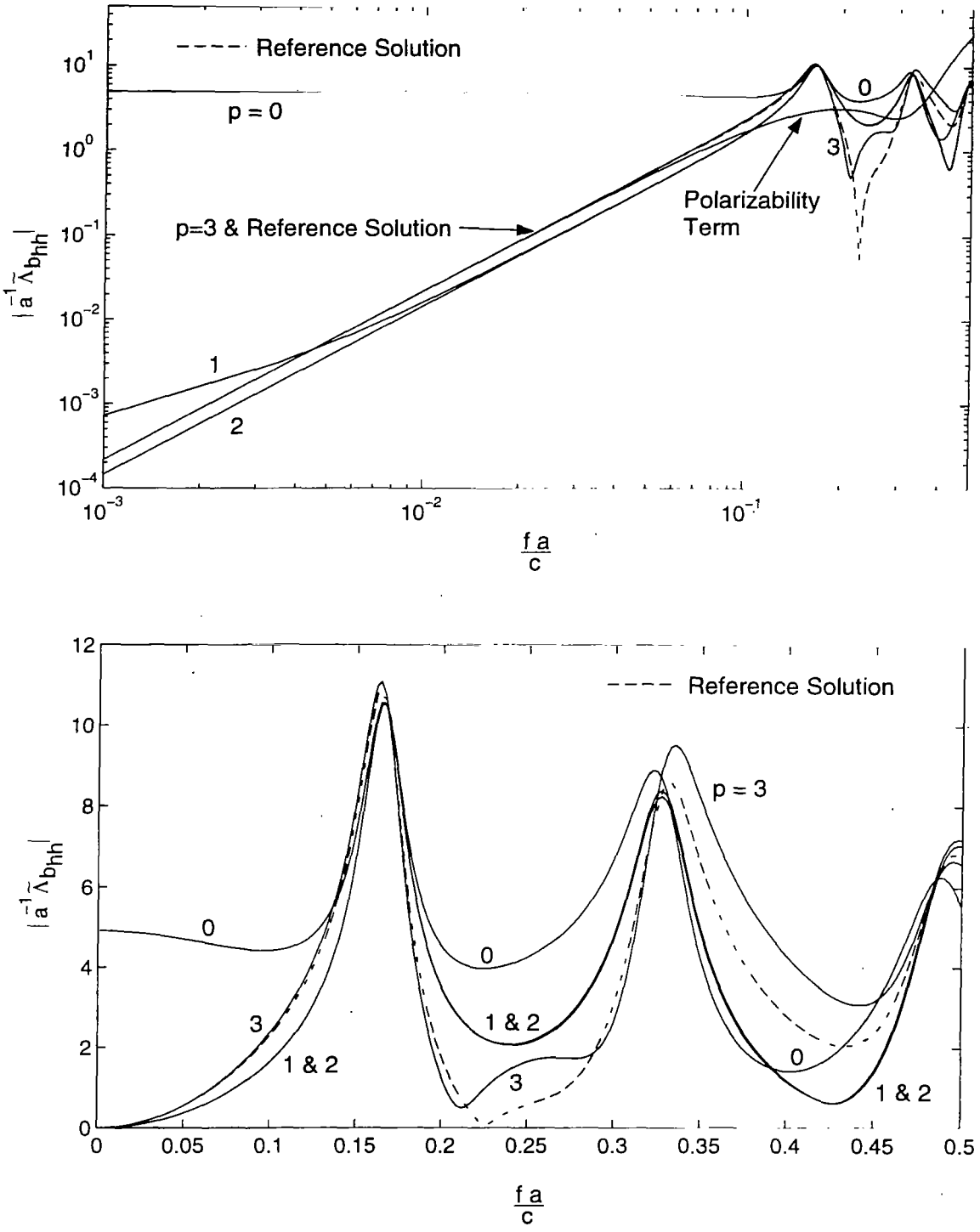

Figure B.15. Magnitude of the backscattering dyadic from a thin circular loop due to an H-polarized plane wave incident from $\theta_{inc} = 90°$, calculated using the class-2 SEM modified pole series (p=0,1,2,3). The reference solution is provided for comparison.

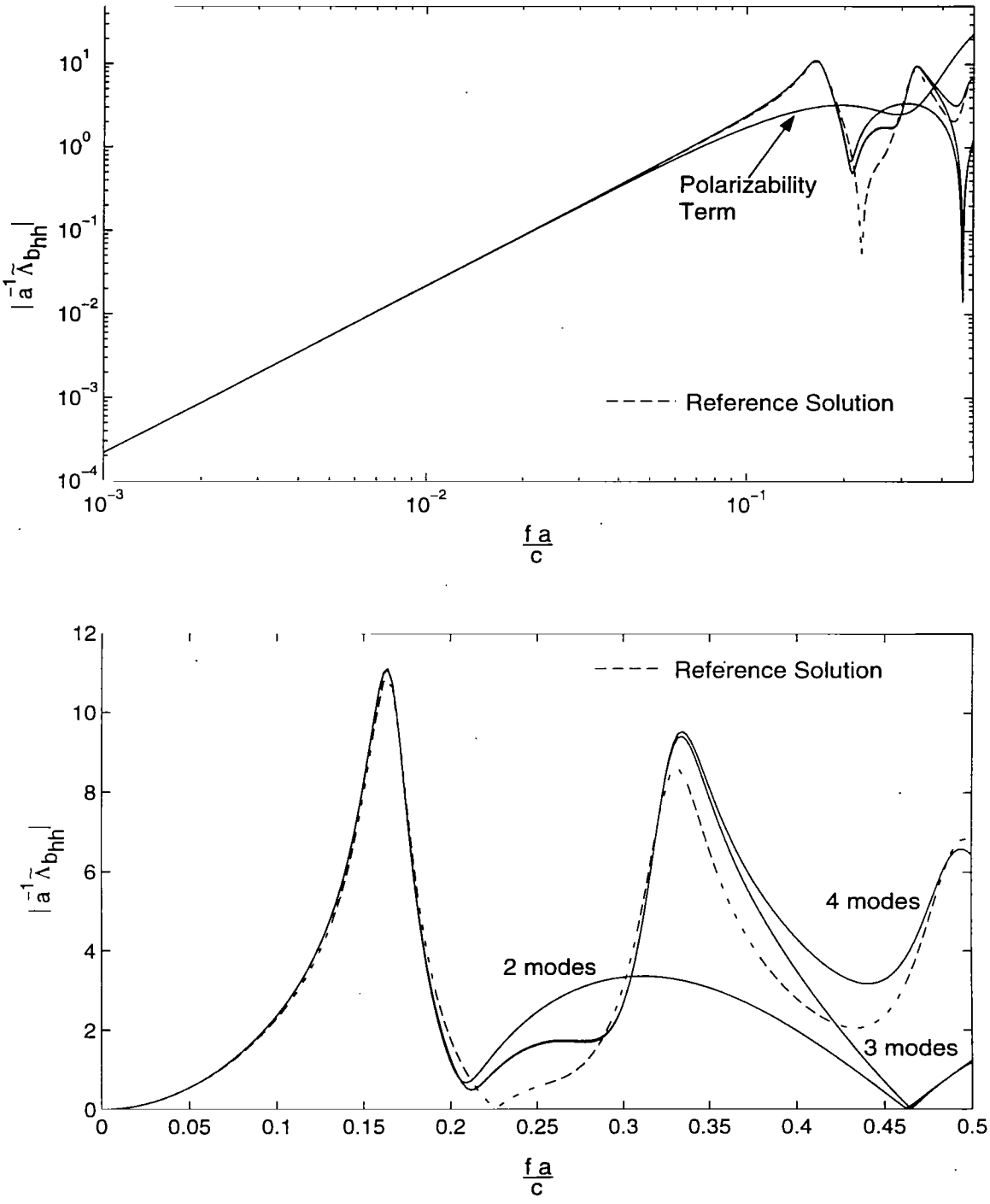

Figure B.16. Magnitude of the backscattering dyadic from a thin circular loop due to an H-polarized plane wave incident from $\theta_{\text{inc}} = 90°$, calculated using the p=3, class-2 SEM representation. The SEM solutions were obtained using 2, 3, and 4 modes.

References

1. C.E. Baum, Some Characteristics of Electric and Magnetic Dipole Antennas for Radiating Transient Pulses, Sensor and Simulation Note 125, January 1971.

2. K.S.H. Lee, Electrically-Small Ellipsoidal Antennas, Sensor and Simulation Note 193, February 1974.

3. R.F. Blackburn, Analysis and Synthesis of an Impedance-Loaded Loop Antenna Using the Singularity Expansion Method, Sensor and Simulation Note 214, May 1976.

4. C.E. Baum, Use of Modified Pole Series for Characterizing the Surface Response of Scatterers, Sensor and Simulation Note 300, December 1986.

5. C.E. Baum, On the Singularity Expansion Method for the Solution of Electromagnetic Interaction Problems, Interaction Note 88, December 1971.

6. K.R. Umashankar and D.R. Wilton, Transient Characterization of Circular Loop Using Singularity Expansion Method, Interaction Note 259, August 1974.

7. C.E. Baum, Emerging Technology for Transient and Broad-Band Analysis and Synthesis of Antennas and Scatterers, Interaction Note 300, November 1976, and Proc. IEEE, 1976, pp. 1598-1616.

8. C.E. Baum, A Priori Application of Results of Electromagnetic Theory to the Analysis of Electromagnetic Interaction Data, Interaction Note 444, February 1985, and Radio Science, 1987, pp. 1127-1136.

9. C.E. Baum, Scattering, Reciprocity, Symmetry, EEM, and SEM, Interaction Note 475, May 1989.

10. C.E. Baum, SEM Backscattering, Interaction Note 476, July 1989.

11. C.E. Baum, Representation of Surface Current Density and Far Scattering in EEM and SEM With Entire Functions, Interaction Note 486, February 1992, and in P.P. Delsanto and A.W. Saenz (eds.), *New Perspectives on Problems in Classical and Quantum Physics*, Gordon and Breach (in publication).

12. C.E. Baum, H. Chang, and J.P. Martinez, Analytical Approximations and Numerical Techniques for the Integral of the Anger-Weber Function, Mathematics Note 25, August 1972.

13. T.T. Crow, B.D. Graves, and C.D. Taylor, Numerical Techniques Useful in the Singularity Expansion Method as Applied to Electromagnetic Interaction Problems, Mathematics Note 27, December 1972.

14. C.O. Beasley, Jr. and H.K. Meier, Subroutine CAUCHY: Complex Roots of a Function Using a Cauchy Integral Technique, Mathematics Note 37, August 1974.

15. B.K. Singaraju, D.V. Giri, and C.E. Baum, Further Developments in the Application of Contour Integration to the Evaluation of the Zeros of Analytic Functions and Relevant Computer Programs, Mathematics Note 42. March 1976.

16. D.V. Giri and C.E. Baum, Application of Cauchy's Residue Theorem in Evaluating the Poles and Zeros of Complex Meromorphic Functions and Apposite Computer Programs, Mathematics Note 55, May 1978.

17. E. Hallén, Theoretical Investigation into Transmitting and Receiving Qualities of Antennae, Nova Acta Regiae, Soc. Sci. Upsaliensis, Ser. IV, Vol. II, Nov. 1938, pp.1-43.

18. J.E. Storer, Impedance of Thin-Wire Loop Antennas, Trans. Am. Inst. Elec. Eng., Vol. 75, pt. 1, No. 27, Nov. 1956, pp. 606-619.

19. T.T Wu, Theory of the Thin Circular Loop Antenna, Journal Math. Physics, 1962, pp. 1301-1304.

20. R.F. Harrington and J.L. Ryerson, Electromagnetic Scattering by Loaded Wire Loops, Radio Science, pp. 347-352.

21. L.W. Pearson and L. Marin, Special Issue on the Singularity Expansion Method, Electromagnetics, 1981, pp. 349-511.

22. C.E. Baum, The Singularity Expansion Method: Background and Developments, IEEE Antennas and Propagation Newsletter/Magazine, Vol. 24, No. 4, August 1986, pp. 15-23.

23. C.E. Baum, T.H. Shumpert, and M.A. Richards, Judicious Choice of the SEM Representation for Scattered Fields, URSI Radio Science Mtg., Chicago, Illinois, July 1992.

24. M. Abramowitz and I.A. Stegun, *Handbook of Mathematical Functions*, AMS 55, U.S. Gov't. Printing Office, 1964.

25. R.W.P. King and C.W. Harrison, *Antennas and Waves: A Modern Approach*, M.I.T. Press, 1969.

26. J.D. Jackson, *Classical Electrodynamics., 2nd. Ed.*, Wiley, 1975.

27. C.E. Baum, The Singularity Expansion Method, Ch.3, pp. 129-179, in L.B. Felson (ed.) *Transient Electromagnetic Fields*, Springer-Verlag, 1976.

28. C.E. Baum, Toward an Engineering Theory of Electromagnetic Scattering: The Singularity and Eigenmode Expansion Methods, Ch. 15, pp. 571-651, in P.L.E Uslenghi (ed.), *Electromagnetic Scattering*, Academic Press, 1978.

29. J. Van Bladel, *Electromagnetic Fields*, Hemisphere (Taylor & Francis), 1985.

30. K.S.H. Lee (ed.), *EMP Interaction: Principles, Techniques, and Reference Data*, Hemisphere (Taylor & Francis), 1986.

31. W.R. Smythe, *Static and Dynamic Electricity, 3rd Ed.*, Hemisphere (Taylor & Francis), 1989.

32. C.E. Baum, SEM and EEM Scattering Matrices and Time-Domain Scatterer Polarization in the Scattering Residue Matrix, Ch. I-10, pp.427-486, in W.-M. Boerner et al (eds.), *Direct and Inverse Methods in Radar Polarimetry*, Kluwer Academic Publishers, 1992.

33. C.E. Baum and H.N. Kritikos, Symmetry in Electromagnetics, Ch. 1, pp. 1-90, in C.E. Baum and H.N. Kritikos (eds.), *Electromagnetic Symmetry*, Taylor & Francis, 1995.